▷ Structure of Matter - Subatomic Physics

Strongly Interacting Matter in the Early Universe Prior to Confinement [B,E]

D. Seipt, M. Bluhm, R. Schulze, B. Kämpfer

Part of Diploma thesis D. Seipt

Strongly interacting matter (quarks and gluons) dominates the energy density e, pressure p and entropy density s in the early universe all the way from electro-weak transition at temperature $T \sim 100$ GeV down to confinement at $T \sim 170$ MeV. This is evidenced in Fig. 1, where we exhibit the effective numbers of degrees of freedom for energy density, h_{eff} in $e = \frac{\pi^2}{30} h_{eff}(T)\, T^4$, for pressure, f_{eff} in $p = \frac{\pi^2}{90} f_{eff}(T)\, T^4$, and for entropy density, g_{eff} in $s = \frac{2\pi^2}{45} g_{eff}(T)\, T^3$, respectively. The dotted curves depict the electro-weak contributions (photons, leptons, $W^{\pm}$ and Z^0). The total numbers including the contribution of strongly interacting matter are displayed as solid curves (based on our quasi-particle model adjusted to lattice QCD data at low temperatures; the drop at 170 MeV is due to confinement, where quarks and gluons are converted into hadrons). Below confinement, clearly the electro-weak matter dominates for a long period. The dashed curves are for an ideal gas approximation not containing any interaction effects. Of course, it can not account for the strong correlations build up at confinement and reducing strongly the effective degrees of freedom. Remarkable is the failure of the naive standard perturbation theory below 1 GeV (not shown).

In searching for weakly interacting massive relic particles (WIMPs) one can estimate their cosmic abundance from the freeze-out at about $T \sim m_X/25$. Thus, the freeze-out temperature is in the range from 400 MeV till 40 GeV assuming masses m_X in the range 10 - 1000 GeV. It turns out that the exact relic densities for dark matter candidates (say, sterile neutrinos etc.) depend on two essential functions, $g_{eff}(T)$ and

$$g_*^{1/2}(T) = \frac{h_{eff}}{\sqrt{g_{eff}}} \left(1 + \frac{T}{3} \frac{d \log h_{eff}}{d T} \right). \qquad (1)$$

As pointed out in [1] an uncertainty of 10 % in the strong interaction component for pressure translates into an uncertainty up to 1 % in the corresponding relic densities. WMAP measurements have determined the matter density (including the hitherto unknown dark matter) to an accuracy of better than 10 %. The Planck mission will improve the determination better than 1 % (cf. [1] for references). In this respect the precise determination of the effective degrees of freedom in the early universe in the above quoted temperature range is tempting, in particular for the strong interaction sector. The future direct detection experiments at LHC will further constrain the particle zoo beyond the present standard model of particle physics.

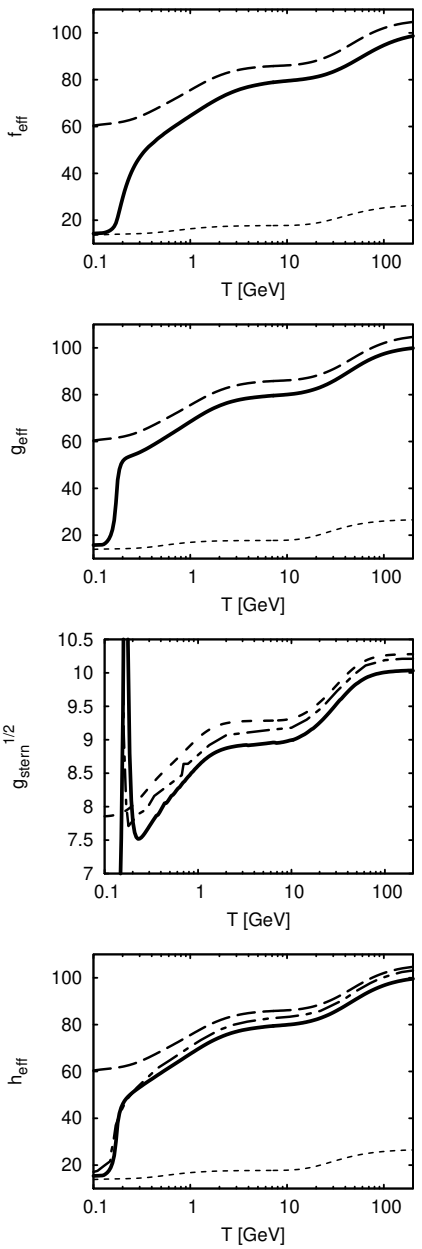

Fig. 1 *The dependence of various parameters quantifying the number of degrees of freedom in the early universe. Solid curves: electro-weakly + strongly interacting matter (the latter one calculated within our quasi-particle model [2]), dotted curves: only electro-weak particles, dashed curves: neglecting any interaction effects. The dot-dashed curves reproduce the assessment in [1].*

[1] M. Hindmarsh, O. Philipsen, Phys. Rev. D 71 (2005) 087302

[2] M. Bluhm, B. Kämpfer, G. Soff, Phys. Lett. B 620 (2005) 131

Anti-Matter in Big Bang and Little Bang [B,E]

H. Schade, B. Kämpfer

Part of PhD thesis H. Schade

The Boltzmann equations for nucleons and anti-nucleons integrated over momentum read

$$\frac{dY_+}{dx} = -\frac{\Lambda}{x^\xi}\left(Y_+(Y_+ - \eta) - Y_{eq}^2\right), \quad (1)$$

$$\frac{dY_-}{dx} = -\frac{\Lambda}{x^\xi}\left(Y_-(Y_- - \eta) - Y_{eq}^2\right), \quad (2)$$

where $Y_\pm = n_\pm/s$ are the baryon densities $n_\pm$ normalized to entropy density $s = \frac{2\pi^2}{45} h_{eff}(T) T^3$. We attribute Y_+, n_+ to baryons (protons) and Y_+-, n_- to anti-baryons (anti-protons). $h_{eff}(T)$ is the effective number of all degrees of freedom in the fireball with comoving volume $V(t)$. We apply the Boltzmann approximation, as for the following $x \equiv m_N/T$ is larger than unity. Therefore, $Y_{eq} = \frac{45}{4\pi^4}\frac{2}{h_{eff}} x^2 K_2(x)$.

In Little Bang, $\Lambda = 3\langle\sigma v\rangle \tau m_N^3 \frac{2\pi^2}{45} h_{eff}$ encodes the thermally averaged annihilation cross section $\langle\sigma v\rangle$. In Big Bang, $\Lambda = \langle\sigma v\rangle\, g_{eff}^{1/2}\, M_{Pl}\, m_N\, (\pi/45)^{1/2}$ holds with g_{eff} determining the effective degrees of freedom relevant for the energy density and M_{Pl} as Planck mass and m_N as nucleon mass.

In deriving eqs. (1, 2) we use adiabaticity of the expanding fireball, i.e. $sV = const$. Both evolution equations are related by baryon conservation, $Y_+ - Y_- = \eta = const$, i.e. $\dot{Y}_+ = \dot{Y}_-$. For the Little Bang in heavy-ion collisions we utilize $V/\dot{V} = \tau$ with τ as characteristic time scale. This allows us to formulate the evolution as a function of x instead as a function of time t. In Big Bang the expansion of the comoving volume is governed by Friedmann's equations. Tab. 1 evidences the huge differences of Little Bang and Big Bang dynamics.

Tab. 1 *Orders of magnitude of the parameter Λ and initial conditions for η, and the power ξ as well.*

	Λ	η	ξ
Little Bang	10^3	10^{-1}	4
Big Bang	10^{21}	10^{-9}	2

The generic features of the Ricatti like eqs. (1, 2) are: For large values of Λ, $Y_\pm$ are dragged by $Y_\pm^{eq}$ for a long time, while for small values of Λ, $Y_\pm$ depart rapidly from $Y_\pm^{eq}$ even when starting at equilibrium, as supposed in the thermo-statistical interpretation of hadron abundances in relativistic heavy-ion collisions, see [1] and Fig. 1. This off-equilibrium evolution causes the ratio of anti-protons to protons to stay roughly constant from chemical freeze-out till kinetic freeze-out. In such way the "anti-proton puzzle" [2] is solved.

In contrast, in the Big Bang the small value of η, represented by the small value of the ration of baryons to photons, causes Y_+ to be frozen in at 45 MeV (Fig. 2), while the anti-baryons are annihilated for long time span yielding at freeze-out an exceedingly small fraction. In particular, the anti-baryon fraction in this homogeneous scenario is so small that the standard primordial nucleosynthesis is not influenced.

While the evolution of $n_\pm$ can be described by such kinetic equations, the origin of the initial conditions remains to be addressed separately and represents a mystery in both Little Bang and Big Bang.

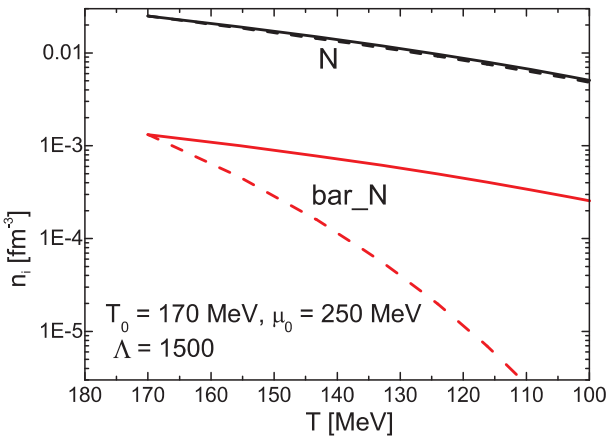

Fig. 1 *The proton density ("N") and anti-proton density ("bar-N") as a function of temperature. Initial conditions for CERN-SPS. Solid curves: actual densities $n_\pm$ for the off-equilibrium evolution, dashed curves: equilibrium densities $n_\pm^{eq}$.*

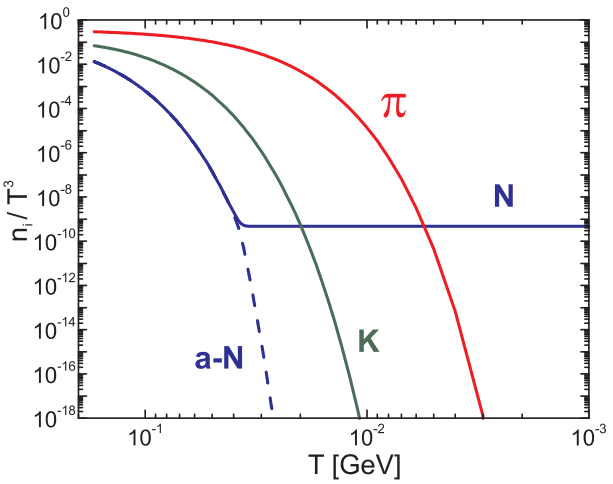

Fig. 2 *Evolution of densities of nucleons (N), anti-nucleons (a-N), pions (π) and kaons (K) as a function of temperature in Big Bang. From [3].*

[1] J. Cleymans, B. Kämpfer, M. Kaneta, S. Wheaton, N. Xu, Phys. Rev. C 71 (2005) 054901

[2] R. Rapp, E.V. Shuryak, Phys. Rev. Lett. 86 (2001) 2980

[3] B. Kämpfer, M. Bluhm, J. Phys. G 31 (2005) S1141

Dielectron Production in ^{12}C+^{12}C Collisions at 2 AGeV with HADES [B,G]

G. Agakichiev, C. Agodi, H. Alvarez-Pol, A. Bałanda, D. Bertini, J. Bielcik, G. Bellia, M. Böhmer, H. Bokemeyer, J.L. Boyard, P. Braun-Munzinger, P. Cabanelas, S. Chernenko, T. Christ, R. Coniglione, L. Cosentino, J. Díaz, **F. Dohrmann**, I. Durán, T. Eberl, **W. Enghardt**, L. Fabbietti, O. Fateev, C. Fernandez, P. Finocchiaro, J. Friese, I. Fröhlich, B. Fuentes, C. Garabatos, J. A. Garzón, R. Gernhäuser, M. Golubeva, D. González-Díaz, **E. Grosse**, F. Guber, T. Hennino, S. Hlavac, R. Holzmann, J. Homolka, A. Ierusalimov, I. Iori, A. Ivashkin, M. Jaskuła, M. Jurkovic, M. Kagarlis, M. Kajetanowicz, **B. Kämpfer**, **K. Kanaki**, T. Karavicheva, A. Kastenmüller, L. Kidoń, P. Kienle, I. Koenig, W. Koenig, H. J. Körner, B. W. Kolb, **R. Kotte**, R. Krücken, A. Kugler, W. Kühn, R. Kulessa, A. Kurepin, S. Lang, S. Lange, J. Lehnert, E. Lins, D. Magestro, C. Maiolino, A. Malarz, J. Markert, V. Metag, J. Mousa, M. Münch, C. Müntz, **L. Naumann**, A. Nekhaev, J. Novotny, J. Otwinowski, Y. C. Pachmayer, V. Pechenov, T. Pérez, P. Piattelli, J. Pietraszko, R. Pleskac, M. Płoskoń, V. Pospísil, W. Prokopowicz, W. Przygoda, B. Ramstein, A. Reshetin, J. Ritman, M. Roy-Stephan, A. Rustamov, **A. Sadovsky**, B. Sailer, P. Salabura, M. Sánchez, P. Sapienza, A. Schmah, H. Schön, W. Schön, C. Schröder, E. Schwab, R. S. Simon, V. Smolyankin, L. Smykov, S. Spataro, B. Spruck, H. Ströbele, J. Stroth, C. Sturm, M. Sudoł, M. Suk, A. Taranenko, P. Tlusty, A. Toia, M. Traxler, H. Tsertos, D. Vassiliev, A. Vázquez, V. Wagner, W. Waluś, M. Wiśniowski, T. Wójcik, **J. Wüstenfeld**, Y. Zanevsky, K. Zeitelhack, D. Zovinec and P. Zumbruch (HADES collaboration)

Published in Phys. Rev. Lett. 98 (2007) 052302, 1-5

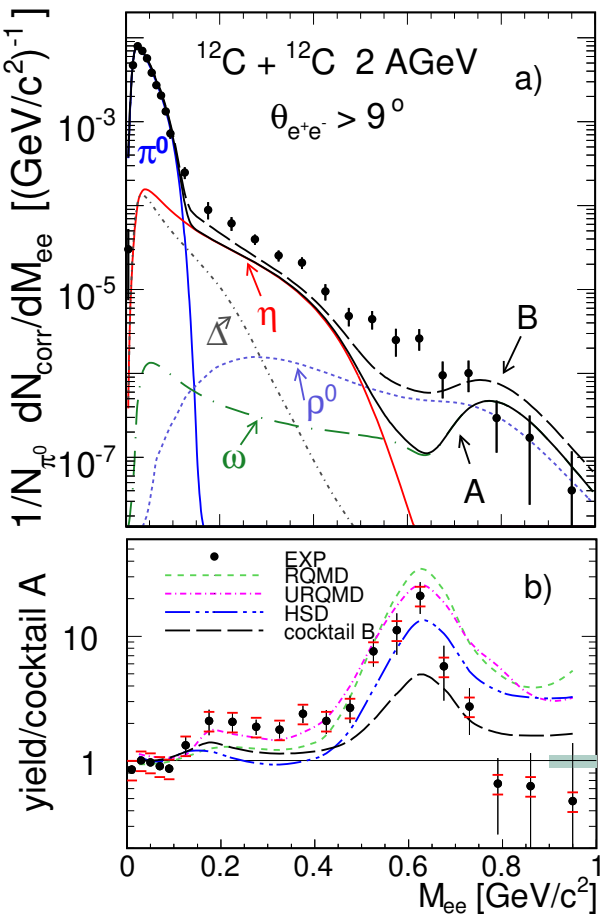

(a) Efficiency- and background-corrected e^+e^- invariant-mass distribution for $\theta_{e+e-} > 9^o$ (symbols) compared to a thermal dielectron cocktail of free π^0, η and ω decays (cocktail A, solid line), as well as including ρ and Δ resonance decays (cocktail B, long-dashed line). Only statistical errors are shown. (b) Ratio of data and cocktail A (dots), compared to ratios of various model calculations and cocktail A. All calculations have been filtered and folded with the HADES [1-4] acceptance and mass resolution. Statistical and systematic errors of the measurement are shown as vertical and horizontal lines, respectively. The overall normalization error of 11% is depicted by the shaded area.

The invariant-mass spectrum of e^+e^- pairs produced in ^{12}C+^{12}C collisions at an incident energy of 2 GeV per nucleon has been measured for the first time. The measured pair production probabilities span over five orders of magnitude from the π^0-Dalitz to the ρ/ω invariant-mass region. Dalitz decays of π^0 and η account for all the yield up to 0.15 GeV/c^2, but for only about 50% above this mass. A comparison with model calculations shows that the excess pair yield is likely due to baryon-resonance and vector-meson decays. Transport calculations based on vacuum spectral functions fail, however, to describe the entire mass region.

[1] R. Schicker et al., Nucl. Instr. Meth. A 380 (1996) 586
[2] J. Friese et al. (HADES collaboration), Prog. Part. Nucl. Phys. 42 (1999) 42
[3] H. Bokemeyer et al., Nucl. Instr. Meth. A 477 (2002) 397
[4] P. Salabura et al. (HADES collaboration), Nucl. Phys. A 749 (2005) 150

HADES Experiment: Di-Lepton Spectroscopy in p+p (2.2 GeV) and C + C (1 and 2 A GeV) Collisions [B,G]

W. Przygoda, G. Agakishiev, C. Agodi, H. Alvarez-Pol, A. Balanda, R. Bassini, G. Bellia, D. Belver, J. Bielcik, A. Blanco, M. Boehmer, C. Boiano, A. Bortolotti, J. Boyard, S. Brambilla, P. Braun-Munzinger, P. Cabanelas, S. Chernenko, T. Christ, R. Coniglione, M. Dahlinger, J. Diaz, R. Djeridi, **F. Dohrmann**, I. Duran, T. Eberl, **W. Enghardt**, L. Fabbietti, O. Fateev, P. Finocchiaro, P. Fonte, J. Friese, I. Froehlich, J. Garzon, R. Gernhaeuser, M. Golubeva, D. Gonzalez-Diaz, **E. Grosse**, F. Guber, T. Heinz, T. Hennino, S. Hlavac, J. Hoffmann, R. Holzmann, A. Ierusalimov, I. Iori, A. Ivashkin, M. Jaskula, M. Jurkovic, M. Kajetanowicz, **B. Kämpfer**, **K. Kanaki**, T. Karavicheva, D. Kirschner, I. Koenig, W. Koenig, B. Kolb, U. Kopf, **R. Kotte**, J. Kotulic-Bunta, R. Kruecken, A. Kugler, W. Kuehn, R. Kulessa, S. Lang, J. Lehnert, L. Maier, P. Maier-Komor, C. Maiolino, J. Marin, J. Markert, V. Metag, N. Montes, E. Moriniere, J. Mousa, M. Muench, C. Müntz, **L. Naumann**, R. Novotny, J. Novotny, W. Ott, J. Otwinowski, Y. Pachmayer, T. Perez, V. Pechenov, J. Pietraszko, J. Pinhao, R. Pleskac, V. Pospisil, A. Pullia, N. Rabin, B. Ramstein, S. Riboldi, J. Ritman, P. Rosier, M. Roy-Stephan, A. Rustamov, **A. Sadovsky**, B. Sailer, P. Salabura, P. Sapienza, A. Schmah, W. Schön, C. Schröder, E. Schwab, P. Senger, R. Simon, V. Smolyankin, L. Smykov, S. Spataro, B. Spruck, H. Ströbele, J. Stroth, C. Sturm, M. Sudol, V. Tiflov, P. Tlusty, A. Toia, M. Traxler, H. Tsertos, I. Turzo, V. Wagner, W. Walus, C. Willmott, S. Winkler, M. Wisniowski, T. Wojcik, **J. Wüstenfeld**, Y. Zanevsky, P. Zumbruch (HADES collaboration)

Published in Acta Phys. Pol. B 37 (2006) 139-151

The HADES (High Acceptance Di-Electron Spectrometer) is a tool designed for lepton pair (e^+e^-) spectroscopy in pion, proton and heavy ion induced reactions in the 1–2 A GeV energy range. One of the goals of the HADES experiment is to study in-medium modifications of hadron properties like effective masses, decay widths, electromagnetic form factors etc. Such effects can be probed with vector mesons (ρ, ω, ϕ) decaying into e^+e^- channel. The identification of vector mesons by means of a HADES spectrometer is based on invariant mass reconstruction of e+e- pairs. The combined information from all spectrometer subdetectors is used to reconstruct the di-lepton signal. The recent results from 2.2 GeV p+p, 1 A GeV and 2 A GeV C + C experiments are presented.

[1] J. Friese et al. (HADES collaboration), Prog. Part. Nucl. Phys. 42 (1999) 42

[2] H. Bokemeyer et al., Nucl. Instr. Meth. A 477 (2002) 397

[3] P. Salabura et al. (HADES collaboration), Nucl. Phys. A 749 (2005) 150

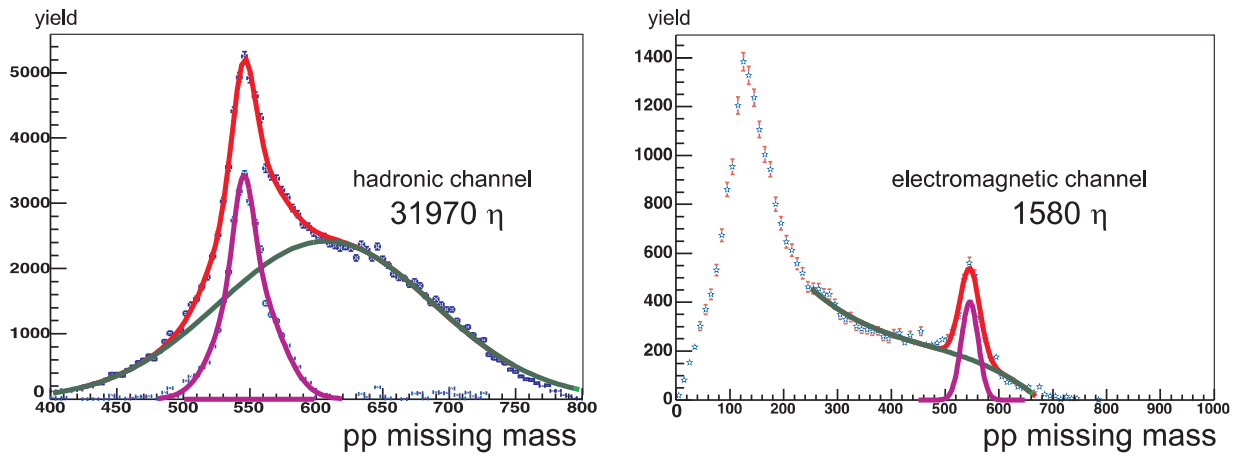

η meson signal retrieved from pp missing mass spectrum for hadronic (left) and electromagnetic (right) channels (no acceptance corrections). For each track the minimization procedure (kinematic fit, varying momentum, polar and azimuthal angles) was performed.

Dielectron Detection Capabilities of HADES for Beam Energies accessible at FAIR [G]

B. Bannier, F. Dohrmann, E. Grosse[1], B. Kämpfer, R. Kotte, L. Naumann, J. Wüstenfeld

Part of diploma thesis B. Bannier

For the FAIR project considerable updates of existing accelerator facilities at the GSI Darmstadt are projected. The available beam energies of the new SIS100 and SIS300 accelerators will be in the range of 2 AGeV to 25 AGeV and above. Experiments with both elementary probes and heavy-ions at beam energies $\leq$ 3.5 AGeV have been performed with the HADES detector at SIS18. The possible dielectron detection capabilities of HADES at the new facilities, focusing on Carbon–Carbon collisions at kinetic beam energies $T = 8 - 25$ AGeV were studied. An event generator based on the state of the art relativistic transport code UrQMDv1.3p1 [1] has been implemented and is available. Based on this event generator dielectron spectra for 8 AGeV and 25 AGeV are shown in Fig. 1 taking into account the geometrical acceptance of the HADES detector as it is currently installed.

For both energies a peak in the ρ, ω mass region is visible, although the background situation at the higher energy deteriorates considerably. The simulations indicate that a determination of the yield of true pairs from particle decays in the $\rho - \omega$ mass region after one week of beam time may be feasible. This study [2] has to be seen in line with other studies [3,4] on this subject.

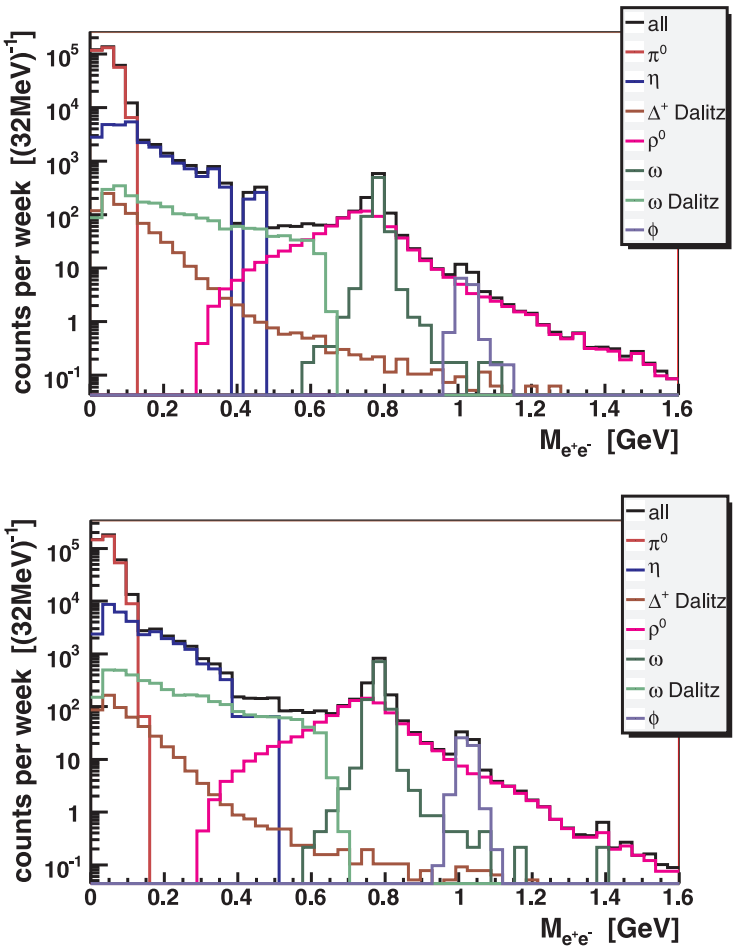

Fig. 1 *Invariant mass spectra for central Carbon-Carbon collisions at beam energies of 8 AGeV (upper panel) and 25 AGeV (lower panel) after one week of beamtime. Pairs are created from all e^+ and e^- emitted into the HADES acceptance with momenta $p >$ 50 MeV. Leptons from pairs with opening angles smaller than 9° are excluded. Particle momenta have been convolved with a momentum dependent error following the procedure given in [5]. For clarity, the simulated combinatorial background was omitted from these figures. Details on how to subtract combinatorial background using the like-sign method are given in [2].*

[1] http://www.th.physik.uni-frankfurt.de/~urqmd
[2] B. Bannier, Diploma Thesis, Technische Universität Dresden, Sep. 2006
[3] T. Galatyuk and J. Stroth, CBM-PHYS-note-2006-001, internal report, GSI Darmstadt 2006
[4] A. Kugler, Talk at CBM meeting, GSI Darmstadt 2004; Proc. Nucl. Phys. Winter meeting, Bormio 2006
[5] R. Holzmann, HAFT: Hades Acceptance Filter for Theorists, internal report, GSI Darmstadt 2006, http://hades-wiki.gsi.de/cgi-bin/view/SimAna/HadesAcceptanceFilter

[1] *also TU Dresden*

Validation of HADES-MDC Data [B,G]

P. Zhou, F. Dohrmann, B. Kämpfer, K. Kanaki, R. Kotte, L. Naumann, A. Sadovsky, J. Wüstenfeld
for the HADES collaboration

Part of PhD thesis P. Zhou

It is the goal of the HADES (High Acceptance Di-Electron Spectrometer) [1] collaboration to study the properties of mesons which are produced in the nuclear medium, in particular light vector mesons ρ, ω and ϕ. In order to investigate the dielectron elementary production mechanisms in pp reactions at an incident beam energy of 1.25 AGeV, the HADES collaboration performed the experiment in April 2006 at GSI.

Before data analysis, valuing the quality of the raw data taken from DAQ (data acquisition), must be done at first. The procedure of "File Validation" is an indispensable first step of data analysis. During data analysis, tracking of particle is the committed step, which have to use the signals taken from MDC (Multi-Wire Drift Chambers). One important part of the "File Validation" is MDC file selection which is presented here step by step.

1. Monitor Rate of HV (high voltage) changes: To protect the detectors the power supply system can automatically control the HV. Once a short-circuit has happened in one of the detectors, it immediately shuts the HV down slowly. This is a so called HV trip. During the HV trip the output signals of the detector are unusable, thus the first step of data analysis is to find out whether any data was taken during that time and then mark out the file which contains the data. Therefore, it is necessary to plot the rate of HV changes as per 10 minutes for each day. An example plot of one day is given in Fig. 1.

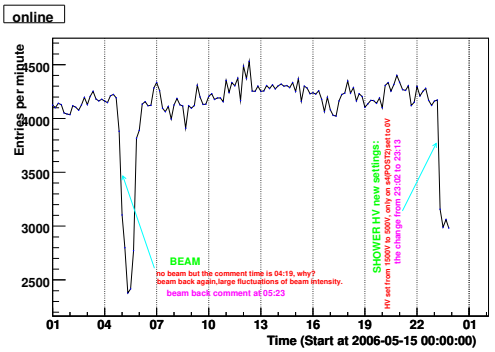

Fig. 1 *An example of the slow control system HV monitor rate of one day.*

2. MDC HV Summary for one HV Channel per Chamber: To find out a good value for the decision of a HV trip in a chamber, the potential of the Field channel 0 was checked for each chamber (see Fig. 2). The important values are the mean, minimum and maximum values of the potential. For this beam time a new safety mechanism was set up in EPICS (Experimental Physics and Industrial Control System, a kind of slow control system), i. e. an automatic ramp up of a tripped channel after some seconds, to limit the amount of downtime. Thus, the mean value is no longer a good value to decide on. Instead, the minimum value was chosen, as it provides a clear signal. If the value goes below 1000 V during the recording time of a file, it is assumed that the chamber tripped.

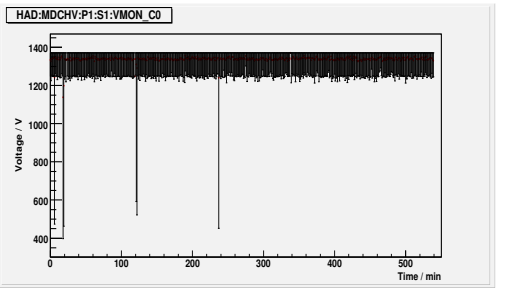

Fig. 2 *An instance of MDC HV summary for one HV channel per chamber.*

3. MDC Files Selection : One has to loop over all files taken from the beam time, checking for each of the HV values for the criteria discussed above. In each file the minimum voltage of all channels is checked and compared against the reference voltage defined in the previous step. If there are two or more trips in one file, it is declared to be unusable (see Fig. 3). Finally, separate lists containing different type of files can be retrieved.

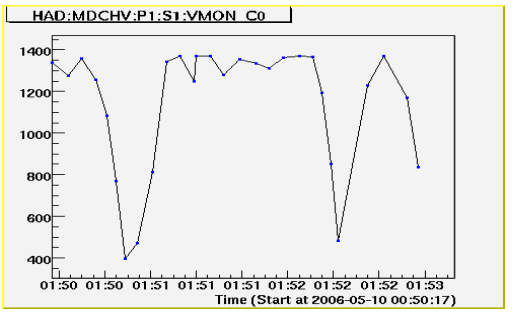

Fig. 3 *A case of HV trips in one file, which is unusable.*

4. MDC Final Validation: The files are validated with these quality factors, according to the following rules. If one of the chambers of plane II to IV had a trip, the file is set unusable. If the trip occurred in plane I, the file is of restricted usability. All other files are fully usable. Three different lists containing the name of the three kind of files separately are formed and put into the HADES database, in order to be used during subsequent step of data analysis.

The introduction of MDC file selection for the Apr06 beam-time of HADES in GSI is complete. For details of this work, please see www-hades.gsi.de.

[1] G. Agakichiev et al., Phys. Rev. Lett. 98 (2007) 052302

Propagation of Broad Meson Resonances in a BUU Type Transport Model: Application to Di-Electron Production [B,E]

H.W. Barz, B. Kämpfer, Gy. Wolf [1], M. Zetenyi[1]

Di-electrons serve as direct probes of dense nuclear matter stages during the course of heavy-ion collisions. The superposition of various sources, however, requires a deconvolution of the spectra by means of models. Of essential interest are the contributions of the light vector mesons ρ and ω. The spectral functions of both mesons are expected to be modified in a strongly interacting environment in accordance with chiral dynamics, QCD sum rules etc. After the first pioneering experiments with the DLS spectrometer now improved measurements with HADES [1] start to explore systematically the baryon-dense region accessible in fixed-target heavy-ion experiments at beam energies in the few AGeV region.

To implement properly the propagation of broad resonances we utilize the kinetic approach of [2] and the spectral function of mesons as a function of the self-energy Σ^{ret}

$$\mathcal{A}(p) = \frac{\hat{\Gamma}(x,p)}{(E^2 - \vec{p}^2 - m_0^2 - Re\Sigma^{ret}(x,p))^2 + \frac{1}{4}\hat{\Gamma}(x,p)^2}, \quad (1)$$

where the resonance widths Γ and $\hat{\Gamma}$ are connected via $\hat{\Gamma}(x,p) = -2Im\Sigma^{ret} \approx 2m_0\Gamma$, and m_0 is the vacuum pole mass of the respective particle. The dynamical evolution of spectral function is accomplished within the test particle method. There, the change of the particle mass m is evidenced in the combined transport equation emerging from the separate time evolution of the particle's three-position, three-momentum and energy [2]

$$\frac{dm^2}{dt} = \frac{1}{1-C}\left(\frac{d}{dt}Re\Sigma^{ret} + \frac{m^2 - m_0^2 - Re\Sigma^{ret}}{\hat{\Gamma}}\frac{d}{dt}\hat{\Gamma}\right) \quad (2)$$

with the comoving derivative $d/dt \equiv \partial_t + \vec{p}/E\vec{\partial}_x$ and renormalization factor C. This equation means that the square of the particle mass tends to reach a value shifted by the real part of the self-energy within a range of the value of $\hat{\Gamma}$. Thus, the vacuum spectral function is recovered when the particle leaves the medium. This ensures the smooth transition from the in-medium behavior to the vacuum properties. In Fig. 1 we exhibit the temporal change of the test particle's mass for ρ and ω mesons together with the local density. The spread of the ρ, ω masses is clearly seen as well as the evolution towards the vacuum spectral function in case of long-living ω mesons. The ρ mesons are short-living, thus often rapidly decaying. Fig. 2 exhibits the resulting di-electron spectra from direct ρ and ω decays.

A first comparison with HADES data is published in [3].

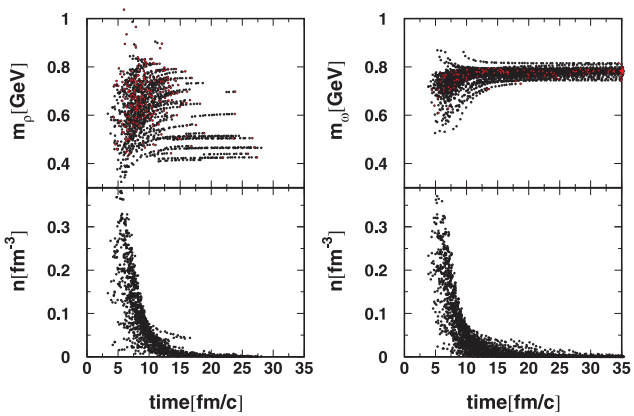

Fig. 1 *Temporal change of selected test particle masses for ρ (left top panel) and ω (right top panel) mesons. The bottom row exhibits the local density of baryon matter surrounding the respective test particle. For the reaction C(2 AGeV) + C. Open circles indicate instances of pion decay.*

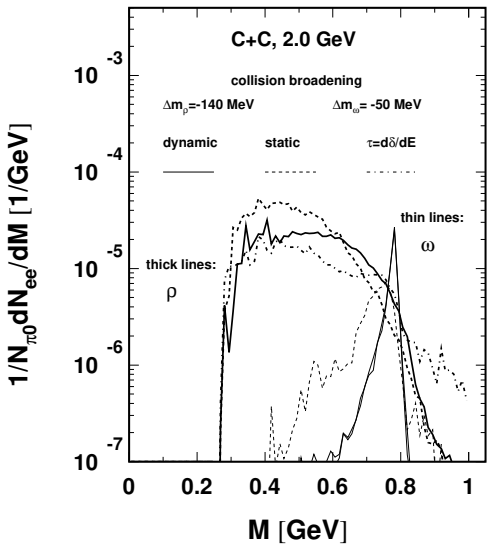

Fig. 2 *Contributions to di-electron spectra from ρ and ω decays calculated with the effect of the mass evolution (solid lines ("dynamic"): using the above evolution equations, dot-dashed lines ("$\tau = d\delta/dE$"): employing $\tau^{-1} = b_c\Gamma^{tot} = b_c(d\delta/dE)^{-1}$ as prescription for the life time). For comparison, the dashed curves ("static") neglect the time evolution of the spectral functions.*

[1] H. Agakishev et al. (HADES collaboration), Phys. Rev. Lett. 98 (2007) 052302

[2] W. Cassing and S. Juchem, Nucl. Phys. A 672 (2000) 417

[3] H.W. Barz, B. Kämpfer, Gy. Wolf, M. Zetenyi, nucl-th/0605036 (2006)

[1] *KFKI Budapest,Hungary*

Di-Electron Bremsstrahlung in Intermediate-Energy *Dp* Collisions [B,E]

L.P. Kaptari [1], **B. Kämpfer**

Published in Nucl. Phys. A 764 (2006) 338-370

Invariant mass spectra of di-electrons stemming from bremsstrahlung processes are calculated in a covariant diagrammatical approach for the exclusive reaction $Dp \to p_{\rm sp}\, np\, e^+e^-$ with detection of a forward spectator proton, $p_{\rm sp}$. We employ an effective nucleon-meson theory for parameterizing the sub-reaction $np \to npe^+e^-$ and, within the Bethe-Salpeter formalism, derive a factorization of the cross section in the form $d\sigma_{Dp\to p_{\rm sp}\, np\, e^+e^-}/dM = d\sigma_{np\to np\, e^+e^-}/dM \times$ kinematical factor related solely to the deuteron (M is the e^+e^- invariant mass). The effective nucleon-meson interactions, including the exchange mesons π, σ, ω and ρ as well as excitation and radiative decay of $\Delta(1232)$, have been adjusted to the process $pp \to pp\, e^+e^-$ at energies below the vector meson production threshold. At higher energies, contributions from ω and ρ meson excitations are analyzed in both, NN and Dp collisions. A relation to two-step models is discussed. Subthreshold di-electron production in Dp collisions at low spectator momenta is investigated as well. Calculations have been performed for kinematical conditions envisaged for forthcoming experiments at HADES.

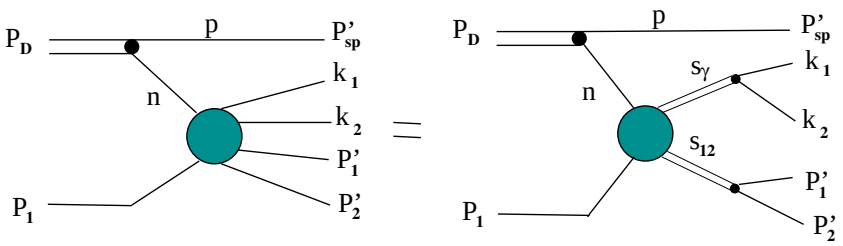

Fig. 1 *Kinematics of the process* $D(P_D) + p(P_1) \to p(P_{\rm sp} + p(P_1') + n(P_2') + e^+(k_1) + e^-(k_2)$ *within the spectator mechanism.*

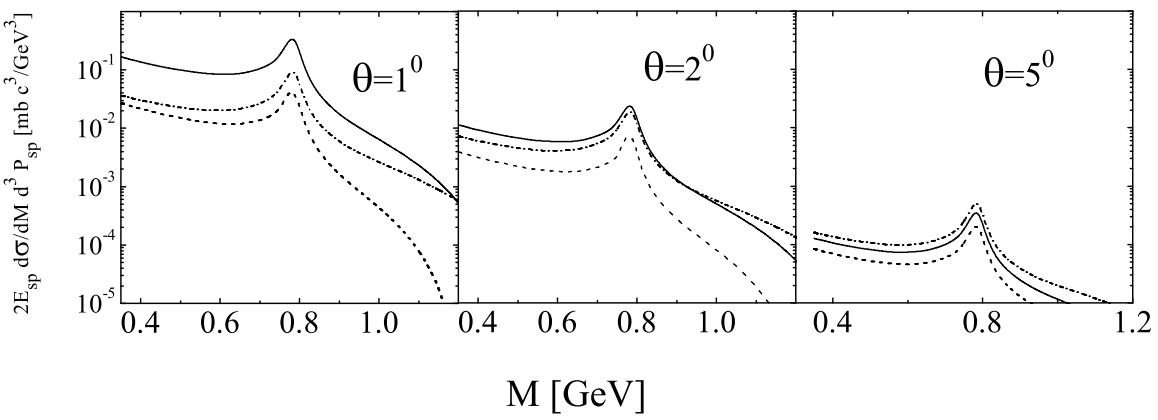

Fig. 2 *Invariant mass distribution* $2E_{\rm sp}\dfrac{d\sigma}{dMd^3p_{\rm sp}}$ *for the reaction* $Dp \to p_{\rm sp}\ np\ e^+e^-$, *at deuteron beam energy* $T_{kin} = 3.5$ *AGeV and three values of the spectator angle in the laboratory system,* $\theta = 1^\circ, 2^\circ$ *and* 5°. *Dot-dashed, solid and dashed curves correspond to values of the spectator momenta as indicated in the legends. Effects of VMD have been taken into account.*

[1] *JINR Dubna, 141980, Russia*

Di-Electrons from η Meson Dalitz Decay in Proton-Proton Collisions [B,E]

L.P. Kaptari [1], **B. Kämpfer**

Published in nucl-th/0702033, submitted to Eur. Phys. J. A

The reaction $pp \to pp\eta \to pp\gamma e^+e^-$ is discussed within a covariant effective meson-nucleon theory. Our focus is on di-electrons from Dalitz decays of η mesons, $\eta \to \gamma\gamma^* \to \gamma e^+e^-$. Numerical results are presented for the intermediate energy kinematics of envisaged HADES experiments.

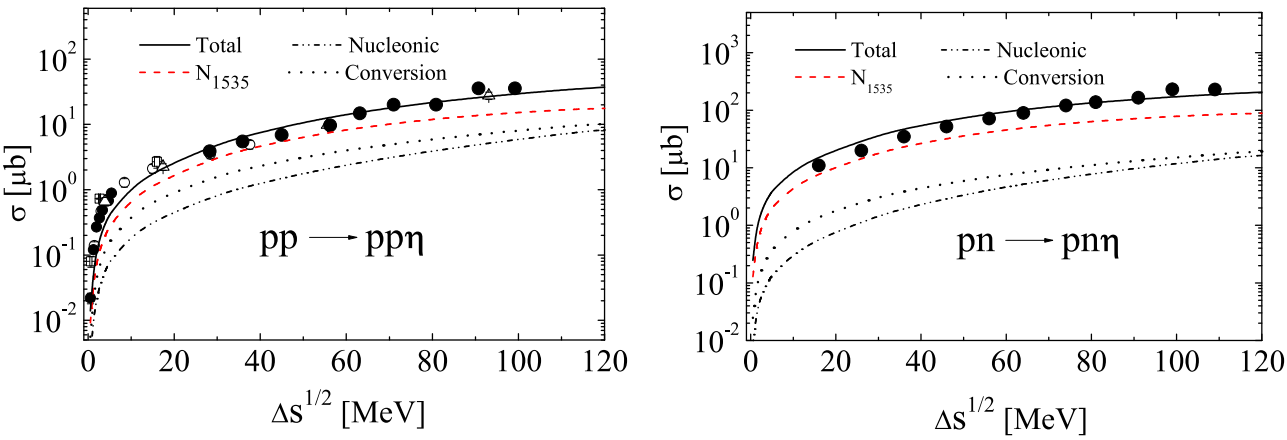

Fig. 1 *Total cross section for the reactions $pp \to pp\eta$ (left panel) and $np \to np\eta$ (right panel) as a function of the excess energy $\Delta s^{1/2} = \sqrt{s} - 2m - m_\eta$. The dot-dashed line corresponds to the nucleon current contribution (without resonances), while the dotted line is for the internal meson conversion diagram. The dashed curve exhibits the contribution of the $S_{11}(1535)$ resonance (nucleon resonance current). Contributions from $P_{11}(1440)$ and $D_{13}(1520)$ are smaller and not displayed. The solid curve is the total contribution with all interferences. References for data are quoted in the full article of this contribution; error bars are suppressed.*

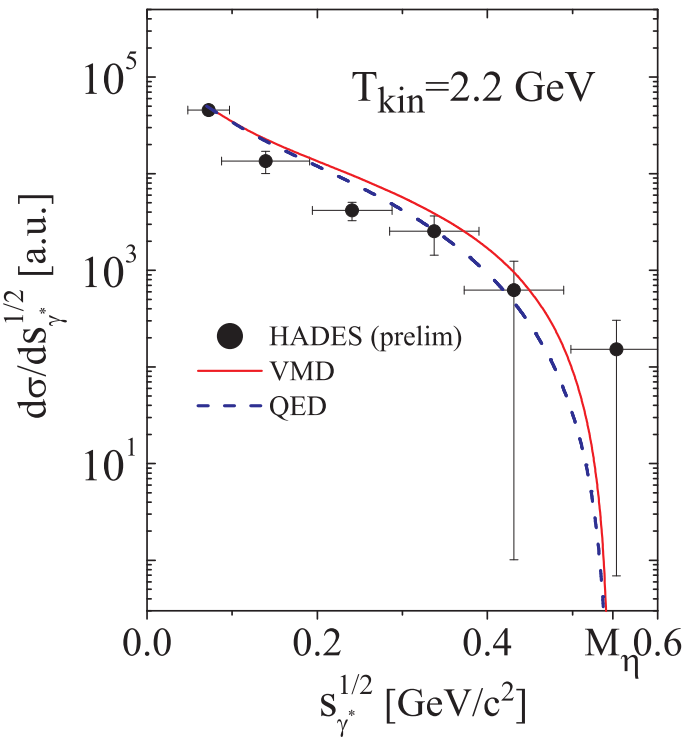

Fig. 2 *Invariant mass distribution of di-electrons produced by Dalitz decay of η mesons in the reaction $pp \to pp\gamma e^+e^-$ at initial kinetic energy $T_{kin} = 2.2\,GeV$. The solid line is for results with the $\eta\gamma\gamma^*$ transition form factor computed within the VMD model, while the dashed line corresponds to a purely QED calculation of the $\eta\gamma\gamma^*$ vertex, i.e., for $|F_{\eta\gamma\gamma^*}|^2 = 1$. The η pole mass position is exposed. Preliminary experimental data are from [1].*

[1] I. Fröhlich et al. (HADES), nucl-ex/0610048

[1] *JINR Dubna, 141980, Russia*

$\omega - \pi\gamma^*$ Transition Form Factor in Proton-Proton Collisions [B,E]

L.P. Kaptari [1], **B. Kämpfer**

Published in Eur. Phys. J. A 31 (2007) 233-243

Dalitz decays of ω and ρ mesons, $\omega \to \pi^0\gamma^* \to \pi^0 e^+e^-$ and $\rho^0 \to \pi^0\gamma^* \to \pi^0 e^+e^-$, produced in pp collisions are calculated within a covariant effective meson-nucleon theory. We argue that the ω transition form factor $F_{\omega\to\pi^0\gamma^*}$ is experimentally accessible in a fairly model independent way in the reaction $pp \to pp\pi^0 e^+e^-$ for invariant masses of the $\pi^0 e^+e^-$ subsystem near the ω pole. Numerical results are presented for the intermediate energy kinematics of envisaged HADES experiments.

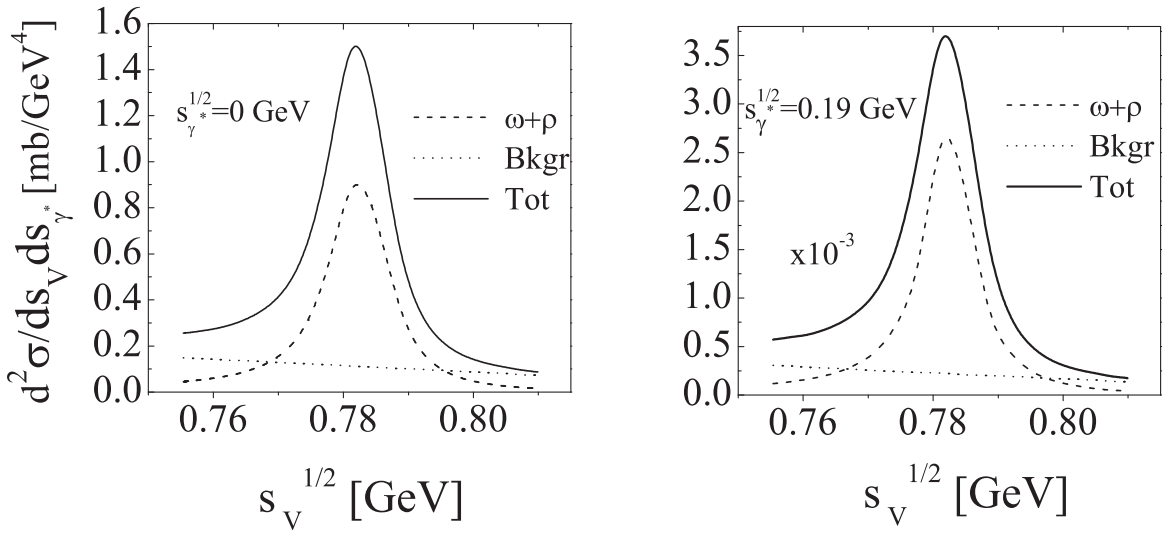

Fig. 1 *The double differential cross section $d\sigma/ds_V ds_{\gamma^*}$ as a function of $s_V^{1/2}$ in the vicinity of the ω pole for $T_{beam} = 2.2\,GeV$ with background contribution taken into account. The relative sign between the resonant and background amplitudes is chosen positively resulting in a constructive interference. The dashed line corresponds to the resonant contributions of diagrams with ω and ρ Dalitz decays, the dotted line corresponds to the background contribution alone, and the solid line is the resulting total cross section. The employed transition form factor is for the VMD model. Left (right) panel is for $\sqrt{s_{\gamma*}} = 2m_e \to 0$ (0.19) GeV.*

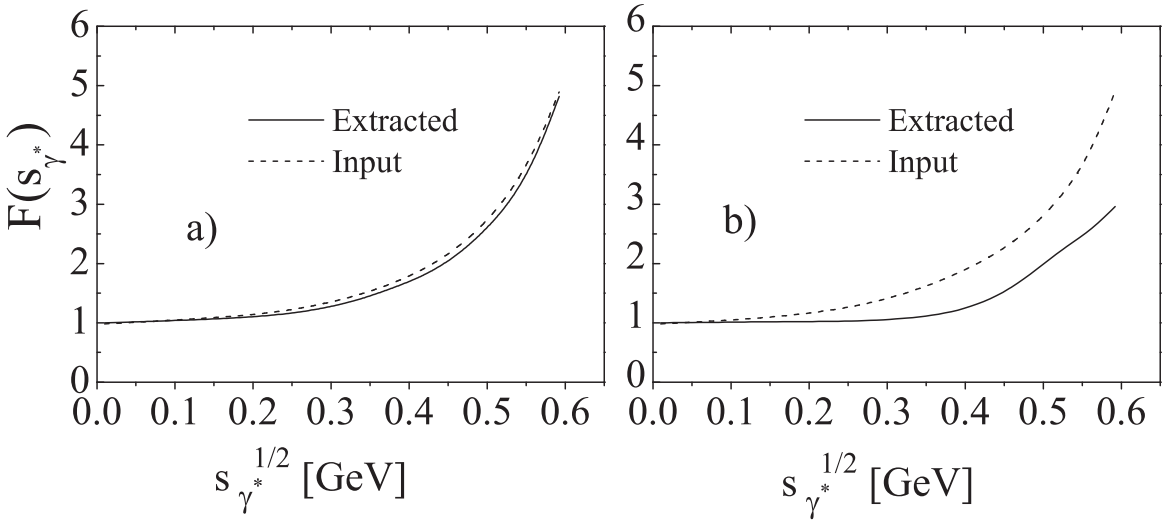

Fig. 2 *The extracted form factor (solid curves) calculated at $T_{beam} = 2.2\,GeV$ with inclusion of the background contribution. Dashed lines correspond to the input FF taken from the VMD model. The averaging has been performed in the ±3.5 % vicinity of the ω pole mass. Panels a) and b) correspond to destructive and constructive interference effects, respectively.*

[1] *JINR Dubna, 141980, Russia*

K^+ and Λ Production in C + C Collisions at 2 AGeV with HADES [B,G]

K. Kanaki, A. Sadovsky, F. Dohrmann, E. Grosse[1], B. Kämpfer, R. Kotte, L. Naumann, J. Wüstenfeld
and the HADES collaboration

Part of the PhD theses K. Kanaki and A. Sadovsky

An analysis of associated strangeness production in Carbon Carbon collisions at 2 AGeV has been performed. The data were taken with the HADES detector. In particular, multiplicities of Λ hyperons [1] and K^+ mesons [2] were determined and new valuable information on strangeness balance, complementary to existing data was gained. Here we present double-differential yields $d^2\sigma/dm_t dy_0$ normalized by $1/m_t^2$, where $m_t = \sqrt{m_0^2 + p_t^2}$ is the transverse mass, p_t is the transverse momentum and m_0 is the kaon rest mass. The statistics collected allowed for evaluating the data in six bins of normalized rapidity $y_0 = (y/y_{\rm cm} - 1)$, where $y = \tanh^{-1}(\beta_z)$ is the Lorentz-invariant longitudinal velocity. This differential information was not available before. Comparisons with results obtained previously by the KaoS collaboration [3] showed consistency within errors for both, inverse slope parameter as well as total cross section (see [2] for details).

Λ hyperons were identified via their charged decay $\Lambda \to p\pi^-$. The multiplicity per event for Λ production in C + C collisions at 2 AGeV was determined to be $\mathcal{M}_{\Lambda+\Sigma^0} = 0.0092 \pm 0.0012(\text{stat.})^{+0.0034}_{-0.0017}(\text{syst.})$. This number includes Λ from Σ^0 decay ($\Sigma^0 \to \Lambda\gamma$, BR $\simeq 100\%$), which experimentally cannot be distinguished from the primary ones with HADES.

[1] K. Kanaki, Ph.D. thesis, TU Dresden (2006)
[2] A. Sadovsky, Ph.D. thesis, TU Dresden (2006)
[3] F. Laue, C. Sturm et al. Phys. Rev. Lett. 82 (1999) 1640; F. Laue, I. Boettcher et al., Eur. Phys. J. A 9 (2000) 397

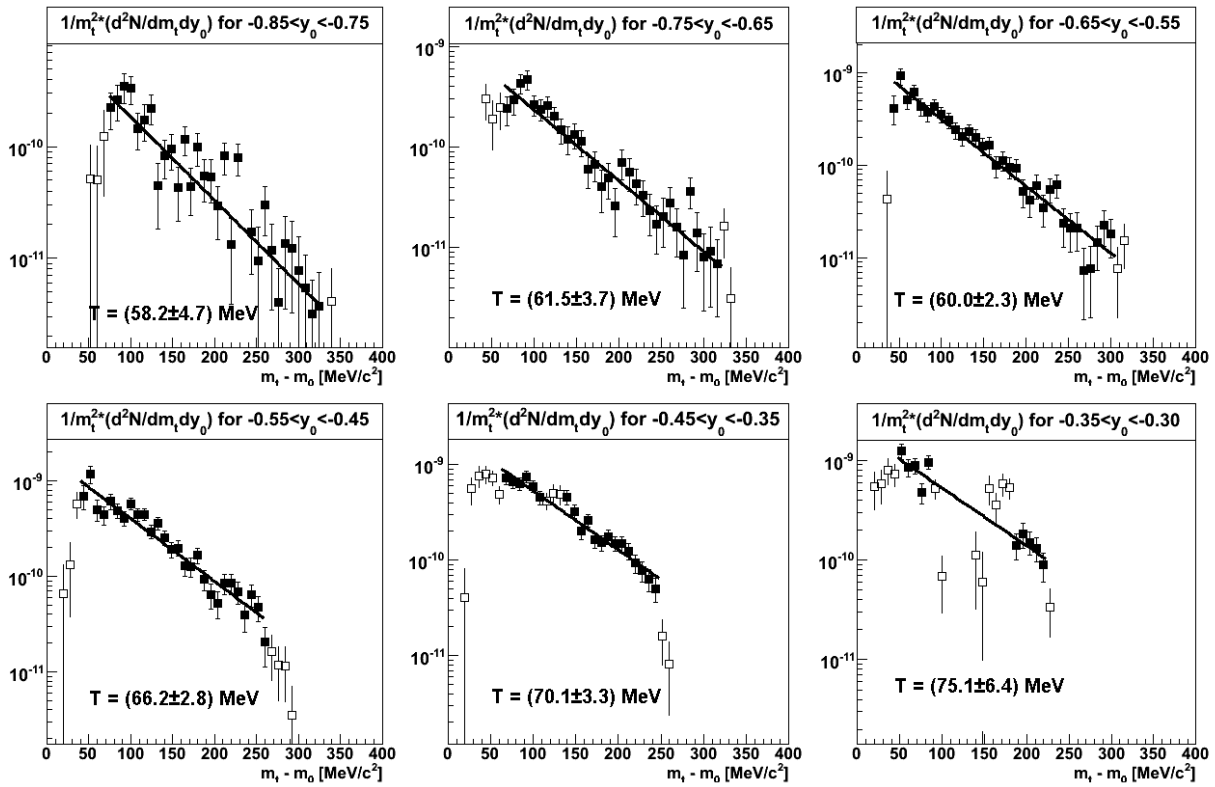

Fig. 1 $\frac{1}{m_t^2} \cdot \frac{d^2\sigma}{dm_t dy_0}$ *distributions of* K^+ *mesons for different rapidity regions. The units for vertical axis are* $b\,[MeV/c^2]^{-3}$. *The data (symbols) are fitted assuming a thermally equilibrated source given by a Maxwell-Boltzmann like distribution with a normalization factor* $A(y_0)$ *and an apparent temperature* T_B

$$\frac{1}{m_t^2} \cdot \frac{d^2\sigma}{dm_t dy_0} = A(y_0) \cdot \exp\Big(-\frac{m_t - m_0}{T_B}\Big).$$

Both parameters, $A(y_0)$ *and* T_B, *are determined by the fits for each of the six intervals in* y_0. *The selected* m_t *regions (filled symbols) used for the fits (solid lines) correspond to the limits given by the phase space accessible with HADES during this experiment. Empty symbols denote data excluded from the fits (see ref. [2] for details).*

[1] *also TU Dresden*

In-Medium Effects on Phase Space Distributions of Antikaons Measured in Proton-Nucleus Collisions [B]

W. Scheinast, F. Dohrmann, E. Grosse[1], L. Naumann, H.W. Barz, B. Kämpfer and the KaoS Collaboration

Published in Phys. Rev. Lett. 96 (2006) 072301, 1-4

Differential production cross sections of $K^{\pm}$ mesons have been measured in p + C and p + Au collisions at 1.6, 2.5 and 3.5 GeV proton beam energy. At beam energies close to the production threshold, the K^- multiplicity is strongly enhanced with respect to proton-proton collisions. According to microscopic transport calculations, this enhancement is caused by two effects: the strangeness exchange reaction $NY \rightarrow K^-NNN$ and an attractive in-medium K^-N potential at saturation density.

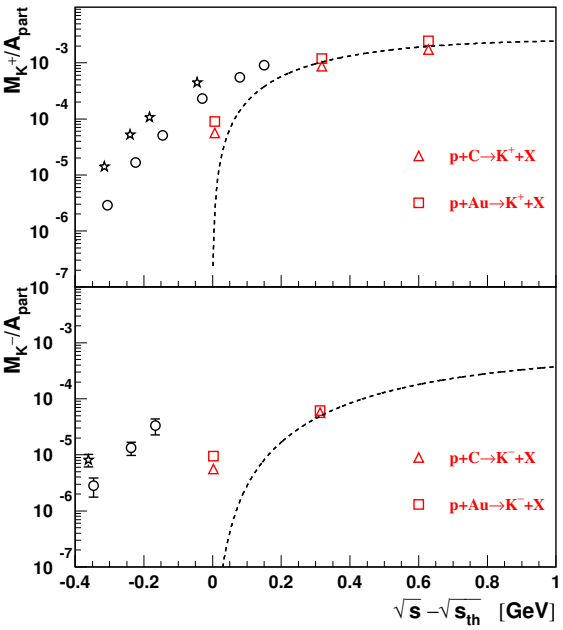

Fig. 1 *Multiplicity normalized by the number of participants as a function of the number of participants for K^+ (upper panel) and K^- (lower panel) for inclusive pAu (open squares) and pC (open triangles) collision as function of the excess energy.*

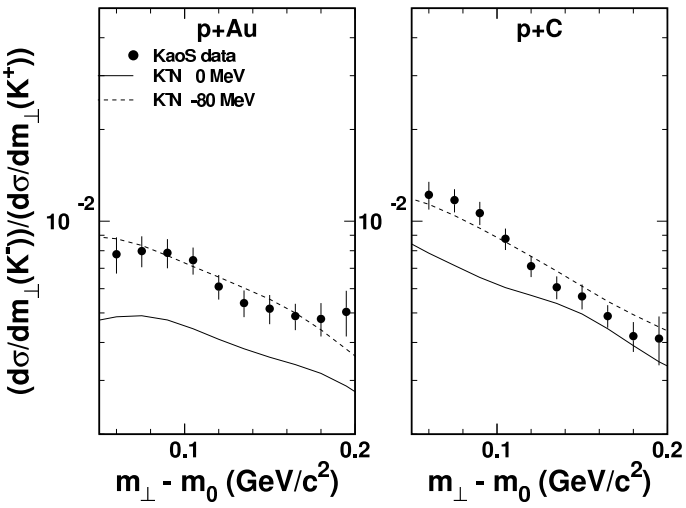

Fig. 2 *Average normalized densities at which $K^{\pm}$ are observed, inferred from BUU calculations for pAu and $AuAu$ collisions.*

[1] *also TU Dresden*

Production of K^+ and of K^- Mesons in Heavy-Ion Collisions from 0.6 to 2.0 A GeV Incident Energy [B]

A. Förster, F. Uhlig, I. Böttcher, D. Brill, M. Dębowski, **F. Dohrmann**, **E. Grosse**[1], P. Koczoń, B. Kohlmeyer, S. Lang, F. Laue, M. Mang, M. Menzel, C. Müntz, **L. Naumann**, H. Oeschler, M. Płoskoń, **W. Scheinast**, A. Schmah, T. J. Schuck, E. Schwab, P. Senger, Y. Shin, J. Speer[†], H. Ströbele, C. Sturm, G. Surówka, A. Wagner, W. Waluś (KaoS Collaboration)

Published in Phys. Rev. C 75 (2007) 024906, 1-19

This paper summarizes the yields and the emission patterns of K^+ and of K^- mesons measured in inclusive C+C, Ni+Ni and Au+Au collisions at incident energies from 0.6 A GeV to 2.0 A GeV using the Kaon Spectrometer KaoS at GSI. For Ni+Ni collisions at 1.5 and at 1.93 A GeV as well as for Au+Au at 1.5 A GeV detailed results of the multiplicities, of the inverse slope parameters of the energy distributions and of the anisotropies in the angular emission patterns as a function of the collision centrality are presented. When comparing transport-model calculations to the measured K^+ production yields an agreement is only obtained for a soft nuclear equation of state (compression modulus $K_N \approx 200$ MeV). The production of K^- mesons at energies around 1 to 2 A GeV is dominated by the strangeness-exchange reaction $K^-N \rightleftharpoons \pi Y$ ($Y = \Lambda, \Sigma$) which leads to a coupling between the K^- and the K^+ yields. However, both particle species show distinct differences in their emission patterns suggesting different freeze-out conditions for K^+ and for K^- mesons.

[1] C. Hartnack, H. Oeschler, J. Aichelin, Phys. Rev. Lett. 96 (2006) 012302

[2] C. Fuchs, A. Faessler, E. Zabrodin, Y. M. Zheng, Phys. Rev. Lett. 86 (2001) 1974

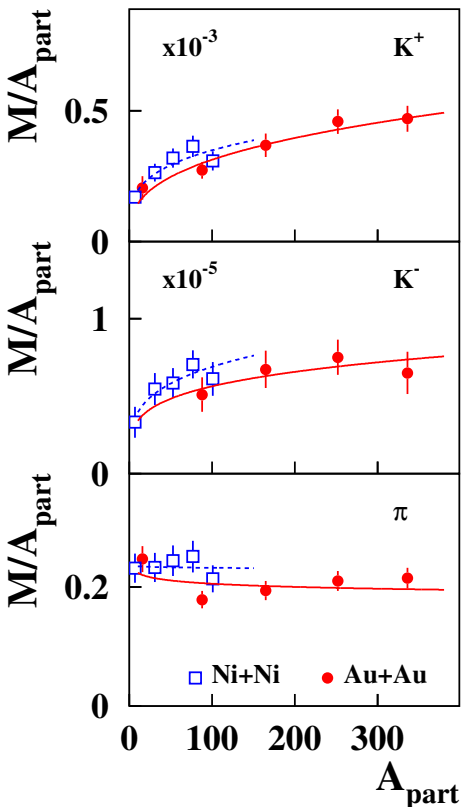

Fig. 1 *Dependence of the multiplicities of K^+ (upper panel) and of K^- mesons (middle panel) as well as of pions (lower panel) on $A_{\rm part}$. Full symbols denote Au+Au, open symbols Ni+Ni, both at 1.5 A GeV. The lines are functions $M \sim A_{\rm part}^{\alpha}$ fitted to the data separately for Au+Au (solid lines) and Ni+Ni (dashed lines). The data have been measured at $\theta_{\rm lab} = 40°$.*

[1] *also TU Dresden* [†] *deceased*

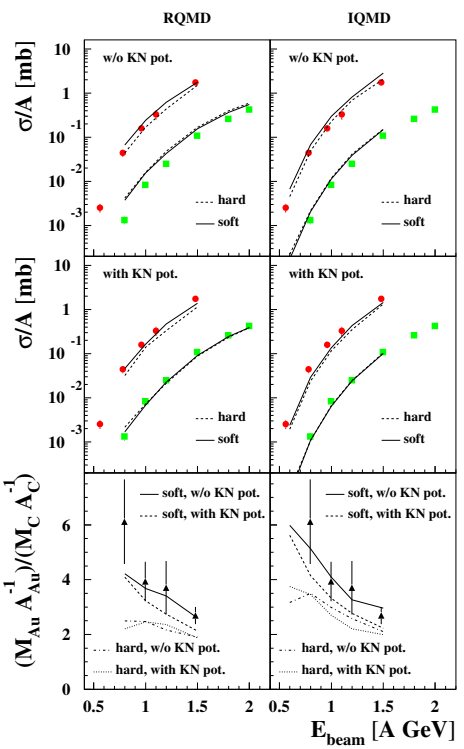

Fig. 2 *Upper and middle panels: Comparison of the K^+ excitation functions ($\sigma(K^+)/A$) for Au+Au (red circles) and for C+C collisions (green squares) with RQMD [2] (left hand side) and with IQMD calculations [1] (right hand side). Solid lines depict a hard EoS, dashed lines depict a soft EoS. The upper panels show calculations without KN potentials, the middle panels calculations with KN potentials. Lower panels: Double ratio of the K^+ multiplicities per mass number M/A in Au+Au divided by the one in C+C and the comparison to the various transport-model calculations.*

Isospin Dependence of Relative Yields of K^+ and K^0 Mesons at 1.528 AGeV [G]

X. Lopez, Y.J. Kim, N. Herrmann, A. Andronic, V. Barret, Z. Basrak, N. Bastid, M.L. Benabderrahmane, R. Caplar, E. Cordier, P. Crochet, P. Dupieux, M. Dzelalija, Z. Fodor, I. Gasparic, Y. Grishkin, O.N. Hartmann, K.D. Hildenbrand, B. Hong, T.I. Kang, J. Kecskemeti, M. Kirejczyk, M. Kis, P. Koczon, M. Korolija, **R. Kotte**, A. Lebedev, Y. Leifels, M. Merschmeyer, **W. Neubert**, D. Pelte, M. Petrovici, F. Rami, W. Reisdorf, M.S. Ryu, A. Schüttauf, Z. Seres, B. Sikora, K.S. Sim, V. Simion, K. Siwek-Wilczynska, V. Smolyankin, G. Stoicea, Z. Tyminski, P. Wagner, K. Wisniewski, **D. Wohlfarth**, Z.G. Xiao, I. Yushmanov, X.Y. Zhang, A. Zhilin (FOPI Collaboration), G. Ferrini, T. Gaintanos

Published in Phys. Rev. C 75 (2007) 011901, 1-5

Results on K^+ and K^0 meson production in $^{96}_{44}$Ru + $^{96}_{44}$Ru and $^{96}_{40}$Zr + $^{96}_{40}$Zr collisions at a beam kinetic energy of 1.528A GeV, measured with the FOPI detector at GSI-Darmstadt, are investigated as a possible probe of isospin effects in high density nuclear matter. The measured double ratio $(K^+/K^0)_{Ru}/(K^+/K^0)_{Zr}$ is compared to the predictions of a thermal model and a Relativistic Mean Field transport model using two different collision scenarios and under different assumptions on the stiffness of the symmetry energy. We find a good agreement with the thermal model prediction and the assumption of a soft symmetry energy for infinite nuclear matter while more realistic transport simulations of the collisions show a similar agreement with the data but also exhibit a reduced sensitivity to the symmetry term.

[1] A. Andronic, P. Braun-Munzinger, J. Stachel, Nucl. Phys. A 772 (2006) 167
[2] T. Gaitanos, Phys. Lett. B 595 (2004) 209
[3] T. Gaitanos, Nucl. Phys. A 732 (2004) 24
[4] G. Ferini, M. Colonna, T. Gaitanos, M. Di Toro, Nucl. Phys. A 762 (2005) 147

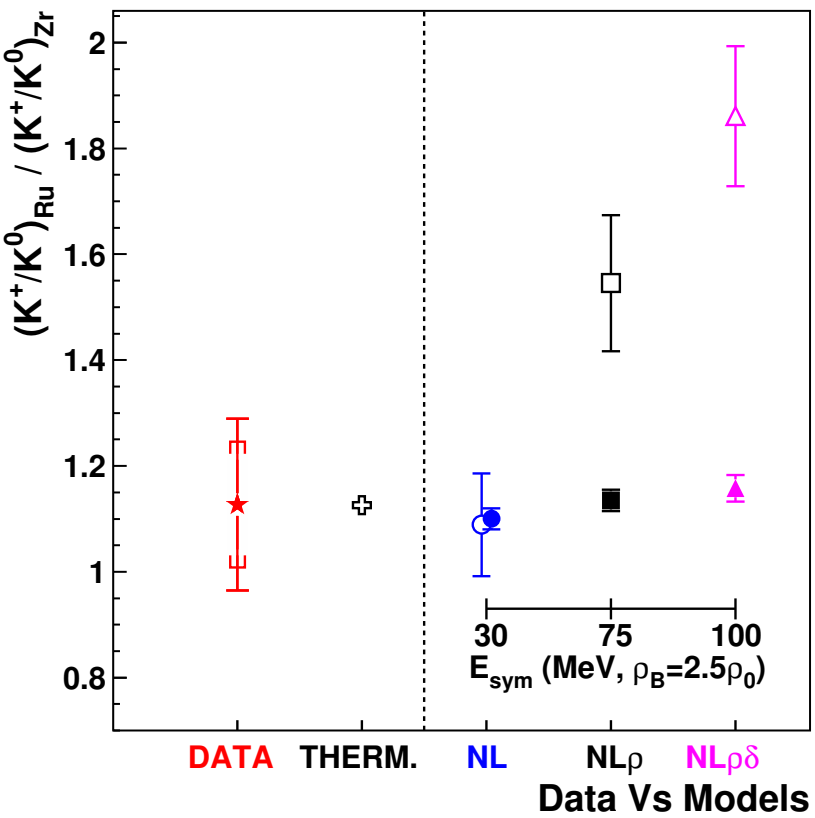

Experimental ratio $(K^+/K^0)_{Ru}/(K^+/K^0)_{Zr}$ (star) and theoretical predictions of the thermal model [1] (cross) and the transport model [2, 3, 4] with 3 different assumptions on the symmetry energy: NL (circles), NLρ (squares) and NL$\rho\delta$ (triangles). The INM and HIC calculations are represented by open and full symbols, respectively. The statistic and systematic errors are represented by vertical bars and brackets, respectively.

Hyperon Production in the Channel $pp \to K^+\Lambda p$ Near the Reaction Threshold [B, J]

S. Abd El-Samad, R. Bilger, A. Böhm, K.-Th. Brinkmann, H. Clement, S. Dshemuchadse, A. Erhardt, W. Eyrich, C. Fanara, A. Filippi, H. Freiesleben, M. Fritsch, R. Geyer, J. Hauffe, A. Hassan, P. Herrmann, D. Hesselbarth, B. Jakob, K. Kilian, H. Koch, J. Kress, E. Kuhlmann, S. Marcello, S. Marwinski, A. Metzger, **P. Michel**, **K. Möller**, H.P. Morsch, **L. Naumann**, E. Roderburg, **A. Schamlott**, P. Schönmeier, M. Schulte-Wissermann, W. Schroeder, M. Steinke, F. Stinzing, G.Y. Sun, J. Wächter, G.J. Wagner, M. Wagner, A. Wilms, S. Wirth, U. Zielinski
(COSY-TOF Collaboration)

Published in Phys. Lett. B 632 (2006) 27-34

Hyperon production in the threshold region was studied in the reaction $pp \to K^+\Lambda p$ using the time-of-flight spectrometer COSY-TOF. Exclusive data, covering the full phase-space, were taken at three different beam momenta p_{beam}= 2.59, 2.68 and 2.85 GeV/c (corresponding to excess energies of ε = 85, 115 and 171 MeV). Total cross-sections were deduced to be $7.4\pm0.5\mu b, 8.6 \pm 0.6\mu b$ and $16.5\pm0.4\mu b$, respectively. Differential observables including Dalitz plots were obtained. From the investigation of the Dalitz plot at p_{beam}=2.85 GeV/c a dominant contribution of the $N^\star(1650)$-resonance to the reaction mechanism was found. In addition the $p\Lambda$-final-state interaction turned out to have a significant influence on the Dalitz plot distribution even 171 MeV above threshold.

[1] J.M. Laget, Phys. Lett. B 259 (1991) 24
[2] A. Sibirtsev et al., nucl-th/0004022
[3] F. Kleefeld, M. Dilling, F. Pilotto, Acta Phys. Pol. B 27 (1996) 2867
[4] R. Shyam, Phys. Rev. C 60 (1999) 055213

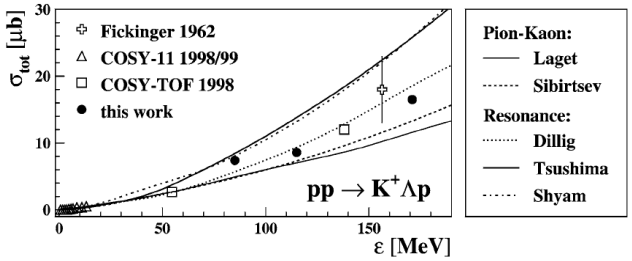

Fig. 1 *Total cross-sections of the channel $pp \to K^+\Lambda p$. All recent data up to $\varepsilon \leq 200MeV$ are shown in comparison with model calculations: pion-kaon exchange model of Laget [1] and Sibirtsev [2], resonance model of Dillig [3], Tsushima as given in [2] and Shyam [4]. The statistical errors are smaller than the size of the symbols. The systematic errors (not shown) are about 10%.*

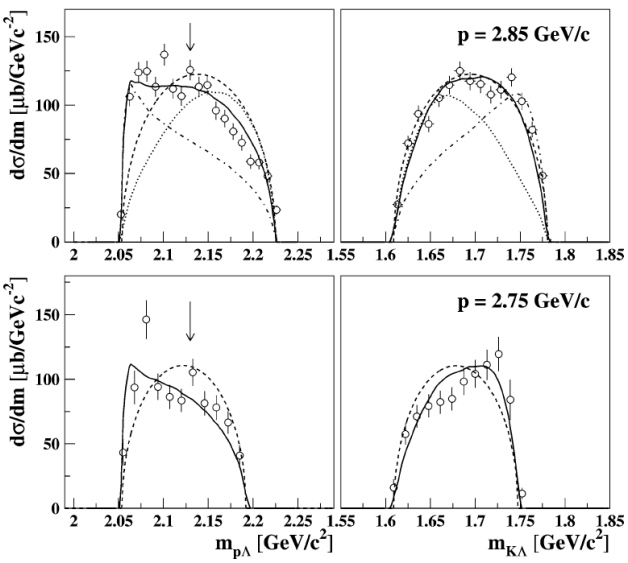

Fig. 2 *Distributions of the invariant mass of the $p\Lambda$- (left) and $K\Lambda$-subsystem (right) at $p_{beam} = 2.85GeV/c$ (top) and 2.75 GeV/c (bottom) in comparison with the model of Sibirtsev (solid line) and pure phase space (dashed line). For the data at $p_{beam} = 2.85GeV/c$ in addition the contributions from the individual components are shown: only resonances (dotted line) and only $p\Lambda$-final-state interaction (dashed-dotted line). Arrows indicate the $p\Sigma^0$-threshold.*

Hunting ϕ Mesons in C + C Collisions at 2 AGeV

R. Kotte and the HADES Collaboration

The HADES spectrometer at SIS/GSI, initially designed for investigating the production of vector mesons via their leptonic decay into e^+e^- pairs, is able to detect hadronic probes, too. Here, we study the channel $\phi \to \mathrm{K^+K^-}$ in collisions of C + C at a beam energy of $E_{beam} = 2$ AGeV [1].

First, we have to find out whether the number of expected ϕ mesons in the data sample of about $N = 10^8$ events is large enough to justify such an experimental analysis. The number of ϕ mesons decaying into charged kaons can be calculated as $N_{\phi\to K^+K^-} = N_{ev}\cdot\epsilon_{trig}\cdot(P_{\phi\to K^+K^-}/P_{K^-})\cdot(\sigma_{K^-}/\sigma_{tot})\cdot\epsilon_{acc}(\Delta p_K, \Delta\theta_K, n_{sec}, E_{beam}, T_\phi)$. $\epsilon_{trig} \simeq 2.8$ is the 1st level trigger vs. minimum bias enhancement as estimated in ref. [2] aimed at $\mathrm{K^+}$ production. The number of anti kaons arising from ϕ decay, $P_{\phi\to K^+K^-}/P_{K^-} \geq 0.22$, is taken from the system Ni + Ni at 1.9 AGeV investigated by the FOPI collaboration [3]. The $\mathrm{K^-}$ production probability, i.e. the ratio of $\mathrm{K^-}$ and total geometrical cross sections, $\sigma_{K^-}/\sigma_{tot} = 2\cdot10^{-4}$, was measured by the KaoS collaboration [4]. Finally, the detector acceptance (including kaon decay) of the decay channel $\phi \to \mathrm{K^+K^-}$ is estimated applying Monte Carlo (MC) simulations. For the daughter kaons a momentum range of $\Delta p_K = (100 - 800)$ MeV/c is assumed. Only the outer part of the time-of-flight detector (TOF system) which exhibits much better time resolution than the inner part (TOFino) will be used in the analysis, hence $\Delta\theta_K = 45^o - 85^o$ was set in MC. Since only three out of six sectors could be used for the present analysis, sectors $n_{sec} = 0, 2, 3$ are activated in MC. The essential parameter of the midrapidity fireball modelled in MC is the inverse slope parameter T_ϕ of the Boltzmann-like c.m. kinetic energy distribution. So far, there is no published data on the momentum-space distribution of ϕ mesons in heavy-ion collisions at SIS energies. Thus, this parameter was chosen to be equal to the corresponding proton one, $T_\phi = T_p = 120$ MeV [5], which yields an acceptance factor of $\epsilon_{acc} = 2.5\cdot10^{-3}$. Having all these numbers at hand, in the above event sample we expect to see $N_{\phi\to K^+K^-} \geq 30$ ϕ mesons via their charged-kaon decay.

For the analysis of the experimental data, "kaon-pair-candidate" N-tuples are filled with the only condition of a ±150 MeV mass window around the nominal kaon mass, roughly corresponding to a 3σ cut at 10% mass resolution. (For masses we set $c = 1$.) Scanning these N-tuples, the same phase-space-relevant cuts as used in MC, i.e. i) TOF system only, ii) sectors 0, 2, 3, and iii) $100 < p_K/(\mathrm{MeV/c}) < 800$, are applied. To enhance the ratio of a possible signal over background, also quality cuts are investigated and optimized, i.e. iv) upper χ^2 limits on the inner ($\chi^2 < 15$) and outer ($\chi^2 < 30\,(17)$ for sectors 0, 3 (2)) track segments fitted to the hit positions measured with multiwire drift chambers (MDCs) in front and behind the HADES magnet, and v) MDC-TOF matching, $\Delta x < 40$ mm and $\Delta y < 10$ mm. About 400 kaon-pair candidates passed these conditions. Finally, kinematically suppressed opening angles ($> 120^o$) are rejected. Figure 1 displays the corresponding invariant mass distribution. Indeed, a peak is visible at the position of the nominal ϕ mass. Integrating the peak over ±8 MeV, an excess yield of about 22 entries with a significance of 2.8 is observed. Note, however, that the deduced width is a factor of $2 \div 3$ smaller than expected from MC simulations.

An order of magnitude more ϕ's is expected for the system Ar + KCl at 1.8 AGeV, due to a larger data sample and full azimuthal coverage of the spectrometer with at least three MDCs. This system is presently prepared for data-summary-tape production.

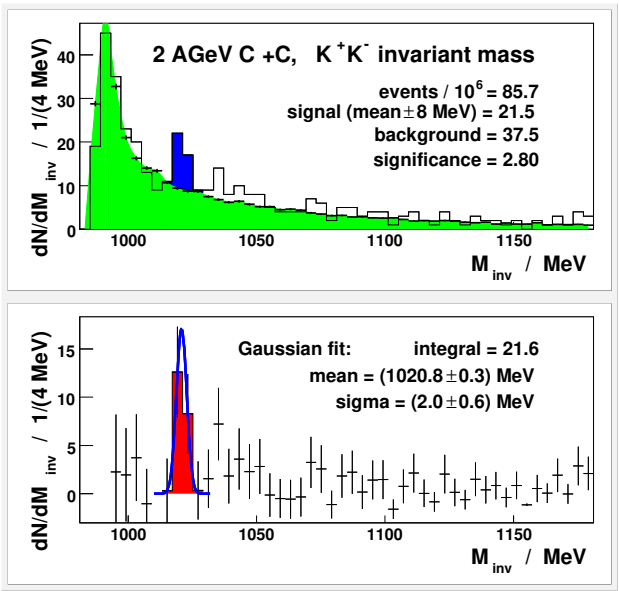

Fig. 1 *Upper panel: The invariant mass distribution of K^+K^- pair candidates (histogram). The light hatched (green) distribution gives the (renormalized at large invariant masses) corresponding uncorrelated background. The dark (blue) histogram is the potential signal within a 8 MeV wide mass window around the peak center. Lower panel: The difference of both distributions. The full line is a Gaussian fit to the yield excess at masses of 1010 MeV - 1030 MeV.*

[1] R. Kotte, HADES collab. meeting, GSI, Oct 2006
[2] A. Sadovsky, Ph.D. thesis, TU Dresden (2007)
[3] A. Mangiarotti et al., Nucl. Phys. A 714 (2003) 89
[4] F. Laue et al., Phys. Ref. Lett. 82 (1999) 1640
[5] P. Tlusty, Proc. XLII Wintermeeting on Nuclear Physics, Bormio 2004, Vol. 120 (2005) 171

Coherent Photo-Excitation of Θ^+ [B,E]

A.I. Titov [1], **B. Kämpfer**, S. Date [2], Y. Ohashi [2]

Published in Phys. Rev. C 74 (2006) 055206, 1-17

We analyze the possibility to produce an intermediate Θ^+ via a $KN \to \Theta^+$ formation process in $\gamma D \to pK^-X$ ($X = nK^+, pK^0$) reactions at some specific kinematical conditions, in which a pK^- pair is knocked out in the forward direction and its invariant mass is close to the mass of Λ^* ($\Lambda^* \equiv \Lambda(1520)$). The Θ^+ signal may appear in the $[\gamma D, pK^-]$ missing mass distribution. The ratio of the signal (cross section at the Θ^+ peak position) to the smooth background processes varies from 0.7 to 2.5 depending on the spin and parity of Θ^+, and it decreases correspondingly if the pK^- invariant mass is outside of the Λ^*-resonance region. We analyze the recent CLAS search for the Θ^+ in the $\gamma D \to pK^-nK^+$ reaction and show that the conditions of this experiment greatly reduce the Θ^+ formation process making it difficult to extract a Θ^+ peak from the data.

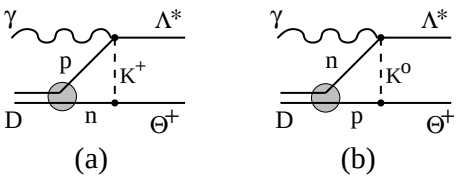

Fig. 1 *Tree level diagrams for the reaction $\gamma D \to \Lambda^*\Theta^+$. The exchange of charged and neutral kaons is shown in (a) and (b), respectively.*

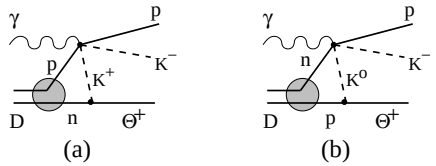

Fig. 2 *Diagrammatic representation of the associated non-resonant $pK^-\Theta^+$ photoproduction.*

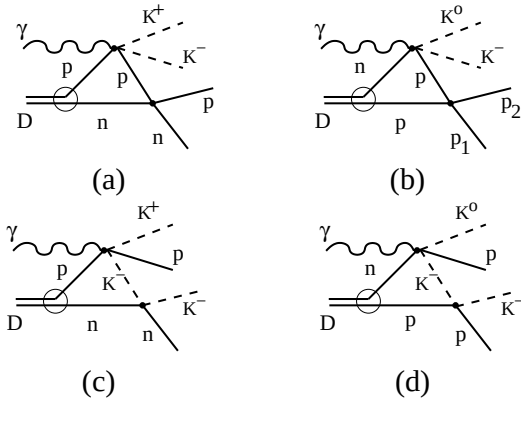

bf Fig. 3 Rescattering of the proton (a,b) and K^- meson (c,d) in pK^-NK photoproduction from the deuteron.

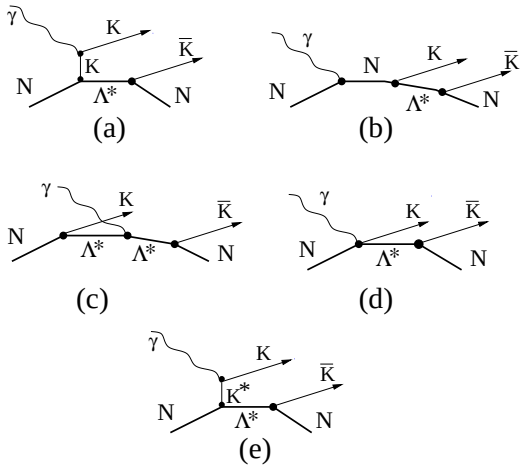

Fig. 4 *Tree level diagrams for the non-resonant subreaction $\gamma N \to \Lambda^* K \to NK\bar{K}$.*

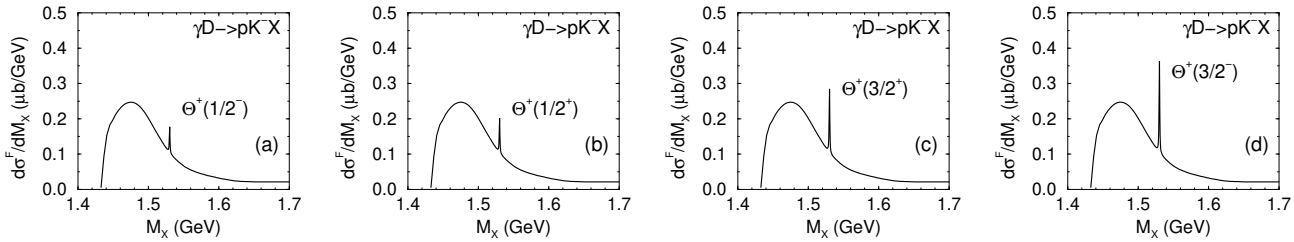

Fig. 5 *Missing mass distribution in the $\gamma D \to pK^-X$ reaction at $E_\gamma = 1.7 - 2.3$ GeV and $M_0 = 1.52$ GeV for different Θ^+ spin and parity: $J^P = \frac{1}{2}^-$ (a), $\frac{1}{2}^+$ (b), $\frac{3}{2}^+$ (c), and $\frac{3}{2}^-$ (d).*

The full article to this contribution is based on preceding ones [1,2].

[1] A.I. Titov, B. Kämpfer, S. Date, Y. Ohashi, Phys. Rev. C 72 (2005) 014005
[2] A.I. Titov, B. Kämpfer, Phys. Rev. C 71 (2005) 062201(R)

[1] *JINR Dubna, 141980, Russia*
[2] *Synchrotron Radiation Research Inst., Sayogun Hyogo 679-5198, Japan*

Production of Strangeness in Hot and Cold Nuclear Matter induced by both Leptonic and Hadronic Projectiles [B]

F. Dohrmann

Published in Int. J. Mod. Phys. E 15 (2006) 761-851

Strangeness production by both hadronic and leptonic projectiles with beam energies of up to a few GeV is reviewed. The focus is on the production of strangeness using proton and ion beams, as well as the photo- and electroproduction of strangeness, as observed at modern facilities. The elementary production of $K^{\pm}$ and ϕ mesons as well as Λ, Σ hyperons on the nucleon is described. Based on these results, the production of strange mesons and strange baryons on nuclear targets, as well as the creation of light hypernuclei is discussed, emphasizing the influence of the nuclear medium.

reaction	observable	experiment
$\gamma p \to K^+\Lambda$	$\frac{d\sigma}{d\cos\theta_K^{\rm CM}}$, P_Λ	CLAS (Jlab Hall B)
$\gamma p \to K^+\Lambda/\Sigma^0$	$\frac{d\sigma}{d\Omega}$, $\sigma_{\rm tot}$, P_{Λ/Σ^0}	SAPHIR (ELSA)
$\gamma p \to K^0\Sigma^+$	$\frac{d\sigma}{d\Omega}$, $\sigma_{\rm tot}$, P_{Σ^+}	SAPHIR (ELSA)
$\gamma p \to K^0\Sigma^+$	$\frac{d\sigma}{d\Omega}$, $\sigma_{\rm tot}$	CLAS (Jlab Hall B)
$\gamma p \to K^+\Sigma^0$	Σ	LEPS (SPring-8)
$\gamma p \to K^+\Lambda$	P, Σ	GRAAL
$\gamma n \to K^+\Sigma^-$	$\frac{d\sigma}{d\Omega}$	CLAS (Jlab Hall B)
$\gamma p \to p\phi$	$\frac{d\sigma}{dt}$, ρ^0_{00} (tensor polarization)	CLAS (Jlab Hall B)
$\gamma p \to p\phi$	K^+ azimuthal decay angle	LEPS (SPring-8)
$\gamma p \to \Xi K^+K^-$	missing mass	CLAS (Jlab Hall B)
$\gamma p \to K^+\Lambda(1405)$	missing mass	LEPS (SPring-8)
$\gamma n \to K^0\Lambda$	missing mass	LNS (Tohoku)
$\gamma A \to \phi X$	$\sigma_{\phi N}$, A-dependence	LEPS (SPring-8)
$\gamma^* p \to K^+\Lambda/\Sigma^0$	$\frac{d\sigma}{d\Omega}$, σ_L/σ_T	E93018 (Jlab Hall C)
$\gamma^* A \to K^+X$	$\frac{d\sigma}{d\Omega}$ (quasifree for Λ,Σ hyperons)	E91016 (Jlab Hall C)
$\gamma^{*\,3,4}{\rm He} \to K^{+\,3,4}_{\Lambda}{\rm H}$	$\frac{d\sigma}{d\Omega}$	E91016 (Jlab Hall C)
$\gamma^* p \to K^+\Lambda$	σ_L/σ_T	CLAS (Jlab Hall B)
$\gamma^* p \to K^+\Lambda$	transfer polarization	CLAS (Jlab Hall B)
$\gamma^* p \to K^+\Lambda(1520)$	$\frac{d\sigma}{d\Omega}$, decay angular distr.	CLAS (Jlab Hall B)
$\gamma^* p \to p\phi$	$\frac{d\sigma}{dt}$, σ	CLAS (Jlab Hall B)

Table 1 *Elementary electro- and photoproduction reactions and the observables studied at modern accelerators over the last year. For the references see the full article.*

Systematics of Pion Emission in Heavy Ion Collisions in the 1 AGeV Regime [G]

W. Reisdorf, M. Stockmeier, A. Andronic, M.L. Benabderrahmane, O.N. Hartmann, N. Herrmann, K.D. Hildenbrand, Y.J. Kim, M. Kis, P. Koczon, T. Kress, Y. Leifels, X. Lopez, M. Merschmeyer, A. Schüttauf, V. Barret, Z. Basrak, N. Bastid, R. Caplar, P. Crochet, P. Dupieux, M. Dzelalija, Z. Fodor, Y. Grishkin, B. Hong, T.I. Kang, J. Kecskemeti, M. Kirejczyk, M. Korolija, **R. Kotte**, A. Lebedev, T. Matulewicz, **W. Neubert**, M. Petrovici, F. Rami, M.S. Ryu, Z. Seres, B. Sikora, K.S. Sim, V. Simion, K. Siwek-Wilczynska, V. Smolyankin, G. Stoicea, Z. Tyminski, K. Wisniewski, **D. Wohlfarth**, Z.G. Xiao, H.S. Xu, I. Yushmanov and A. Zhilin (FOPI Collaboration)

Published in Nucl. Phys. A 781 (2007) 459-508

Using the large acceptance apparatus FOPI, we study pion emission in the reactions (energies in A GeV are given in parentheses): $^{40}Ca + ^{40}Ca$ (0.4, 0.6, 0.8, 1.0, 1.5, 1.93), $^{96}Ru + ^{96}Ru$ (0.4, 1.0, 1.5), $^{96}Zr + ^{96}Zr$ (0.4, 1.0, 1.5), $^{197}Au + ^{197}Au$ (0.4, 0.6, 0.8, 1.0, 1.2, 1.5). The observables include longitudinal and transverse rapidity distributions and stopping, polar anisotropies, pion multiplicities, transverse momentum spectra, ratios $(\pi^+/\pi-)$ of average transverse momenta and of yields, directed flow, elliptic flow. The data are compared to earlier data where possible and to transport model simulations.

[1] J. W. Harris et al., Phys. Lett. B 153 (1985) 377
[2] J. W. Harris et al., Phys. Rev. Lett. 58 (1987) 463

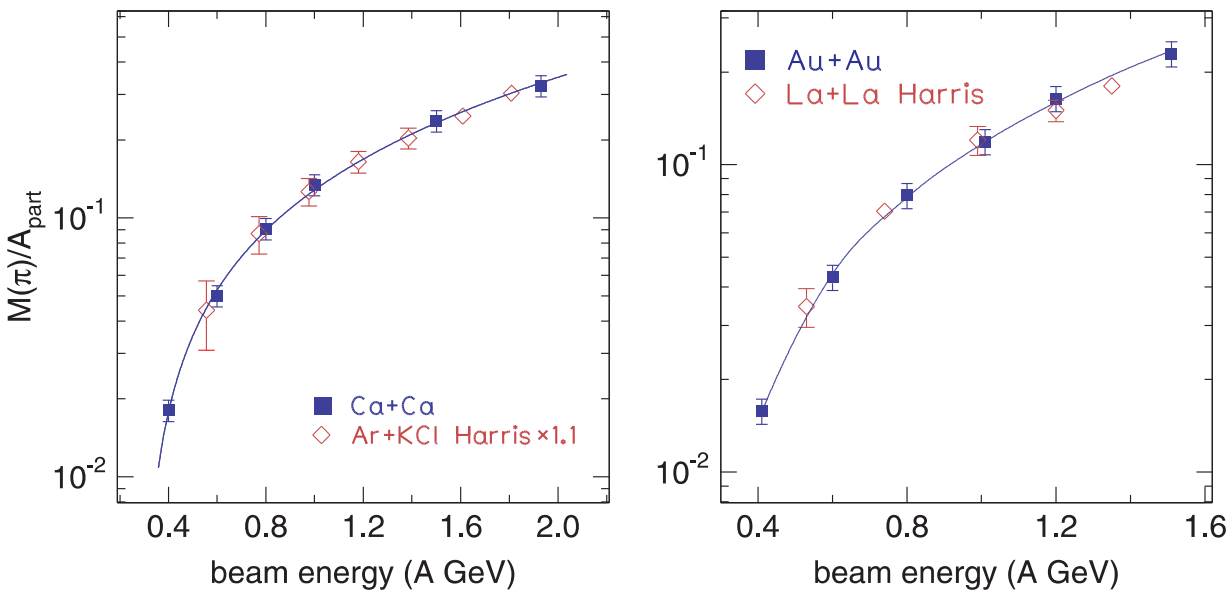

Excitation functions of the reduced pion multiplicity (per participant). The left panel compares the FOPI data for Ca + Ca with the data of Harris et al. [1] for Ar + KCl. The right panel compares the FOPI data for Au + Au with the La + La data [2].

Single-Pion Production in *pp* Collisions at 0.95 GeV/c (I) [B,D,J]

S. Abd El-Samad, R. Bilger, K.-Th. Brinkmann, H. Clement, M. Dietrich, E. Doroshkevich, S. Dshemuchadse, A. Erhardt, W. Eyrich, A. Filippi, H. Freiesleben, M. Fritsch, R. Geyer, A. Gillitzer, J. Hauffe, D. Hesselbarth, R. Jaekel, B. Jakob, L. Karsch, K. Kilian, H. Koch, J. Kress, E. Kuhlmann, S. Marcello, S. Marwinski, R. Meier, **K. Möller**, H.P. Morsch, **L. Naumann**, E. Roderburg, P. Schönmeier, M. Schulte-Wissermann, W. Schroeder, M. Steinke, F. Stinzing, G.Y. Sun, J. Wächter, G.J. Wagner, M. Wagner, U. Weidlich, A. Wilms, S. Wirth, G. Zhang, P. Zupranski
(COSY-TOF Collaboration)

Published in Eur. Phys. J. A 30 (2006) 443-453

The single-pion production reactions $pp \to d\pi^+$, $pp \to np\pi^+$ and $pp \to pp\pi^0$ were measured at a beam momentum of 0.95 GeV/c ($T_p \approx 400$ MeV) using the short version of the COSY-TOF spectrometer. The implementation of a central calorimeter provided particle identification, energy determination and neutron detection in addition to time-of-flight and angle measurements. Thus all pion production channels were recorded with 1-4 overconstraints. The total and differential cross sections obtained are compared to previous data and theoretical calculations. Main emphasis is put on the discussion of the $pp\pi^0$ channel, where we obtain angular distributions different from previous experimental results, however, partly in good agreement with recent phenomenological and theoretical predictions. In particular we observe very large anisotropies for the π^0 angular distributions in the kinematical region of small relative proton momenta revealing there a dominance of proton spinflip transitions associated with π^0 *s*- and *d*-partial waves and emphasizing the important role of π^0 d-waves.

[1] R. Bilger et al., Nucl. Phys. A 693 (2001) 633

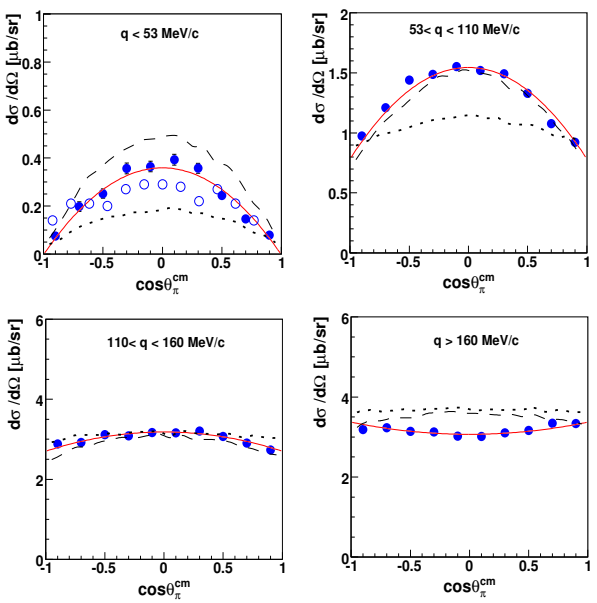

Fig. 1 *Pion angular distribution for four different q-ranges as indicated for $pp \to pp\pi^0$ reaction. Data from this work are shown by full circles, the fit to the data by solid lines. The open circles show data of Bilger et al. [1]. A strong anisotropy with a_2= -1.01 is indicated for $q < 53 MeV/c$.*

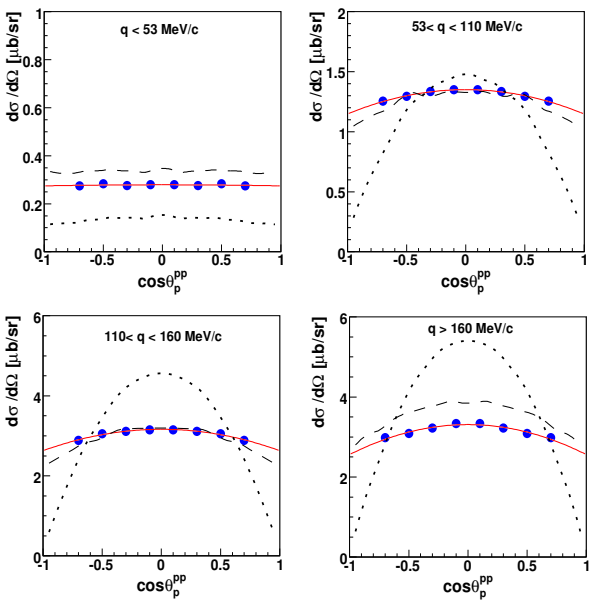

Fig. 2 *Proton angular distribution for four different q-ranges as indicated for $pp \to pp\pi^0$ reaction. Data from this work are shown by full circles, the fit to the data by solid lines.*

Study of Spectator Tagging in the Reaction $np \to pp\pi^-$ with a Deuteron Beam [B,J]

M. Abdel-Bary, K.-Th. Brinkmann, H. Clement, E. Doroshkevich, S. Dshemuchadse, A. Erhardt, W. Eyrich, H. Freiesleben, A. Gillitzer, R. Jaekel, L. Karsch, K. Kilian, E. Kuhlmann, **K. Möller**, H.P. Morsch, **L. Naumann**, N. Paul, C. Pizzolotto, J. Ritman, E. Roderburg, P. Schönmeier, W. Schroeder, M. Schulte-Wissermann, G.Y. Sun, A. Teufel, A. Ucar, G.J. Wagner, M. Wagner, P. Wintz, P. Wüstner and P. Zupranski
(COSY-TOF Collaboration)

Published in Eur. Phys. J. A 29 (2006) 353-361

The reaction $dp \to ppp\pi^-$ has been studied in a kinematically complete experiment at a single beam momentum p_d = 1.85 GeV/c (T = 759MeV). All four ejectiles have been detected in the large-acceptance time-of-flight spectrometer COSY-TOF. We analyzed the data along the lines of the spectator model as a means to isolate the quasi-free $np \to pp\pi^-$ reaction. The spectator proton was identified by its momentum and flight direction thus yielding access to the associated Fermi motion of the bound neutron. A comparison is carried out with Monte Carlo simulations based on two different parameterizations of the deuteron wave function. Up to a Fermi momentum of roughly 150MeV/c no significant deviations between experimental and simulated data of various observables were found from which we conclude that the deuteron can indeed be taken as a valid substitute for the neutron.

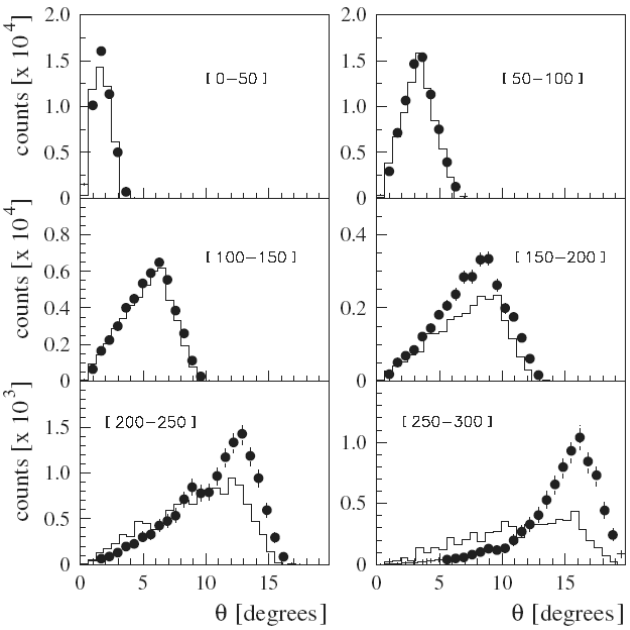

Fig. 1 *Experimentally deduced angular distributions of the spectator proton in the laboratory system (dots with error bars) for indicated bins in Fermi momentum (given in MeV/c) in comparison with Monte Carlo data (solid histograms).*

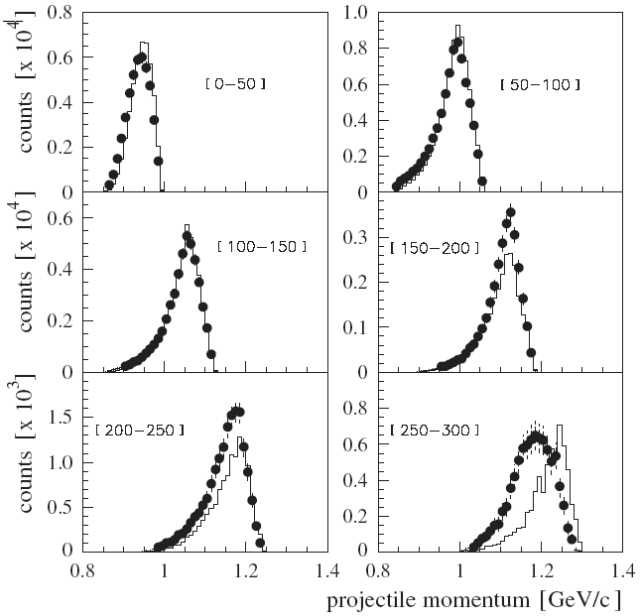

Fig. 2 *Experimentally deduced effective neutron projectile momenta (dots with error bars) for indicated bins in Fermi momentum (given in MeV/c) in comparison with Monte Carlo data (solid histograms).*

Upper Limits on Resonance Contributions to Proton-Proton Elastic Scattering in the c.m. Mass Range 2.05-2.85 GeV/c^2 [B]

H. Rohdjess, D. Albers, J. Bisplinghoff, R. Bollmann, K. Büsser, O. Diehl, **F. Dohrmann**, H.-P. Engelhardt, P. D. Eversheim, J. Greiff, A. Gross, R. Gross-Hardt, F. Hinterberger, M. Igelbrink, R. Langkau, R. Maier, F. Mosel, M. Müller, M. Münstermann, D. Prasuhn, P. von Rossen, H. Scheid, N. Schirm, F. Schwandt, W. Scobel, H. J. Trelle, A. Wellinghausen, W. Wiedmann, K. Woller, R. Ziegler (EDDA Collaboration)

Published in Eur. Phys. J. A 28 (2006) 115-124

Recently published excitation functions [1,2] in proton-proton (pp) elastic scattering observables in the laboratory energy range 0.5-2.5 GeV provide an excellent data base to establish firm upper limits on the elasticities $\eta_{\rm el} = \Gamma_{\rm el}/\Gamma_{\rm tot}$ of possible isovector resonant contributions to the nucleon-nucleon (NN) system. Such contributions have been predicted to arise from dibaryonic states, with c.m. masses between 2.1-2.9 GeV/c^2, but have not been confirmed experimentally. A method to determine quantitatively the maximum value of $\eta_{\rm el}$ compatible with experimental data is presented. We use energy-dependent phase shift fits to the pp data base to model the non-resonant interaction. Based upon the differential cross-section data measured by the EDDA Collaboration an unbiased statistical test is constructed to obtain upper limits on $\eta_{\rm el}$, that exclude larger values with a 99% confidence level. Results in the c.m. mass range 2.05-2.85 GeV/c^2 and total widths of 10-100 MeV/c^2 in the partial waves 1S0, 1D2, 3P0, 3P1, and 3F3 are presented and discussed.

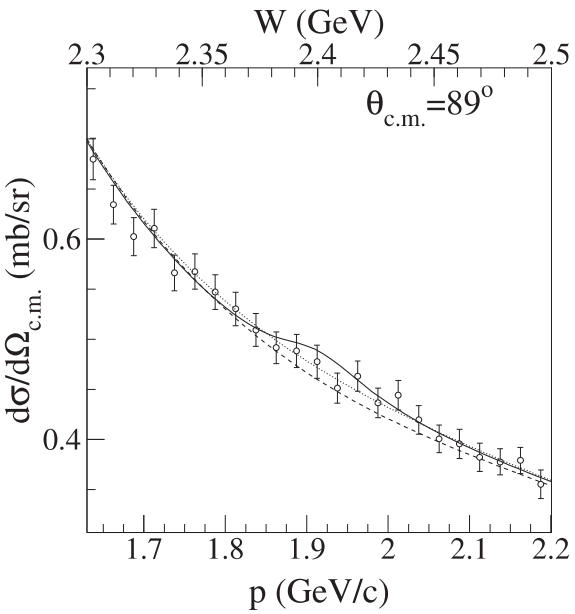

Fig. 1 *Example of an excitation function from [1,2] in comparison to a best-fit PSA without (dotted line) and with (solid line) a resonance in the $^1S_0$ partial wave at $W_R = 2.4$ GeV, with a total width of 50 MeV and a partial elastic width of 2.8 MeV. The non-resonant part of the latter is shown as the dashed line. The presence of this resonance is exclude with 99% CL, based on 28 excitation functions at different scattering angles.*

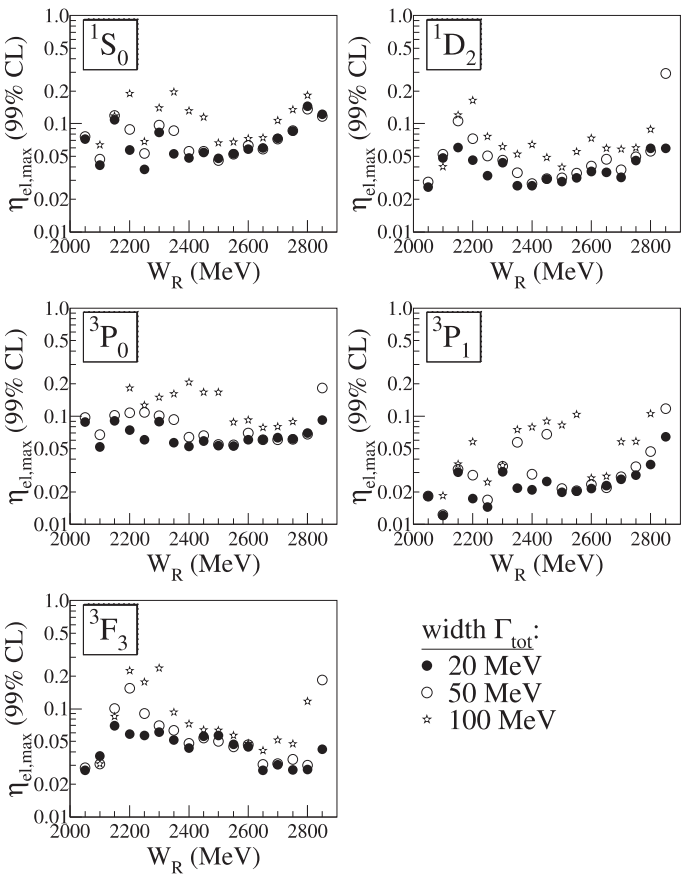

Fig. 2 *Upper limits (99% CL) on $\eta_{\rm el} = \Gamma_{\rm l} = \Gamma_{\rm tot}$ for the lowest uncoupled partial waves as a function the resonance energy W_R for three different total widths $\Gamma_{\rm tot}$ based on the cross-section data of [1,2].*

[1] D. Albers et al., Phys. Rev. Lett. 78 (1997) 1652
[2] D. Albers et al., Eur. Phys. J. A 22 (2004) 125

Four-Quark Condensates at Finite Density in Nucleon QCD Sum Rules [B,G]

R. Thomas, T. Hilger, B. Kämpfer

Part of PhD thesis R. Thomas

The complex hadronic spectrum is governed by the strong interaction which is described by Quantum Chromodynamics (QCD) resting on quarks and gluons as fundamental degrees of freedom. Understanding properties of hadrons is thus impeded by the unsettled confinement mechanism which forms for instance nucleons (protons and neutrons) as building blocks for normal nuclear matter on a microscopic level. A way to gain insight into properties of the ground state of QCD is by probing the impact of this medium at different baryon densities on hadrons, test particles, which are then expected to modify their known vacuum properties (e. g. their spectral density), as pursued by the HADES collaboration where the ρ meson is utilized as probe. The behavior of nucleon effective masses or potentials, respectively, at finite density is strongly related to the stable formation of saturated nuclear matter and can be quantified in scalar and vector nucleon self-energies. For these self-energies chiral effective field theory predicts comparable magnitudes but opposite signs (e. g. [1]).

QCD sum rules relate the nucleon self-energies at non-vanishing baryon densities to properties of the QCD ground state encoded in QCD condensates, which can similarly enter properties of a large set of other hadrons. A specific type, namely four-quark condensates, significantly determine the behavior of nucleon self-energies [2]. We extend such investigations to a more detailed treatment of four-quark condensates and therefore spell out the linear combinations of four-quark condensates

$$\sum c_{i,M} \langle \bar{q} \hat{M}_1 q \bar{q} \hat{M}_2 q \rangle = A \kappa_{\rm i}^{\rm vac} + B \kappa_{\rm i}^{\rm med} n \,,$$

entering the set of three ($i = 1,2,3$) coupled sum rule equations as done for the vacuum case in [3]. The matrices $\hat{M}$ denote the flavor, color and Dirac structures building the full catalog of in-medium four-quark condensates. In this given parametrization the value of $\kappa^{\rm med}$ measures the in-medium modification of the combined four-quark condensates and especially signals deviations from the factorization hypothesis where four-quark condensates are simplified to the square of the chiral condensate $\langle \bar{q} q \rangle$.

A rough analytical estimate reveals (for decoupled sum rules with condensates as in [2], Borel mass $\mathcal{M}^2 = 1$ GeV^2 and threshold $s_0 = 2.5$ GeV^2)

$$\Sigma_v \sim (0.16 + 1.22 \tilde{\kappa}_{\rm v}^{\rm med})\ {\rm GeV} \frac{n}{n_0} \,, \qquad (1)$$

$$\Sigma_s \sim -(0.32 + 0.11 \kappa_{\rm s}^{\rm med} - 0.31 \kappa_{\rm q}^{\rm med})\ {\rm GeV} \frac{n}{n_0} \,, \qquad (2)$$

which elucidates the impact of the density dependence of the three respective four-quark condensate combinations. This dependencies are qualitatively reproduced in full QCD sum rule evaluations: The vector self-energy is solely determined by $\tilde{\kappa}_{\rm v}^{\rm med}$ whereas the scalar self-energy depends on the directly opposed impacts of $\kappa_{\rm s}^{\rm med}$ and $\kappa_{\rm q}^{\rm med}$. This prohibits to find a unique configuration of density dependencies ($\kappa_{\rm s}^{\rm med}$, $\kappa_{\rm q}^{\rm med}$) tuned to the self-energies deduced from chiral effective field theory calculations [1] compared to in Fig. 1. Clearly, the figure shows that constant four-quark condensates would not be sufficient on a quantitative level and neither would be the density dependencies derived from nucleon expectation values of four-quark operators from a perturbative chiral quark model (PCQM) [4].

Consideration of the color structures entering the linear combinations of four-quark condensates in baryon sum rules moreover reveals relations between non-flavor-mixing condensates. Already this makes a translation of the nucleon four-quark condensates to those entering QCD sum rules of light vector mesons impossible. For the ω meson e. g. a strong density dependence compared to the factorization limit of the specific four-quark condensate combination was deduced from a comparison with CB-TAPS data [5]. This and the independent conclusions from the nucleon sum rules are examples questioning the reliability of the factorization ansatz and represent constraints on the exhaustive catalog of four-quark condensates.

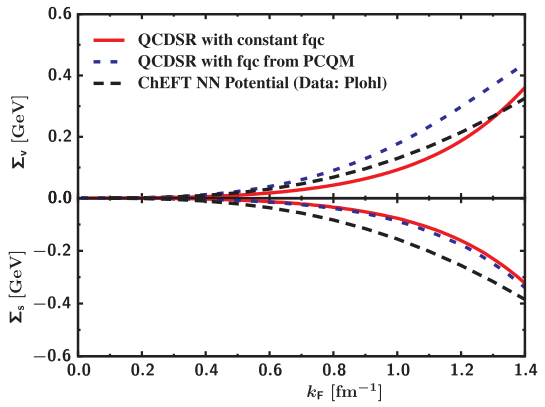

Fig. 1 *Scalar and vector self-energies $\Sigma_{\rm s}$ and $\Sigma_{\rm v}$ of the nucleon as function of the nucleon Fermi momentum $k_{\rm F}$ evaluated from QCD sum rules (SR) for four-quark condensates (fqc) kept constant as well as varied according to [4] compared to advanced nuclear matter calculations [1].*

[1] O. Plohl, C. Fuchs, Phys. Rev. C 74 (2006) 034325
[2] R.J. Furnstahl, D.K. Griegel, T. Cohen, Phys. Rev. C 46 (1992) 1507
[3] R. Thomas, K. Gallmeister et al., Acta. Phys. Hung. A 26 (2006) 35
[4] E.G. Drukarev, M.G. Ryskin et al., Phys. Rev. D 68 (2003) 054021
[5] R. Thomas, S. Zschocke, B. Kämpfer, Phys. Rev. Lett. 95 (2005) 232301

Foundation of the Quasi-Particle Model of Strongly Interacting Matter [B,D,E,G]

M. Bluhm, B. Kämpfer, R. Schulze, D. Seipt

Part of PhD thesis M. Bluhm

The Φ-functional approach [1] allows to derive a formulation of QCD thermodynamics in terms of quasiparticle excitations [2] from the fundamental Lagrangian. In Coulomb gauge, the thermodynamic potential Ω is expressed as a functional of dressed gluon (D) and quark (S) propagators by

$$\frac{\Omega[D,S]}{T} = \frac{1}{2}\mathrm{Tr}[\ln\frac{1}{D} - \Pi D] - \mathrm{Tr}[\ln\frac{1}{S} - \Sigma S] + \Phi[D,S]\,. \tag{1}$$

Here, D consists only of the physical transverse and longitudinal modes and $\Phi[D,S]$ is given by the sum of all 2-particle irreducible skeleton diagrams constructed from D and S. The self-energies are related to the dressed propagators by Dyson's equations. Demanding the stationarity of Ω under functional variation with respect to the dressed propagators, the self-energies follow self-consistently by the gap equations

$$\Pi = 2\frac{\delta\Phi[D,S]}{\delta D}\,,\quad \Sigma = -\frac{\delta\Phi[D,S]}{\delta S}\,. \tag{2}$$

The trace Tr in (1) involves a sum over Matsubara frequencies which can be evaluated by using standard contour integration techniques. With retarded propagators D and S depending on ω and $k = |\vec{k}|$ we find

$$\begin{aligned}\frac{\Omega[D,S]}{V} = {} & \mathrm{tr}\int\tfrac{d^3k}{(2\pi)^3}\int\tfrac{d\omega}{2\pi}n(\omega)\,\mathrm{Im}[\ln D^{-1} - \Pi\, D] \\ & +2\mathrm{tr}\int\tfrac{d^4k}{(2\pi)^4}f(\omega)\,\mathrm{Im}[\ln S^{-1} - \Sigma\, S] + \tfrac{T}{V}\Phi[D,S]\,,\end{aligned} \tag{3}$$

where $n(\omega)$ and $f(\omega)$ denote statistical distribution functions for gluons and quarks. Due to the stationarity property, entropy density $s = -\partial(\Omega/V)/\partial T$ contains only explicit temperature (T) derivatives of $n(\omega)$ and $f(\omega)$. We consider Φ at 2 - loop order given by

$\Phi =$ 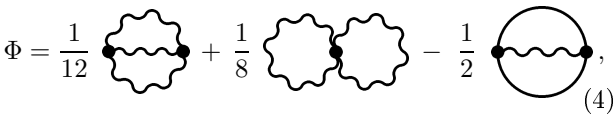 , (4)

and the self-energies read

$\Pi =$ 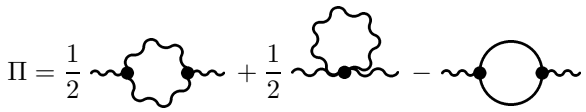 , (5)

$\Sigma =$ 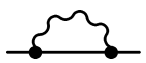 . (6)

Here, wiggly (solid) lines denote gluons (quarks). Truncating Φ, gauge invariance is lost but can be restored by using gauge invariant hard thermal loop (HTL) expressions for Π and Σ [2]. These expressions show the correct behavior near the light cone for momenta $k \sim T, \mu$ as relevant for thermodynamics [3] (Fig. 1). Neglecting imaginary parts in the self-energies, performing the trace tr over color and Dirac indices and approximating the dispersion relations ω_g (ω_q) of gluons (quarks) according to [3], compact expressions for thermodynamic quantities can be derived. Fig. 2 exhibits an example for the entropy density.

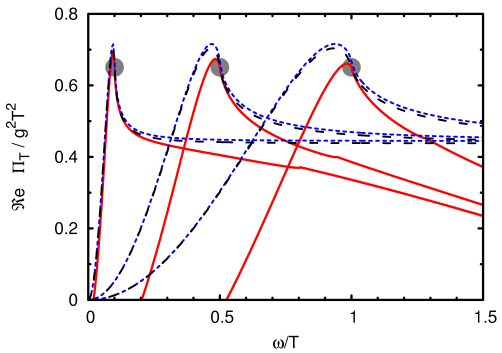

Fig. 1 *Comparison of HTL (dashed; short-dashed with quark mass effects) and 1-loop results (solid) for the transverse gluon self-energy at $k/T = 0.1$, 0.5 and 1 (left to right). Near the light cone (regions marked by circles), both results agree.*

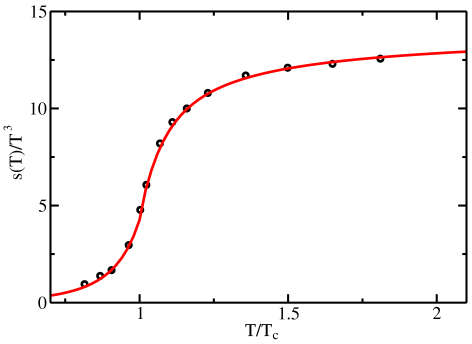

Fig. 2 *Comparison of entropy density s/T^3 as a function of the scaled temperature T/T_c for a two-flavor quark-gluon plasma (solid curve) with lattice QCD data [4] (symbols).*

[1] J.M. Luttinger, J.C. Ward, Phys. Rev. 118 (1960) 1417

[2] J.P. Blaizot, E. Iancu et al., Phys. Rev. D 63 (2001) 065003

[3] M. Bluhm, B. Kämpfer et al., Eur. Phys. J. C 49 (2007) 205

[4] F. Karsch, Nucl. Phys. A 698 (2002) 199

Family of QCD Equations of State within a Quasi-Particle Model [B,D,E,G]

M. Bluhm, B. Kämpfer, R. Schulze, D. Seipt, U. Heinz[1]

Part of PhD thesis M. Bluhm

With growing evidence, ideal hydrodynamics successfully describes the expansion stage of strongly interacting matter created in relativistic heavy-ion collisions. The essential input for solving the equations of motion is the equation of state (EoS) relating pressure p, energy density e and baryon density n_B. Ab initio calculations of QCD on a discretized space-time grid (dubbed lattice) deliver the EoS in form of a Taylor series expansion at small μ/T [1], e.g. the pressure

$$p = T^4 \left(c_0(T) + c_2(T) \left(\frac{\mu}{T}\right)^2 + c_4(T) \left(\frac{\mu}{T}\right)^4 + ... \right) \quad (1)$$

as a function of temperature T and chemical potential μ.

As a flexible parametrization for the EoS, we developed a quasi-particle model (QPM) using dynamically generated self-energies and a non-perturbative coupling as essential input which was shown [2] to successfully reproduce the lattice QCD results. The latter employ too large quark masses at small energy densities e [3]. Thus, we employ the resonance gas model at small energy densities and use our QPM EoS at larger densities. By generating a family of equations of state, cf. Fig. 1, keeping the matching point e_1 to the resonance gas EoS fixed and interpolating linearly to a given matching point e_2 (serving as label) of the QPM EoS, we can study the influence of details in the transition region on observables.

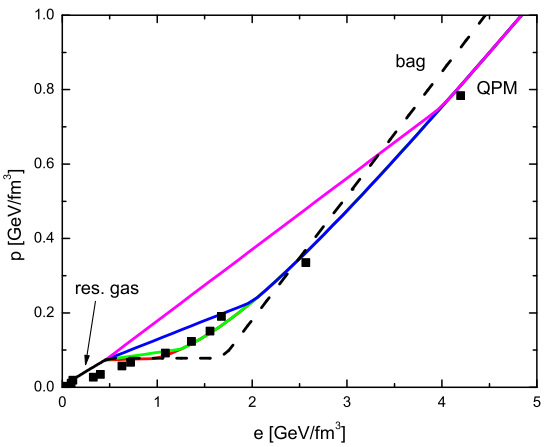

Fig. 1 *Family of equations of state $p(e)$ at small n_B relevant for top RHIC energies: Combination of QPM and resonance gas model as described in the text, $e_1 = 0.45$ GeV/fm^3. Dashed curve represents bag model EoS, squares lattice QCD data [3].*

For instance, in Fig. 2 we compare hydrodynamic calculations obtained with different equations of state with experimental data for the differential elliptic flow at midrapidity $v_2(p_T)$ of strange baryons as a function of transverse momentum p_T. We observe a small but non-negligible impact of EoS details in the transition region on the results.

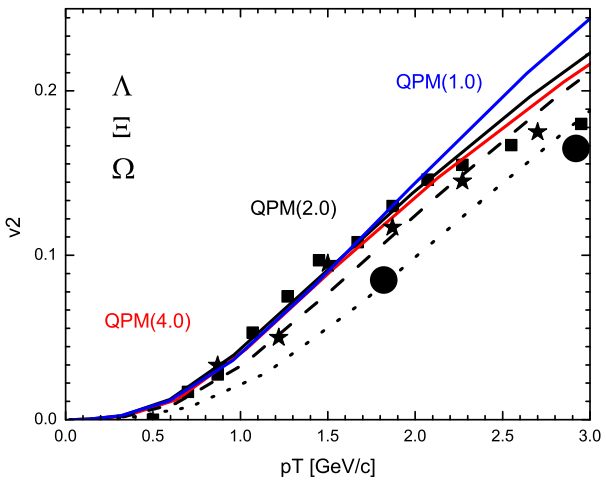

Fig. 2 *$v_2(p_T)$ for strange baryons: Λ (squares), Ξ (stars), Ω (circles); data from [4]. Corresponding results when using the EoS of Fig. 1 with $e_2 = 1$, 2 and 4 GeV/fm^3 (solid curves from top to bottom for Λ) and $e_2 = 2$ GeV/fm^3 (dashed and dotted curves for Ξ and Ω).*

[1] C. R. Allton, M. Doring et al., Phys. Rev. D 71 (2005) 054508

[2] B. Kämpfer, M. Bluhm et al., Nucl. Phys. A 774 (2006) 757

[3] F. Karsch, E. Laermann et al., Phys. Lett. B 478 (2000) 447

[4] J. Adams, M. M. Aggarwal et al. (STAR), Phys. Rev. Lett. 95 (2005) 122301

[1] *Ohio State Univ., Department of Physics, Columbus, OH 43210, USA*

QCD Critical End-Point Effects in a Quasi-Particle Model [B,D,E,G]

M. Bluhm, B. Kämpfer

Part of PhD thesis M. Bluhm

The phase diagram of strongly interacting matter exhibits an astonishing richness. The first-order transition line separating hadronic and quark-gluon fluid phases at large baryo-chemical potentials μ_B terminates in a critical end point (CP) of second order. While its exact location and the extension of the critical region are matter of current investigations, CP belongs to the universality class of the 3D Ising model for QCD with massive quarks. For smaller μ_B the transition turns into a cross over. Across the phase transition line large variations in energy or various susceptibilities are expected as observable consequences. Within our quasi-particle model (QPM) for the QCD equation of state (EoS) we include phenomenologically CP features. In line with [1] we locate CP at $\mu_B^{CP} = 360$ MeV and estimate the transition line by

$$T_c(\mu_B) = T_c^0 \left(1 + \frac{1}{2} d \left(\frac{\mu_B}{3T_c^0}\right)^2\right) \qquad (1)$$

with $d = -0.122$ and $T_c^0 = 175$ MeV for two-flavor QCD. Accordingly, we find for the temperature T of CP, $T^{CP} = 170$ MeV. Following [2], CP features are included through non-analytic contributions in the bulk thermodynamic quantities with adjustable parameters characterizing the extension of the critical region. To be specific, we model the superposition of the smooth regular and the singular contributions to the entropy density as $s = s_{reg} + s_{sing}$ where the regular part is given by our QPM expression for the entropy density [3] and

$$s_{sing}(T, \mu_B) = \frac{2}{9} A\, c_2(T)\, \mu_B^2 T\, tanh\, S_c(T, \mu_B)\,. \qquad (2)$$

Here, A denotes the relative strength between regular and singular part, c_2 is the leading order Taylor expansion coefficient of the μ_B-dependence of the pressure p and the singular function S_c reads with Gibbs' free energy density G for the 3D Ising model

$$S_c(T, \mu_B) = -\sqrt{\Delta T_c^2 + \Delta \mu_{B,c}^2} \left(\frac{\partial G}{\partial T}\right)_{\mu_B}\,. \qquad (3)$$

Assuming the extension of the critical region to be small (defined by the parameters ΔT_c and $\Delta \mu_{B,c}$) implies that the EoS is given to a large extent by its regular contributions [3], in particular for small μ_B.
In contrast, baryon number susceptibility χ_B being a measure of fluctuations in the baryon density n_B is strongly influenced by CP. In Fig. 1, we show n_B as function of μ_B. For $\mu_B > \mu_B^{CP}$, n_B exhibits a discontinuity across the transition line which is significant for a first-order phase transition. The corresponding result for χ_B is depicted in Fig. 2.

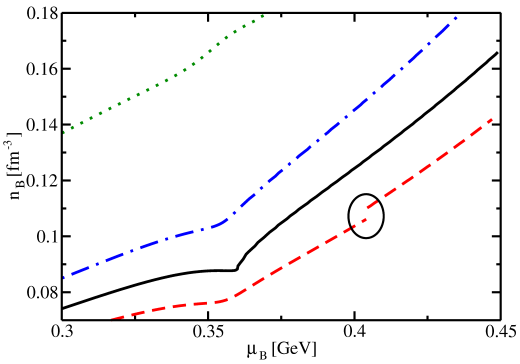

Fig. 1 *n_B as a function of μ_B for different temperatures $T = T^{CP} - 1.25$ MeV, T^{CP}, $T^{CP} + 1.25$ MeV and $T = 176$ MeV (dashed, solid, dash-dotted and dotted curves, respectively). At $T = T^{CP} = T_c(\mu_B^{CP})$, the slope becomes infinite at μ_B^{CP+}, and for $T < T^{CP}$, $n_B(\mu_B)$ exhibits the discontinuous behavior (encircled) of a first-order phase transition.*

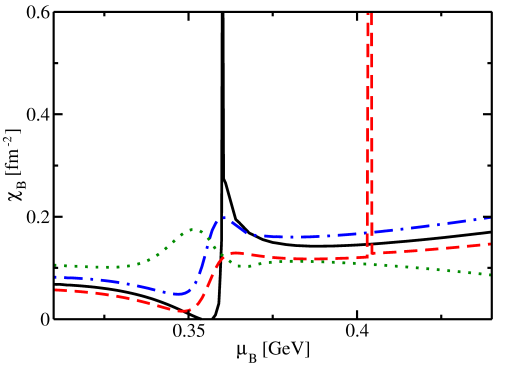

Fig. 2 *Baryon susceptibility $\chi_B = \frac{\partial n_B}{\partial \mu_B}$ as function of μ_B (same line code as Fig. 1). χ_B diverges at μ_B^{CP}, while the spike in the dashed curve at $\mu_B = 0.41$ GeV is an artifact of the numerical differentiation at the discontinuity in n_B.*

[1] Z. Fodor, S. D. Katz, JHEP 0404 (2004) 050
[2] C. Nonaka, M. Asakawa, Phys. Rev. C 71 (2005) 044904
[3] M. Bluhm, B. Kämpfer, PoS (CPOD2006) 004

Relativistic Approaches to Investigations of Few-Nucleon Systems [B,E]

S.M. Dorkin [1], L.P. Kaptari [1], **B. Kämpfer**, S.S. Semikh [1]

Published in Phys. Part. Nucl. 37 (2006) 867-898

Theoretical approaches used in investigations of relativistic effects in high energy lepton and hadron collisions with few nucleon systems are analyzed. The Bethe-Salpeter formalism for describing interacting systems of two spinor particles both in the continuum and bound state is described in detail. Special attention is paid to partial expansions taking into account the analytic properties of Bethe-Salpeter amplitudes and unitary transformations correlating different representations of partial amplitudes. Mathematical methods of numerical solution of equations are considered. Results of calculation of relativistic corrections and effects of interactions in the final state in particular reactions with the deuteron, namely, inelastic pD backward scattering and in reactions of deuteron break-up with production of correlated pairs, are presented.

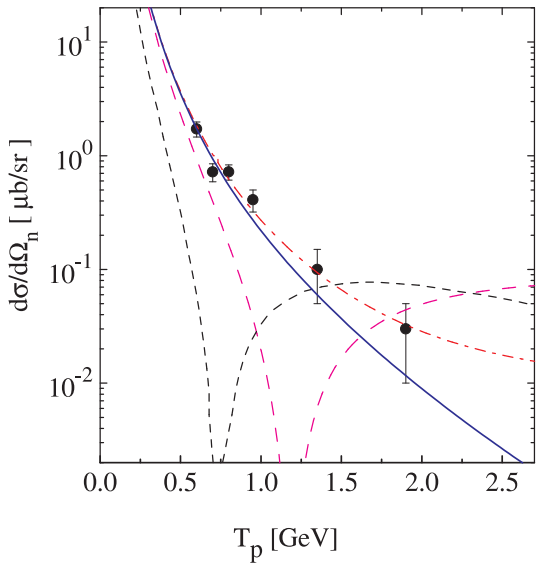

Fig. 1 *Cross section of the reaction* $p + D = (p_1p_2)(0^0) + n_1(180^0)$ *integrated over the excitation energy* E_x *of the outgoing proton pair as a function of the initial energy* T_p. *Dashed line: non-relativistic calculation (only ++ components of* $^1S_0$ *state without Lorentz boosts), dotted line: Lorentz boost in the main component, dot-dashed line: relativistic calculation (including P waves) without cut-off form factors, solid line: relativistic calculations with form factors.*

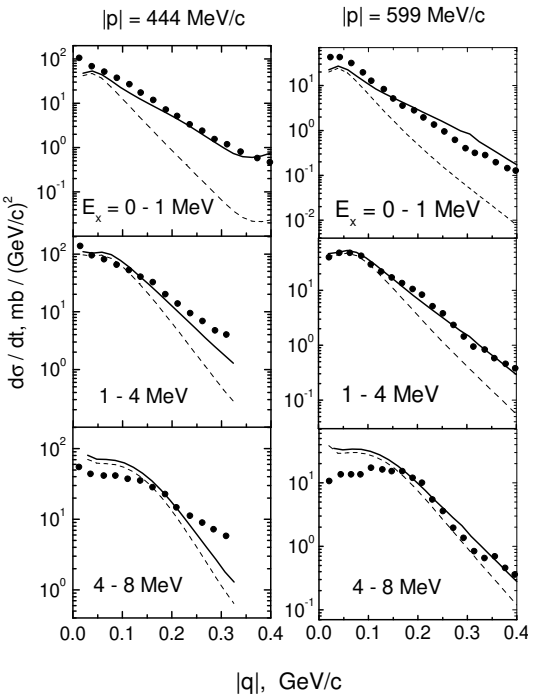

Fig. 2 *Differential cross section of the reaction* $p + \vec{D} = n + (p_1 + p_2)$ *at initial momentum* $|\mathbf{p}| = 0.444\,GeV/c$ *(left column) and* $|\mathbf{p}| = 0.599\,GeV/c$ *(right column). Dashed lines: results of impulse approximation, solid lines: with final state interaction.*

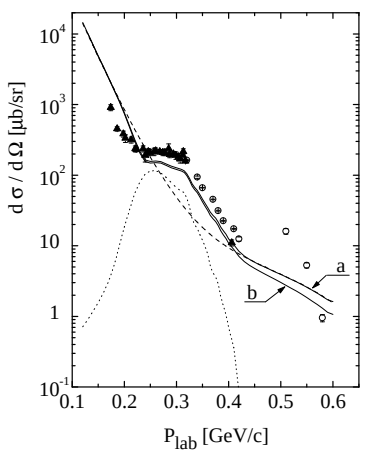

Fig. 3 *Differential cross section for the elastic backward* $pD \to Dp$ *reaction with triangle diagrams and meson exchange corrections. Dashed line: contribution solely from the one-nucleon exchange mechanism, dotted line: meson exchange corrections, solid lines: total contribution with (a) and without (b) P components in the Bethe-Salpeter amplitude.*

[1] *JINR Dubna, 141980, Russia*

Development of Straw Tubes for High Rate Capability Application [G,E]

K. Davkov, V. Davkov, J. Marzec, V. Myalkovskiy, **L. Naumann**, V. Peshekhonov, A. Savenkov, D. Seliverstov, V. Tikhomirov, K. Viryasov, P. Wintz, K. Zaremba, I. Zhukov

The construction of a large size straw tube particle tracking detector for the Compressed Baryonic Matter Experiment at FAIR is under consideration [1]. Drift chambers on the basis of thin-walled drift tubes (straws) have been widely used as tracking detectors in high rate environments [2,3,4]. In the inner part of the first CBM tracker station the expected hit density of charged particles for central Au+Au collisions at 25 AGeV amounts to 0.05 /cm^2. To guarantee a sufficient efficiency of the tracking system, the occupancy of a single drift tube element should be below five percent and the active detector cross-section yields 1 cm^2 for the expected hit density. To realise small area drift detectors long straw tubes with subdivided anodes of different length have been developed. The readout of a section should be independent of each other. Consequently it is possible to reduce the active cross-section of a straw tube to few cm^2. The low-mass inner straw elements and the technology of the multi-anode straw assembly have been devised and checked. A prototype of 19 straws with 57 readout channels has been manufactured. The straws are 500 mm long and 4 mm in diameter. The anodes are subdivided in two, three or four parts of different length. Fig. 1 shows a straw tube layout with four anode segments.

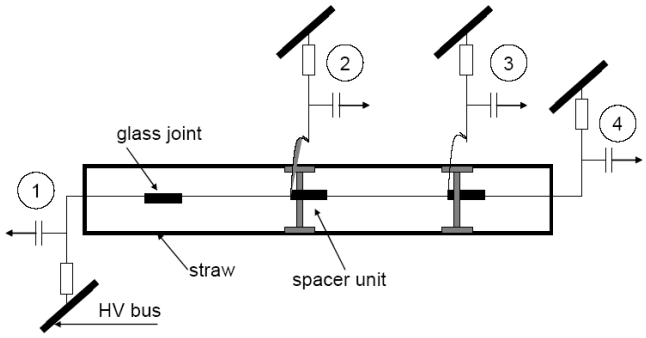

Fig. 1 *Schematical drawing of the straw tube design with four anodes.*

Different readouts have been tested. The front-end readout of the outer anodes has been provided close to the end-plugs. For the inner sectors cables of 15 cm length connect the anode wires with the front-end electronics. In the threefold segmented anode the single glas joint has been removed to investigate the double-sided readout. The current sensitive preamplifiers with an input impedance of 300 Ω are connected to the anodes by a capacitive coupling of 200 pF. Each anode has been supplied with high voltage through a resistor of 1 MΩ. A gas mixture of Ar/CO_2 (70/30) at atmospheric pressure has been supplied through the two end-plugs of each straw. Collimated Gammas (^{55}Fe) irradiated the straws along the anodes with a width of 1 mm perpendicular to the wires. Fig. 2 shows the anode signal amplitude distribution in a threefold subdivided wire. The collimator was moved along the straw. The information from the inner sector is read out over the contact wire fed through the spacer supporting the capillary tube and the hole in the straw wall. To compare the signals going through the straw wall and the end plug, the readout of the right anode has a double-sided layout.

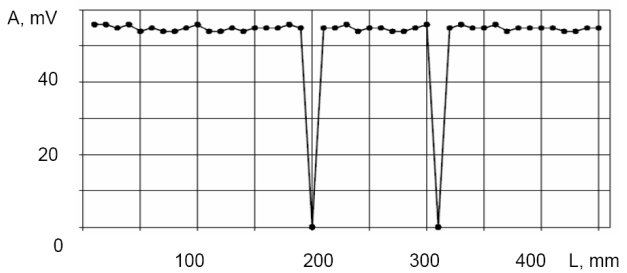

Fig. 2 *Amplitude distribution of the anode signals (A) along the threefold subdivided straw of 500 mm length (L).*

The result shows that detector inefficiencies are only evident in small regions of 7.2 mm length around the spacer units. The straws work stably, no discharges were observed between any construction elements placed inside the straws. The radiation length of the spacer amounts to 0.4 %. For minimum ionizing particles the rate capability amounts up to 4.5 MHz/cm^2 in single straws of 4 mm in diameter with a gain of 5×10^4 [5].

[1] CBM Experiment, Techn. Status Report, GSI Darmstadt (2005)
[2] Y. Arai et al., NIM A381 (1996) 355
[3] ATLAS Inner Tracker Design Report, CERN/LHCC/97-16
[4] V. Bytchkov et al., Particles and Nuclei, Letters N.2 (2002) 75
[5] I. Zhukov et al., JINR Preprint P13-2005-126

Radiation Damage of Polypropylene Fiber Targets in Storage Rings [B]

H. Rohdjess, D. Albers, J. Bisplinghoff, R. Bollmann, K. Büsser, O. Diehl, **F. Dohrmann**, H.-P. Engelhardt, P. D. Eversheim, J. Greiff, A. Gross, R. Gross-Hardt, F. Hinterberger, M. Igelbrink, R. Langkau, R. Maier, F. Mosel, M. Müller, M. Münstermann, D. Prasuhn, P. von Rossen, H. Scheid, N. Schirm, F. Schwandt, W. Scobel, H. J. Trelle, A. Wellinghausen, W. Wiedmann, K. Woller, R. Ziegler (EDDA Collaboration)

Published in Nucl. Instr. Meth. B 243 (2006) 127-133

Thin polypropylene fibers have been used for internal experiments in storage rings as an option for hydrogen targets. The change of the hydrogen content due to the radiation dose applied by the circulating proton beam has been investigated in the range $1{\cdot}10^6$ to $2{\cdot}10^8$ Gy at beam momenta of 1.5 to 3 GeV/c by comparing the elastic pp-scattering yield to that from inelastic p-carbon reactions. It is found that the loss of hydrogen as a function of applied dose receives contributions from a fast and a slow component.

[1] R. Bradley, Radiation Technology Handbook, Marcel Dekker Inc., New York, 1984.

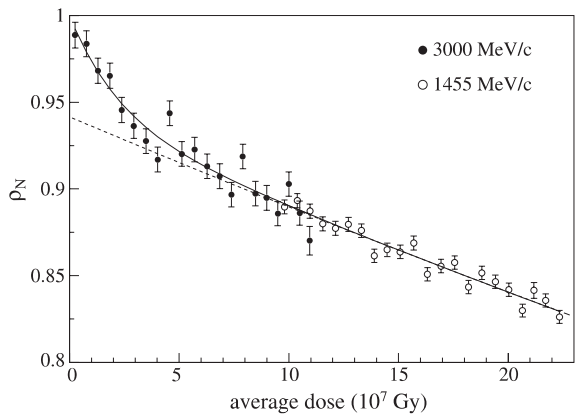

Fig. 1 *Normalized average hydrogen density as a function of the average dose. The result of the fit is shown as the solid line. The dashed line shows the contribution of the slow component only. Note, that the first data point at 1.455 GeV/c corresponds to a lower dose than the last point at 3.0 GeV/c, since the beam is slightly displaced, such that a region of lower accumulated dose is probed.*

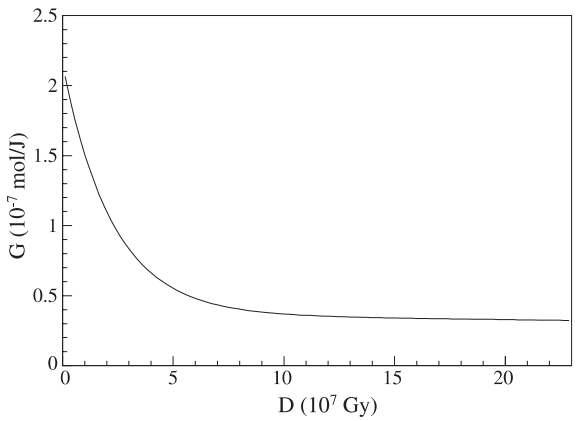

Fig. 2 *G-value for radiolytic loss of H2 as a function of the accumulated dose. The $G(H_2)$-value [1] describes the number of hydrogen molecules δn_X per $\delta E = 100$ eV energy deposited in the polymer. The modern definition of G is the amount of substance n_x (unit mol) per $\delta E = 1$ J, $G = \delta n_x/\delta E$. The old unit 1/(100 eV) corresponds to $1.04{\cdot}10^7$ mol/J. The observed dependence of $G(H_2)$ is very similar to the results shown in this figure.*

Determining Beam Parameters in a Storage Ring with a Cylindrical Hodoscope Using Elastic Proton–Proton Scattering [B]

H. Rohdjess, D. Albers, J. Bisplinghoff, R. Bollmann, K. Büsser, O. Diehl, **F. Dohrmann**, H.-P. Engelhardt, P. D. Eversheim, J. Greiff, A. Gross, R. Gross-Hardt, F. Hinterberger, M. Igelbrink, R. Langkau, R. Maier, F. Mosel, M. Müller, M. Münstermann, D. Prasuhn, P. von Rossen, H. Scheid, N. Schirm, F. Schwandt, W. Scobel, H. J. Trelle, A. Wellinghausen, W. Wiedmann, K. Woller, R. Ziegler (EDDA Collaboration)

Published in Nucl. Instr. Meth. A 556 (2006) 57-65

The EDDA-detector at the cooler-synchrotron COSY/Jülich has been operated with an internal CH_2 fiber target to measure proton"=proton elastic scattering differential cross-sections. For data analysis knowledge of beam parameters, like position, width and angle, are indispensable. We have developed a method to obtain these values with high precision from the azimuthal and polar angles of the ejectiles only, by exploiting the coplanarity of the two final-state protons with the beam and the kinematic correlation. The formalism is described and results for beam parameters obtained during beam acceleration are given.

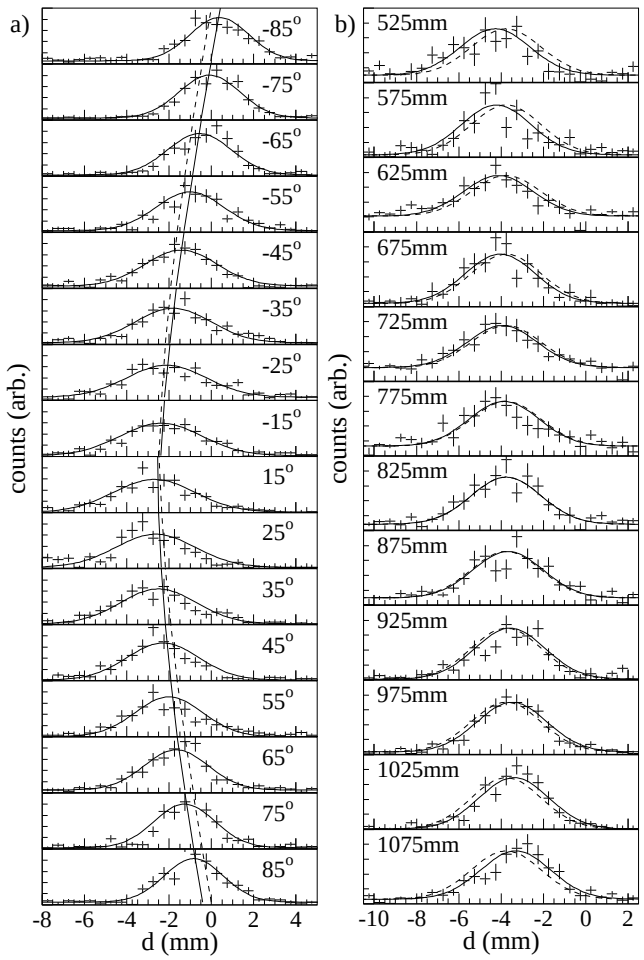

Fig. 1 *(a) Variation of the d-distribution for different bins in ϕ_d. The fit (solid Gaussian) to the data (crosses) yields a beam displacement of $x_b = -2.51$ mm, $y_b = -0.41$ mm. The mean value is shown as the solid vertical curve, for the dashed curve y_b was fixed to zero. (b) Variation of the d-distribution at $\phi_d = 15 \pm 5^\circ$ with $z_1 + z_2$ and the result of the fit (solid line) yielding $x'_b \approx 5$ mrad. The dashed line shows the fit at 825 mm for comparison. The measured value of d for a displaced (x_b, y_b) and tilted (x'_b, y'_b) beam is given by:*

$$d = (x_b + \frac{z_1 + z_2}{2} x'_b) \cos\phi_d + (y_b + \frac{z_1 + z_2}{2} y'_b) \sin\phi_d$$

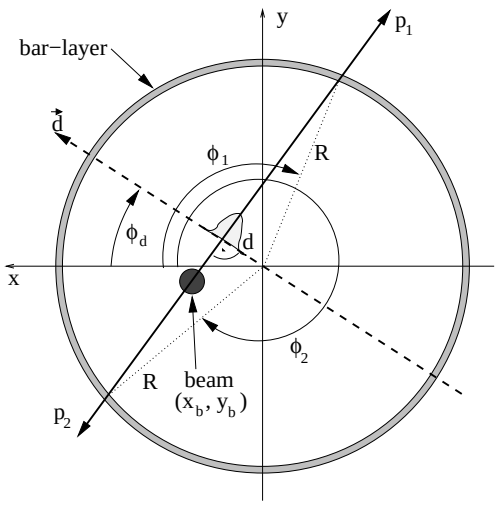

Fig. 2 *Geometry for a beam parallel to the detector symmetry axis. EDDA measures the points of interception of two prongs with a bar layer (R=164 mm).*

Studies of a Separator Dipole Magnet for Tagging Experiments for Photon-Induced Transmutation at ELBE [E]

F. Dohrmann, A. Sytcheva, E. Grosse [1]

The ELBE electron linac provides, in addition to primary electrons, high intensity and highly collimated secondary beams. Irradiating a probe with electrons or photons from bremsstrahlung may be desirable for applications in nuclear physics, cross sections for transmutation as well as studying structural defects and ageing due to high radioactive doses within material.

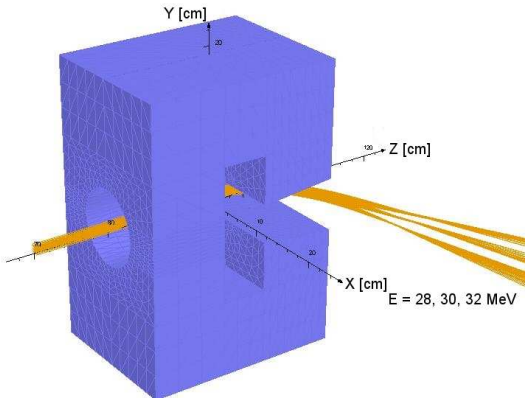

Fig. 1 *Simulation of a clam magnet with rectangular pole shoes. The average magnetic flux density was ∼ 0.8 T, average gap 5 cm (note the clam design). Electron beams of 28–32 MeV are shown.*

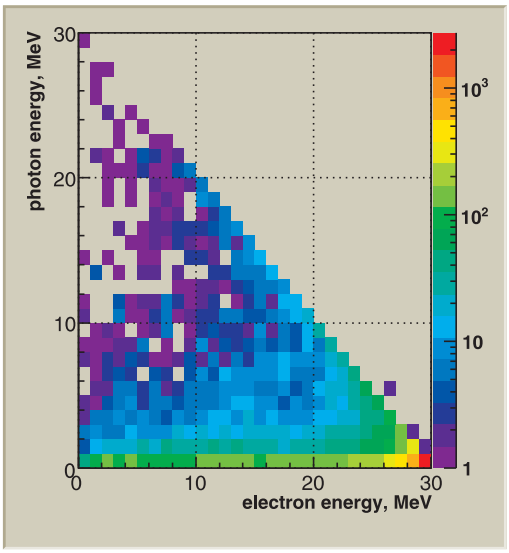

Fig. 2 *Simulation of bremsstrahlung produced on a 0.2 mm Be foil by 30 MeV electrons after a dipole magnet similar as in Fig. 1. The correlation between the electron and bremsstrahlung photon energies is shown.*

In order to separate bremsstrahlung photons from electrons, a conceptual design of a dedicated separator magnet was started and continued. This dipole magnet should be part of a spectrometer setup with which photons may be energetically marked by measuring the residual energy of the electrons, which have undergone bremsstrahlung.

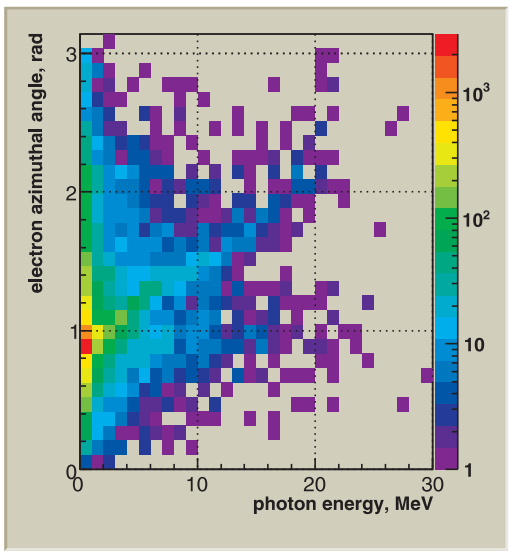

Fig. 3 *Same setup as in Fig. 2. Shown is the correlation between azimuthal angle in radians and energy of bremsstrahlung photons.*

Using the Opera-3D/TOSCA [1] program package several configurations were simulated. A possible use of non-flat pole shoes (clam design) may provide additional focussing. Since space is limited, the yoke of the magnet may be designed with a hole through which the electron beam is directed. Such a configuration is displayed in Fig. 1. The solution (field map) of the simulation result is then extracted and used for further simulations. Using the program package Geant4 a realistic setup of experimental conditions at the ELBE beam may be studied, including beam divergences, material properties etc. In a first step, a dipole magnet has been simulated and correlations of electron and photon energy as well as electron angle and photon energy are displayed in Figs. 2 and 3. The bremsstrahlung takes place in a Be foil of thickness 0.2 mm.

[1] Opera-3D user guide, Vector Fields Ltd., Oxford, England
http://www.vectorfields.co.uk

[2] S. Agostinelli et al. (Geant4 collaboration), Nucl. Instr. Meth. A 506 (2003) 250
http://geant4.web.cern.ch/geant4/

[1] *also TU Dresden*

Testing the Performance of Timing MRPC Detectors at ELBE [E]

R. Kotte, F. Dohrmann, J. Hutsch, L. Naumann, D. Stach

Published in Nucl. Instr. Meth. A 564 (2006) 155-163

The timing performance of multigap resistive plate chambers (MRPCs) [1-7] has been tested at the Rossendorf electron linac ELBE. Electrons with energies of 20 - 40 MeV have been used to mimic minimum ionizing hadrons to be detected in large-scale time-of-flight (TOF) detectors for future heavy-ion collision experiments. Referencing the TOF measurement to the accelerator radio frequency, no fast start detector was necessary. A typical time resolution (including contributions from front-end electronics) of about 70 ps has been achieved for individual strips of the multistrip-anode MRPCs. Rate dependencies and detection efficiencies have been investigated.

[1] P. Fonte et al., Nucl. Instr. Meth. A 443 (2000) 201
[2] P. Fonte et al., Nucl. Instr. Meth. A 449 (2000) 295
[3] A. Blanco et al., Nucl. Instr. Meth. A 485 (2002) 328
[4] M. Petrovici et al., Nucl. Instr. Meth. A 487 (2002) 337
[5] M. Petrovici et al., Nucl. Instr. Meth. A 508 (2003) 75
[6] A. Schüttauf, Nucl. Instr. Meth. A 533 (2004) 65
[7] A. Schüttauf, Nucl. Phys. B (Proc. S.) 158 (2006) 52

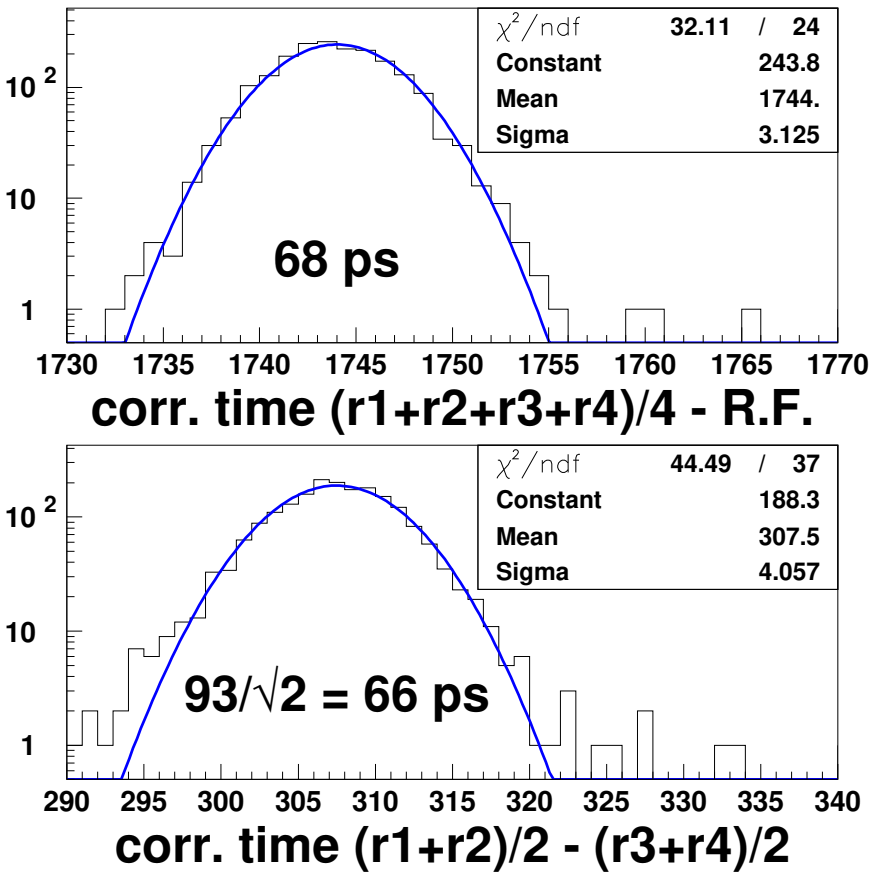

Upper panel: The mean timing w.r.t. the accelerator RF of four (time slewing corrected) signals from two strips of two identical MRPCs built in the detector laboratory of the Institute of Radiation Physics. For the given resolution a 34 ps contribution of the TDC resolution is quadratically subtracted. Lower panel: The time resolution of the difference between the mean timing of two strips from different MRPCs (full lines: Gaussian fits, TDC time slope 24.5 ps/ch).

Dipole Response of ^{88}Sr up to the Neutron-Separation Energy [D]

R. Schwengner, G. Rusev, N. Benouaret, R. Beyer, M. Erhard, E. Grosse, A.R. Junghans, J. Klug, K. Kosev, L.K. Kostov, C. Nair, N. Nankov, K.D. Schilling, A. Wagner

Submitted to Phys. Rev. C

The detailed understanding of the response of atomic nuclei to photons has received increasing attention in recent years. Information on the low-energy tail of the Giant Dipole Resonance is important for an estimate of the effect of high temperatures during the formation of heavy elements in the cosmos. In particular, reaction rates in the so-called p-process are influenced by the behaviour of dipole-strength distributions close to the neutron-separation energy S_n [1]. This behaviour may be affected by excitations like the Pygmy Dipole Resonance (see, e.g., Refs. [2, 3]).

The bremsstrahlung facility [3] at the superconducting electron accelerator ELBE of the research center Dresden-Rossendorf opens up the possibility to study the dipole response of the stable nuclei with even the highest neutron-separation energies in photon-scattering experiments. In the course of a systematic study of dipole-strength distributions for varying neutron and proton numbers in nuclei around $A = 90$ we started with the magic $N = 50$ nuclide ^{88}Sr. Bremsstrahlung was produced with electron beams of 9.0 and 13.2 MeV kinetic energy and with average currents of 520 μA and 400 μA hitting radiators consisting of niobium foils of 4 μm and 7 μm thickness, respectively. Gamma rays were measured with two HPGe detectors placed at 90° and two at 127° relative to the photon beam. Ground-state transitions have been identified by comparing the transitions observed at different electron energies. 160 levels were identified with a total dipole strength of 201 meV/MeV[3]. Spin $J = 1$ could be deduced from the angular correlations of the ground-state transitions for about 90 levels including 84% of the total dipole strength. A measurement of linear polarizations of the γ rays by using polarized bremsstrahlung reveals that almost all transitions with energies greater than 6 MeV are $E1$ transitions. These $E1$ transitions comprise about 63% of the total dipole strength of all ground-state transitions.

The intensity distribution obtained from the measured spectra after a correction for detector response and a subtraction of atomic background in the target contains a continuum part in addition to the resolved peaks. It turns out that the dipole strength in the resolved peaks amounts to about 77% of the dipole strength in the continuum. In order to estimate the intensities of inelastic transitions to low-lying levels we have applied statistical methods [3]. By means of simulations of γ-ray cascades intensities of branching transitions could be removed from this intensity distribution and the intensities of ground-state transitions could be corrected for their branching ratios.
A comparison of the photoabsorption cross section obtained in this way from the present (γ, γ') experiments with (γ, n) data shows a smooth connection of the data of the two different types of experiments and gives new information about the extension of the dipole-strength distribution towards energies around and below the threshold of the (γ, n) reaction. In comparison with a simple approximation of the Giant Dipole Resonance by a Lorentz curve one observes extra dipole strength in the energy range from 6 to 11 MeV which may be considered of a Pygmy Dipole Resonance.

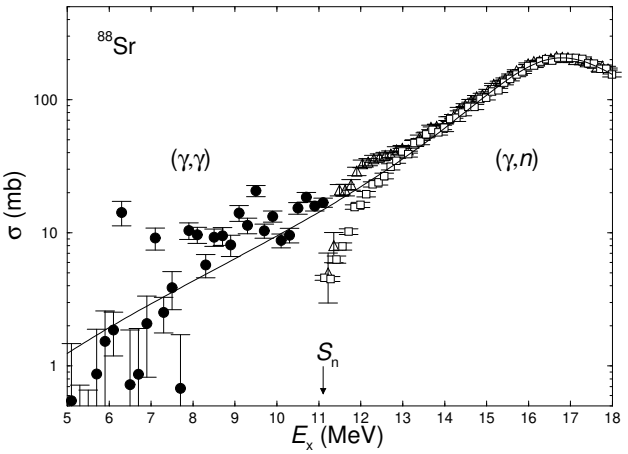

Fig. 1 *Photoabsorption cross section deduced from the present (γ, γ') data for ^{88}Sr after correction for branching transitions (filled circles) in comparison with (γ, n) data taken from Ref. [6] (open triangles) and Ref. [7] (open squares). The solid line is a Lorentz curve with the parameters $E_0 = 16.8$ MeV, $\Gamma = 4.0$ MeV and $\sigma_0 = 206$ mb which are consistent with the Thomas-Reiche-Kuhn sum rule [8] resulting in $\sigma_0 = 2/(\pi\Gamma) \cdot 60NZ/A$ mb.*

[1] M. Arnould and S. Goriely, Phys. Rep. 384 (2003) 1
[2] S. Goriely, Phys. Lett. B 436 (1998) 10
[3] A. Zilges, M. Babilon et al., Progr. Part. Nucl. Phys. 55 (2005) 408
[4] R. Schwengner, R. Beyer et al., Nucl. Instr. Meth. A 555 (2005) 211
[5] G. Rusev, Thesis, TU Dresden 2007, unpublished
[6] A. Lepretre, H. Beil et al., Nucl. Phys. A 175 (1971) 609
[7] A. M. Goryachev and G. N. Zalesnyy, Vopr. Teor. Yad. Fiz. 8 (1982) 121
[8] P. Ring and P. Schuck, in *The Nuclear Many Body Problem*, (Springer, New York, 1980)

Dipole-Strength Distributions in the Stable Even-Mass Mo Isotopes [D]

G. Rusev, R. Schwengner, M. Erhard, E. Grosse[1], A. R. Junghans, K. Kosev, K. D. Schilling, A. Wagner

Part of PhD thesis G. Rusev

Dipole-strength distributions in the stable even-mass Mo isotopes up to the neutron-separation energies have been studied in photon-scattering experiments at the superconducting electron accelerator ELBE. The measurements were performed at identical experimental conditions for an electron-beam energy of 13.2 MeV. Since only about 30 % of the strength is located in the identified peaks a novel method for analysis of the measured spectra was developed [1] in order to determine the total dipole strength below the neutron-separation energy. The measured spectra of scattered photons were corrected for detector response and atomic background obtained from simulations using the code GEANT3 [2]. Simulations of γ-ray cascades [1] were performed in order to correct the transition intensities for feeding from higher-lying levels and to deduce the branching ratios for transitions to the ground state. The cross sections resulting from this correction method for stable even-mass Mo isotopes are directly compared to nuclear photo effect data from literature [3] in Fig. 1 resulting in a photoabsorption cross section covering the full range from 4 to above 15 MeV, which is of interest for nuclear astrophysics network calculations. The dipole strength from the photon-scattering experiments on the even-mass Mo isotopes is compared with results for the dipole strength in the neighbouring odd-mass Mo isotopes obtained from (n,γ) experiments [4] (cf. Fig. 1). Novel information about the low-energy tail of the Giant Dipole Resonance (GDR) and the energy spreading of its strength can be derived. We represent the photoabsorption cross section σ_γ of the GDR as a superposition of three Lorentzian functions:

$$\sigma_\gamma = \frac{2S_{\mathrm{TRK}}}{3\pi} \sum_{i=1}^{3} \frac{E_x^2 \Gamma_0}{(E_x^2 - E_i^2)^2 + E_x^2 \Gamma_0^2}, \qquad (1)$$

where the cross section integral is given by the Thomas-Reiche-Kuhn sum rule: $S_{\mathrm{TRK}} = \int \sigma_\gamma dE = 60ZN/A$ mb MeV. The width Γ_0 is selected to be 4 MeV from the parametrisation of the GDR in the spherical nuclei ^{92}Mo and ^{88}Sr [5]. The maxima E_i of the three Lorentzian curves are calculated according to the Nilsson model [6]:

$$E_i = E_0 \left(1 - \frac{2}{3} \varepsilon \cos\left(\gamma - \frac{2\pi i}{3} \right) \right), \qquad (2)$$

where the deformation parameters ε and γ are taken from our previous investigation on the $M1$ strength in the stable even-mass Mo isotopes [7] and E_0 is a parameter describing the energy of the maximum of the GDR.

[1] *also TU Dresden*

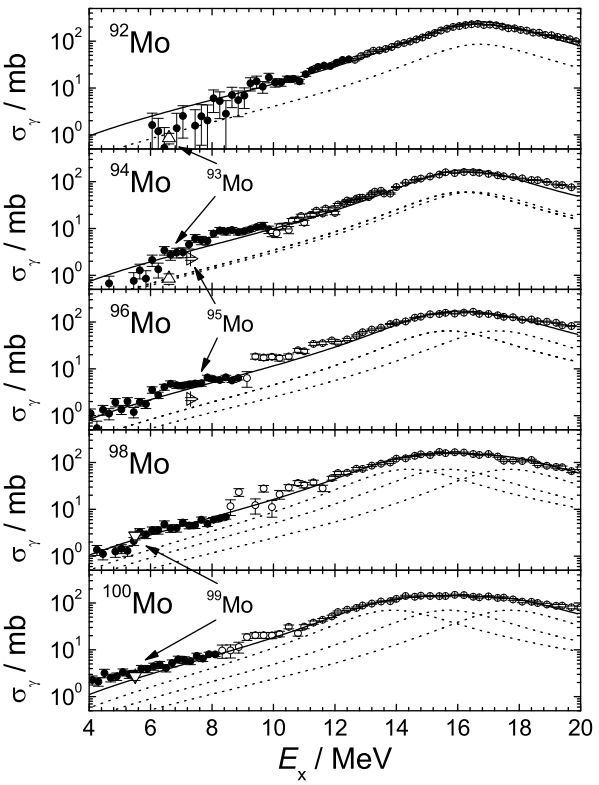

Fig. 1 *Photoabsorption cross sections in the stable even-mass Mo isotopes. The results from our photon-scattering experiments (filled circles) are combined with (γ,n) cross sections [3] (open circles) and compared with the dipole strength in the neighbouring odd-mass Mo isotopes (open triangles) obtained from (n,γ) experiments [4]. A parametrisation of the GDR (solid lines) resulting from a superposition of three Lorentzian curves (dashed lines) is compared with the experimental data.*

The presented results for the photoabsorption cross section and parametrisation of the low-energy tail of the GDR allow an extension of the knowledge for the shape of the GDR to exotic nuclei, which is of importance for a more precise modelling of astrophysical processes.

[1] R. Schwengner, N. Benouaret, at al., Nucl. Phys. A (2007), in print

[2] CERN Program Library Long Writeup W5013, Geneva 1993, unpublished

[3] H. Beil, R. Bergère et al., Nucl. Phys. A 277 (1974) 427

[4] J. Kopecky and M. Uhl, IAEA, Bologna, 1994

[5] R. Schwengner, G. Rusev, et al., Phys. Rev. C, submitted

[6] S. G. Nilsson and I. Ragnarsson, "Shapes and Shells in Nuclear Structure", Cambridge University Press, 1995

[7] G. Rusev, R. Schwengner et al., Phys. Rev. C 73 (2006) 044308

Origin of the Magnetic Dipole Strength in the Stable Even-Mass Mo Isotopes [D]

G. Rusev, R. Schwengner, F. Dönau, M. Erhard, S. Frauendorf, E. Grosse, A.R. Junghans, L. Käubler, K. Kosev, L.K. Kostov, S. Mallion, **K.D. Schilling, A. Wagner**, H. von Garrel, U. Kneissl, C. Kohstall, M. Kreutz, H.H. Pitz, M. Scheck, F. Stedile, P. von Brentano, J. Jolie, A. Linnemann, N. Pietralla, V. Werner

Published in Phys. Rev. C 73 (2006) 044308, 1-12

The nuclides ^{92}Mo, ^{98}Mo and ^{100}Mo were investigated in photon-scattering experiments with bremsstrahlung. Various electron-beam energies were used in order to resolve branching transitions in ^{98}Mo and ^{100}Mo. Five $J = 1$ states up to $E_x = 4$ MeV in ^{98}Mo and 14 in ^{100}Mo were observed for the first time. The transition strengths deduced from the present experiments for ^{92}Mo, ^{98}Mo, and ^{100}Mo together with known values for ^{94}Mo [1, 2] and ^{96}Mo [3] allowed us to study the systematics of the low-lying magnetic dipole excitations in the chain of stable even-even Mo isotopes. The results of the present study have been published in Ref. [4].

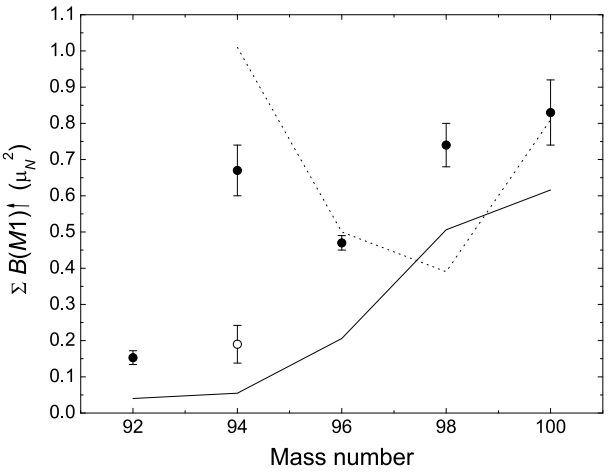

Fig. 1 *Comparison of the experimental summed $M1$ strengths up to 4 MeV (filled circles) with predictions of the QRPA calculations (solid line) and the shell-model calculations (dotted line). The open circle represents the $M1$ strength in ^{94}Mo without the contribution of the four-particle state.*

The experimental results are compared with predictions of QRPA calculations in a deformed basis, and with predictions of the shell model in Fig. 1. The QRPA calculations reproduce the growing and the spread of the $M1$ strength with increasing neutron number. As a result of the QRPA calculations we found the $M1$ strengths in the nearly spherical nuclei to be generated by isovector-spin vibrations only while the $M1$ strengths in the deformed nuclei are a combination of isovector-orbital vibrations and isovector-spin vibrations. The shell-model calculations especially reproduce the large $M1$ strength in ^{94}Mo as caused by a special four-particle configuration that is outside the scope of the QRPA.

In addition to the energy range covered by the present experiments we have performed QRPA calculations up to an excitation energy of 10 MeV. The predicted $M1$-strength distributions are shown in Fig. 2. The contributions of isovector-orbital vibrations to the total $M1$ strengths in the spherical ^{92}Mo and the deformed ^{100}Mo are depicted in Fig. 2.

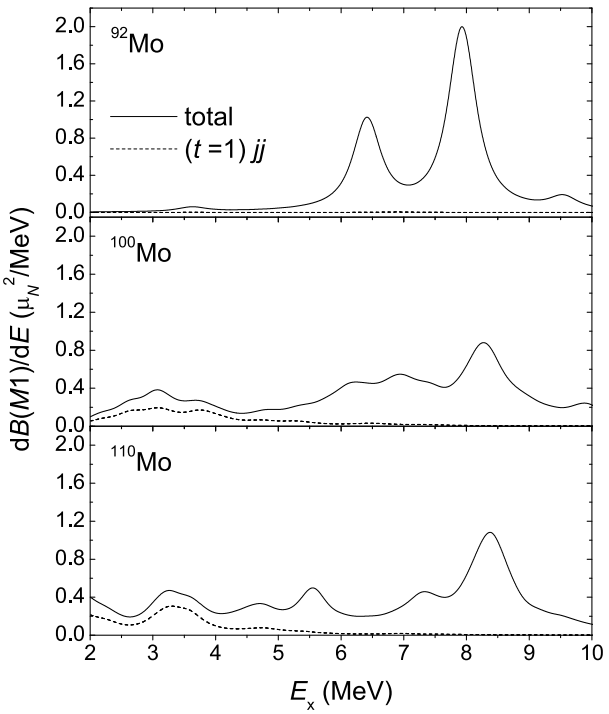

Fig. 2 *Contributions of different types of vibrations to the $M1$-strength distributions in ^{92}Mo (top), ^{100}Mo (middle), and ^{110}Mo (bottom) as predicted from QRPA. The solid lines represent the total strengths while the dashed lines show the isovector-orbital contributions.*

[1] N. Pietralla, C. Fransen et al., Phys. Rev. Lett. 83 (1999) 1303

[2] C. Fransen, N. Pietralla et al., Phys. Rev. C 67 (2003) 024307

[3] C. Fransen, N. Pietralla et al., Phys. Rev. C 70 (2004) 044317

[4] G. Rusev, R. Schwengner et al., Phys. Rev. C 73 (2006) 044308

Effect of Nuclear Deformation on the Electric Dipole Strength in the Particle-Emission-Threshold Region [D]

F. Dönau, G. Rusev, R. Schwengner, A.R. Junghans, K.D. Schilling, A. Wagner

Submitted to Phys. Rev. C

The role of nuclear deformation for the photoabsorption cross section in the tail region of the electric Giant Dipole Resonance (GDR) is studied in terms of a deformed oscillator model and a Nilsson-plus-random-phase-approximation model. It is found within the framework of these approaches that extra electric dipole strength is generated at energies below the GDR maximum if the nuclear system is spatially deformed. This is important for the prediction of the stellar photodisintegration rates knowing that an extra strength can affect these rates even below the particle separation energies through the so-called γ process. Because the nuclear deformation is governed by shell effects this extra strength does not directly correlate with neutron excess.

The effect of the deformation on the photoabsorption cross section is shown in Fig. 1 for the isotopic chain of stable even-even mass samarium isotopes starting at the spherical ^{144}Sm ($N = 82$) and ending at the deformed ^{154}Sm. Fig. 2 compares calculations with and without deformation for the isotopic chain of stable even-even molybdenum isotopes. This comparison clearly demonstrates that the increase of $E1$ strength in the energy range from 8 to 14 MeV while going from the shell closure at ^{92}Mo ($N = 50$) to the heavier isotopes is caused by increasing deformation. This predicted increase of $E1$ strength is consistent with experimental results of recent systematic photon-scattering experiments performed for the Mo isotopes at the ELBE accelerator [3].

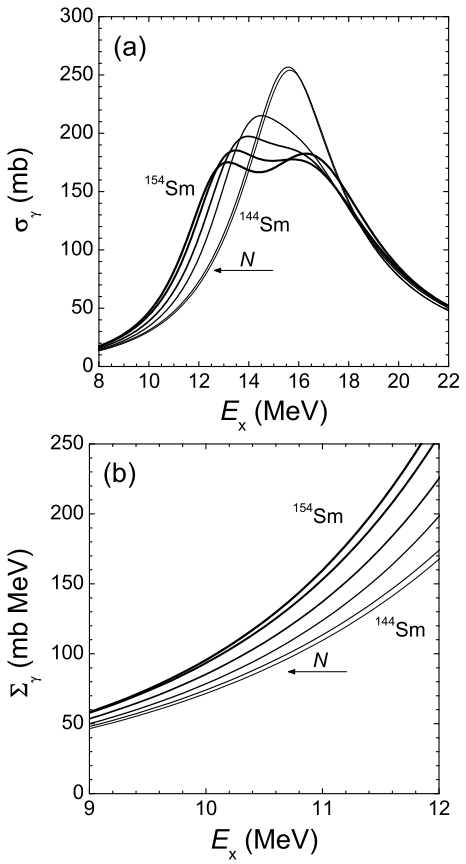

(a) The photoabsorption cross sections of $^{144-154}$Sm calculated in the oscillator approximation adopting the deformation parameters from Ref. [1] and using a Lorentzian-like level broadening (see text). (b) The integrated cross sections of even-even Sm isotopes $\Sigma_\gamma(E_x) = \int_0^{E_x} \sigma_\gamma(E')dE'$ in the interval E_x = 9 – 12 MeV.

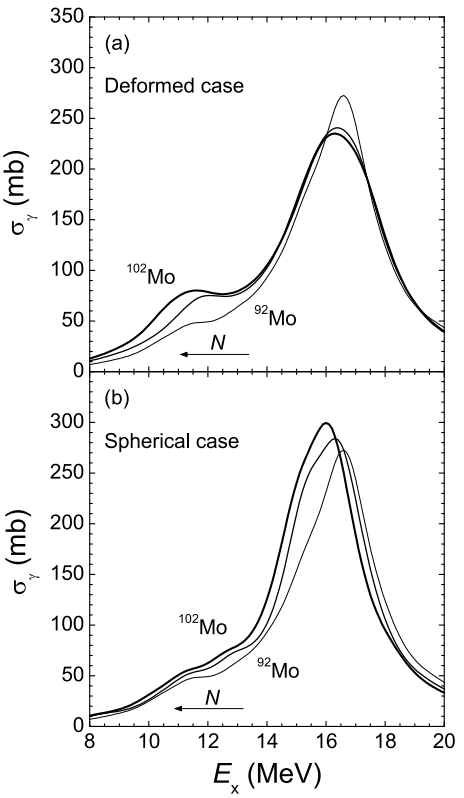

Calculated photoabsorption cross sections σ_γ for ^{92,98,102}Mo (a) including deformation parameters as used in Ref. [2] and (b) assuming spherical shapes.

[1] P. Möller, J. R. Nix, W. D. Myers, and W. J. Swiatecki, At. Data Nucl. Data Tables 59 (1995) 185

[2] G. Rusev, R. Schwengner et al., Phys. Rev. C 73 (2006) 044308

[3] G. Rusev, R. Schwengner et al., contribution to this report, p. 40

Low-Lying $E1$, $M1$, and $E2$ Strengths in ^{124,126,128,129,130,131,132,134,136}Xe: Systematic Photon Scattering Experiments in the Mass Region of a Nuclear Shape or Phase Transition[D]

H. v. Garrel, P. v. Brentano, C. Fransen, G. Friessner, N. Hollmann, J. Jolie, F. Käppeler, **L. Käubler**, U. Kneissl, C. Kohstall, L. Kostov, A. Linnemann, D. Mücher, N. Pietralla, H.H. Pitz, **G. Rusev**, M. Scheck, **K.D. Schilling**, C. Scholl, **R. Schwengner**, F. Stedile, S. Walter, V. Werner, K. Wisshak

Published in Phys. Rev. C 73 (2006) 054315, 1-20

Nuclear shape or phase transitions are a current topic in nuclear structure physics. The properties of spherical, axially deformed, and γ-soft even-even nuclei can well be described in the framework of algebraic models in the dynamical symmetry limits of U(5), SU(3), and O(6), as is well known [1]. Moreover, three newly introduced so-called critical-point symmetries [2] allow the description of nuclei in mass regions of nuclear phase or shape transitions. Nuclei at critical points should exhibit dramatic changes in their structure and hence of the experimental observables, such as level orderings, γ-transition probabilities, and branchings of the deexcitation paths. The Xe isotopic chain crosses the U(5), E(5) values and reaches the O(6) limit. Therefore, this chain provides a unique case to investigate systematically the changes of spectroscopic observables expected for shape or phase transitions near critical points.

The Xe isotopes were studied in photon-scattering experiments using the bremsstrahlung facility at the Dynamitron accelerator of the Stuttgart University [15] at an electron energy of 4.1 MeV. For the first time in photon-scattering experiments thin-walled high-pressure target cells were used containing isotopically enriched Xe gas of about 70 bar. The cells were delivered by Forschungszentrum Karlsruhe [4].

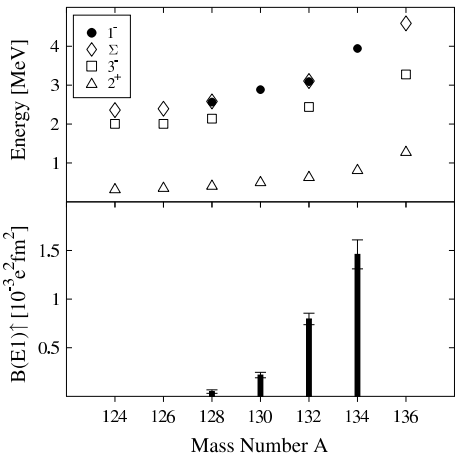

Fig. 1 *Systematics of $2^+ \otimes 3^-$ two-phonon excitations in the even-even Xe isotopes. Upper part: Experimental energies of the 2^+ (open triangles), 3^- (open squares) states and of the observed 1^- two-phonon states (filled circles) in $^{124-136}$Xe compared to the energy sums $\Sigma = E_{2^+} + E_{3^-}$ (open rhombs). Lower part: Experimental $B(E1)\uparrow$ values for the two-phonon excitations.*

Systematics of the 1^- members of $2^+ \otimes 3^-$ two-phonon excitations as resulting from the present work are shown in Fig. 1. The steep decrease of $B(E1)\uparrow$ strengths observed when moving away from the closed shell at $N = 82$ (^{136}Xe) is reproduced by Quasiparticle-Phonon-Model calculations [5, 6].

Systematics of candidates of 1^+ mixed-symmetry states are shown in Fig. 2. The total $B(M1)\uparrow$ strengths exhaust the IBA predictions in the O(6) limit [7] for the light isotopes up to ^{128}Xe but deviate from these predictions for the heavier isotopes which may be a hint for a phase transition near $A = 130$.

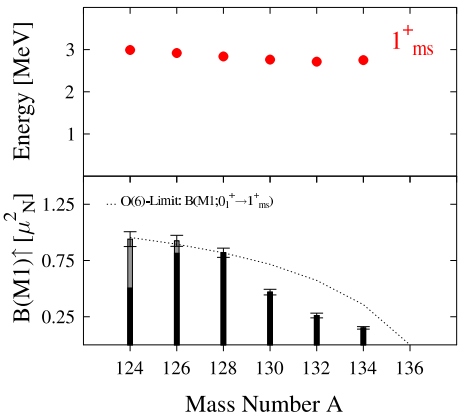

Fig. 2 *Systematics of the candidates for mixed-symmetry $1^+_{\rm ms}$ states in the even-even Xe isotopes versus mass number A. Upper part: Excitation energies. Lower part: $B(M1)\uparrow$ excitation strengths. The dotted line gives the strengths predicted by the IBM-2 model in the O(6) limit. The grey areas in the bars for ^{124,126}Xe represent the summed strengths of the fragments of the $M1$ excitations.*

[1] R. F Casten, *Nuclear structure from a simple perspective*, Oxford University Press, New York, Oxford (1990)
[2] F. Iachello, Phys. Rev. Lett. 85 (2000) 3580; 87 (2001) 052502; 91 (2003) 132502
[3] U. Kneissl, H.H. Pitz and A. Zilges, Prog. Part. Nucl. Phys. 37 (1996) 349
[4] R. Reifarth, M. Heil et al., Phys. Rev. C 66 (2002) 064603
[5] M. Grinberg and Ch. Stoyanov, Nucl. Phys. A 573 (1994) 231
[6] V. Yu. Ponomarev, Ch. Stoyanov et al., Nucl.Phys. A 635 (1998) 470
[7] P. van Isacker, K. Heyde et al., Ann. Phys. (N.Y.) 171 (1986) 253

Quadrupole Moment of the 8^+ Yrast State in ^{84}Kr[E]

R. Schwengner, D.L. Balabanski, G. Neyens, N. Benouaret, D. Borremans, N. Coulier, M. De Rydt, G. Georgiev, S. Mallion, G. Rainovski, **G. Rusev**, S. Teughels, K. Vyvey

Published in Phys. Rev. C 74 (2006) 034309, 1-6

Nuclear moments are very sensitive to the structure of nuclear states and their measurement is therefore a stringent test of nuclear models. States with a structure dominated by a few nucleons outside a closed shell are good candidates for tests of predictions of the shell model. In particular, effective g factors and effective charges accounting for the influence of orbits not included in the model space may be examined.

The quadrupole moment of the 8^+ yrast isomer (τ = 2.65(6) μs) in ^{84}Kr was measured at the CYCLONE facility in Louvain-la-Neuve using level-mixing spectroscopy (LEMS) [1, 2]. In a LEMS experiment recoiling nuclei are implanted into a suitable host with a non-cubic lattice, where they experience a combined electric quadrupole and magnetic dipole interaction. A split-coil superconducting magnet provides an external magnetic field of up to $B = 4.4$ T which is oriented parallel to the beam axis and thus coincides with the normal vector of the plane in which the spins are oriented after a fusion-evaporation reaction. At low strength of the magnetic field, the electric quadrupole interaction between the electric field gradient, V_{zz}, and the quadrupole moment of the isomer of interest, Q, dominate, and destroy the initial spin orientation. At a high magnetic field this interaction is negligible in comparison to the magnetic dipole interaction, and the spins perform a Larmor precession around the magnetic field $\vec{B}$. As the magnetic field is along the normal vector of the spin-orientation plane, a high field leads to an anisotropy of the intensities of isomeric transitions at 0° and 90° relative to the beam as induced by the spin alignment produced in a fusion-evaporation reaction. The anisotropy is measured as a function of the magnetic field, giving rise to the LEMS curve, which yields the ratio of the electric quadrupole frequency, $\nu_Q = eQV_{zz}/h$, to the magnetic interaction frequency, $\nu_\mu = \mu B/hJ$. From the LEMS curve measured in the present experiment we have deduced a quadrupole moment of $Q = 36(4)e\mathrm{fm}^2$ for the 8^+ yrast state in ^{84}Kr. Experimental quadrupole moments of ^{84}Kr and neighboring nuclei [5] are compared with predictions of the shell model in Fig. 1. Shell-model calculations were performed with a model space including the active proton orbits $\pi(0f_{5/2}, 1p_{3/2}, 1p_{1/2}, 0g_{9/2})$ and neutron orbits $\nu(1p_{1/2}, 0g_{9/2}, 1d_{5/2})$ relative to a hypothetic ^{66}Ni core using a combination of various empirical interactions and surface delta interactions. For details see, e.g., Refs. [3, 4]. Various sets of effective charges used in the literature have been applied: $e_\pi = 1.35e$, $e_\nu = 0.35e$ (SM1); $e_\pi = 1.72e$, $e_\nu = 1.44e$ (SM2). While the quadrupole moment in ^{84}Kr deduced in the present work is well reproduced with set SM1, the general behaviour of the quadrupole moments shows that e_π is too large in SM2 and e_ν is too small in SM1. Therefore, we applied a modified set of $e_\pi = 1.35e$, $e_\nu = 1.0e$ (SM1N) which improves the overall agreement between calculated and experimental quadrupole moments of the neutron-dominated states (see Fig. 1).

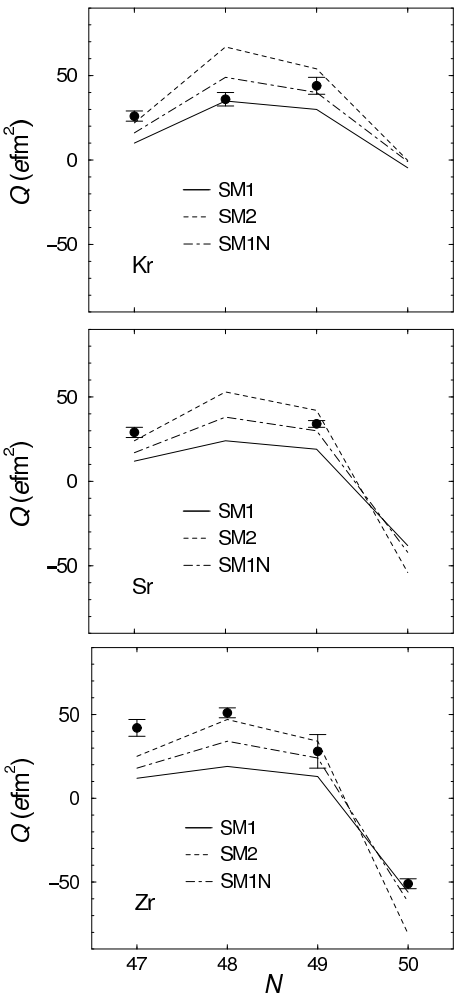

Fig. 1 *Comparison of experimental and calculated quadrupole moments for $9/2^+$ and 8^+ states in the Kr, Sr and Zr isotopes with N = 47 – 50. The calculations were performed with different sets of effective charges (see text).*

[1] F. Hardeman, G. Schevenfeels et al., Phys. Rev. C 43 (1991) 130
[2] G. Neyens, Rep. Prog. Phys. 66 (2003) 633
[3] G. Winter, R. Schwengner et al., Phys. Rev. C 49 (1994) 2427
[4] R. Schwengner, J. Reif et al., Phys. Rev. C 57 (1998) 2892
[5] N.J. Stone, At. Data Nucl. Data Tables 90 (2005) 75

Beta Decay of ^{101}Sn [G]

O. Kavatsyuk, C. Mazzocchi, Z. Janas, A. Banu, L. Batist, F. Becker, A. Blazhev, W. Brüchle, J. Döring, T. Faestermann, M. Górska, H. Grawe, A. Jungclaus, M. Karny, M. Kavatsyuk, O. Klepper, R. Kirchner, M. La Commara, K. Miernik, I. Mukha, C. Plettner, A. Pł'ochocki, E. Roeckl, M. Romoli, K. Rykaczewski, M. Schädel, K. Schmidt, **R. Schwengner**, J. Żylicz

Published in Eur. Phys. J. A 31 (2007) 319-325

The measurement of properties of doubly-magic nuclei and their closest neighbours is of great interest as it provides information on the underlying shell structure. Concerning the closest neighbours of the heaviest particle-stable self-conjugated nucleus $^{100}_{50}$Sn, namely $^{99}_{49}$In, $^{99}_{50}$Sn, $^{101}_{50}$Sn and $^{101}_{51}$Sb, only one of them is known so far: ^{101}Sn. The scarce experimental information available on this nucleus stems from studies of its β^+/EC decay [1, 2] or from investigating the α-decay chains ^{105}Te$\rightarrow^{101}$Sn [3] and ^{109}Xe$\rightarrow^{105}$Te$\rightarrow^{101}$Sn [4]. In order to approach experimentally these nuclei, heavy-ion induced fusion-evaporation reactions have been found to be a suitable production mechanism.

The nuclide ^{101}Sn was produced at the GSI on-line mass separator [5] by using the ^{50}Cr(^{58}Ni,α3n)^{101}Sn fusion-evaporation reaction. A ^{58}Ni beam provided by the linear accelerator UNILAC impinged on a ^{50}Cr target (3 mg/cm^2, enriched to 97%).

In a βp experiment the mass-separated beam was periodically switched between two carbon foils in consecutive grow-in (12 s) and decay (12 s) intervals, the collected βp activity being recorded by two identical ΔE-E Si-detector telescopes. The ΔE singles and ΔE-E coincidence events were tagged by the time elapsed since the start of each 24 s cycle. The resulting time profiles were used to determine the half-life of ^{101}Sn.

In the $\beta\gamma$ experiment, three Si detectors were placed in a cube-like geometry inside of a small vacuum chamber. The other three sides of the cube, which remained open, were used to let the beam pass onto a tape in the centre of the cube and to guide the tape to the implantation position and away from it. Around the Si-detector setup two GSI VEGA-Super Clover detectors and a small Clover detector were mounted. The measurement was performed in grow-in mode, *i.e.* during the time when the mass-separated ion beam was continuously implanted into the tape at rest. After a pre-selected time of 8 s the implanted activity was removed from the implantation position.

Based on the measurement of β-delayed protons the half-life of ^{101}Sn was determined to be $T_{1/2} = 1.9(3)$ s. This result is in good agreement with but considerably more accurate than the previously obtained values of 3(1) s [1] and 1.5(6) s [2].

As a result of the measurement of $\beta - \gamma$ and $\gamma - \gamma$ coincidences, β-delayed γ rays following the decay of ^{102}Sn were tentatively assigned for the first time, yielding weak evidence for a cascade of 352 and 1065 keV transitions in ^{101}In.

The decay scheme of ^{102}Sn including the two tentative transitions is shown in Fig. 1 and compared with the results of shell-model calculations. In these calculations, the model space $\pi(p_{1/2}, g_{9/2})$ $\nu(d_{5/2}, g_{7/2}, d_{3/2}, s_{1/2}, h_{11/2},)$ was used with respect to ^{88}Sr as an inert core and a newly developed interaction [6] was applied.

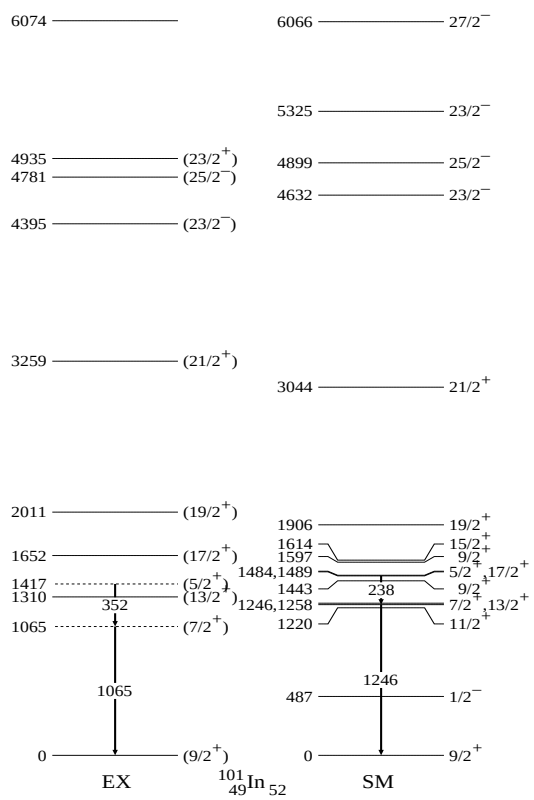

Fig. 1 *Experimental and shell-model high-spin yrast and low-energy low-spin states in ^{101}In. The newly assigned tentative γ-ray cascade observed in the present work and possible shell model predictions are shown, too.*

[1] Z. Janas et al., Phys. Scr. T 56 (1995) 262
[2] A. Stolz, Ph.D. Thesis, TU München (2001)
[3] D. Seweryniak et al., Phys. Rev. C 73 (2006) 061301(R)
[4] S.N. Liddick et al., Phys. Rev. Lett. 97 (2006) 082501
[5] E. Roeckl et al., Nucl. Instr. Meth. B 204 (2003) 53
[6] H. Grawe, to be published

Beta Decay of the Proton-Rich Nuclei ^{102}Sn and ^{104}Sn [G]

M. Karny, L. Batist, A. Banu, F. Becker, A. Blazhev, W. Brüchle, J. Döring, T. Faestermann, M. Górska, H. Grawe, Z. Janas, A. Jungclaus, M. Kavatsyuk, O. Kavatsyuk, R. Kirchner, M. La Commara, S. Mandal, C. Mazzocchi, K. Miernik, I. Mukha, S. Muralithar, C. Plettner, A. Pł'ochocki, E. Roeckl, M. Romoli, K. Rykaczewski, M. Schädel, K. Schmidt, **R. Schwengner**, J. Żylicz

Published in Eur. Phys. J. A 27 (2006) 129-136

Beta decays of nuclei close to ^{100}Sn with $Z \leq 50$ and $N \geq 50$ are characterised by large decay energies and pure Gamow-Teller (GT) transitions between $\pi g_{9/2}$ and $\nu g_{7/2}$ orbits. These features make studies of these decays especially useful to test the nuclear shell model in general and its predictions of (the quenching of) the GT strength in particular. As the half-life of these nuclei are between fraction of a second and few minutes experiments using on-line mass separation are feasible.

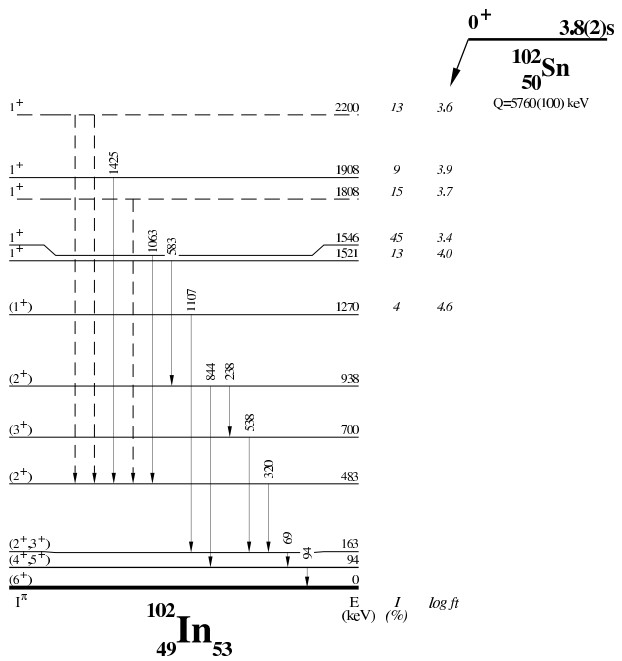

Fig. 1 *Decay scheme of ^{102}Sn established in this work. The γ-ray energies and ^{102}In level energies marked by solid lines represent results from the high-resolution measurement, while dashed lines indicate levels and γ transitions added to the level scheme in order to reproduce the TAS spectrum. The β feeding (I_β) and the comparative half-lives ($log ft$) stem from TAS data.*

In the present experiments, the two isotopes were produced by means of fusion-evaporation reactions between a ^{58}Ni beam delivered by the UNILAC accelerator and a ^{50}Cr target at beam energies between 284 and 302 MeV. After passing the GSI on-line mass separator the ions were directed to either a Total Absorption Spectrometer (TAS) for a β-feeding measurement or to a high-resolution array consisting of one CLUSTER, two CLOVER and two conventional HPGe detectors for measuring γ rays, and of three Si detectors for measuring electrons.

The decay schemes of ^{102}Sn and ^{104}Sn resulting from the present work are shown in Figs. 1 and 2, respectively. The present results have been compared with shell-model calculations using the model space $\pi(p_{1/2}, g_{9/2})^{11}$, $\nu(g_{7/2}, d_{5/2}d_{3/2}, s_{1/2}, h_{11/2})^3$ and the SNC interaction [1, 2].

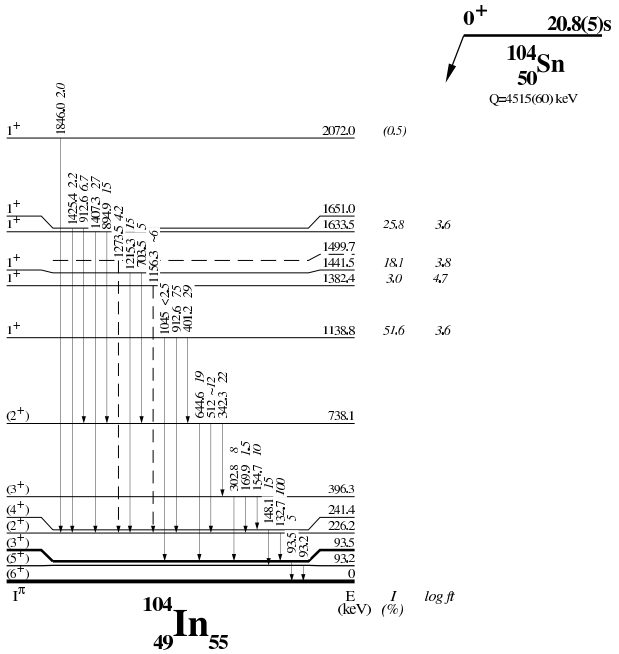

Fig. 2 *Decay scheme of ^{104}Sn. The γ-ray intensities, normalised to that of the 133 keV transition, represent results of the present high-resolution measurement combined with results of Ref. [3]. The β intensities (I_β) and the comparative half-lives ($log ft$) stem from TAS data. Dashed lines indicate tentative assignments.*

[1] B.A. Brown, K. Rykaczewski, Phys. Rev. C 50 (1994) R2270
[2] Z. Hu et al., Phys. Rev. C 62 (2000) 064315
[3] J. Szerypo et al., Nucl. Phys. A 507 (1990) 357

Photon Scattering Experiments on the Quasistable, Odd-Odd Mass Nucleus ^{176}Lu [D]

S. Walter, F. Stedile, J.J. Carroll, C. Fransen, G. Friessner, N. Hollmann, H. von Garrel, J. Jolie, O. Karg, F. Käppeler, U. Kneissl, C. Kohstall, P. von Neumann-Cosel, A. Linnemann, D. Mücher, N. Pietralla, H.H. Pitz, **G. Rusev**, M. Scheck, C. Scholl, **R. Schwengner**, V. Werner, K. Wisshak

Published in Phys. Rev. C 75 (2007) 034301, 1-6

The quasistable odd-odd-mass nucleus ^{176}Lu is of special interest in nuclear structure physics and, moreover, in nuclear astrophysics. This isotope is one of the only nine known stable or quasistable naturally occurring odd-odd mass nuclei. It has a ground-state spin of $J_0^\pi = 7^-$ ($K = 7$) and decays by β^- decay with a halflife of about $4 \cdot 10^{10}$ a [1, 2] to ^{176}Hf. In addition, a low-lying $J^\pi = 1^-, K = 0$ isomer occurs in ^{176}Lu at an excitation energy of 122.9 keV with a halflife of only 3.635 h, which decays also by β^--transitions to ^{176}Hf. Such large spin differences of low-lying levels are common features in heavy odd-odd nuclei and originate from aligned and antialigned couplings of the unpaired protons and neutrons in high-spin Nilsson orbits. In the case of ^{176}Lu these orbits are the $\pi 7/2^+[404]$ and $\nu 7/2^-[514]$ orbits [3]. Because of the long halflife of 40 Ga and the fact that the isotope is shielded against an r-process synthesis, ^{176}Lu was suggested to be an appropriate s-process chronometer [4, 5, 6]. However, answering the question to what extent ^{176}Lu may serve as a cosmic clock or represents rather a stellar thermometer is complicated because of its nuclear structure and depends critically on a possible photoexcitation of the 1^- isomer and its subsequent short-lived 3.635 h β-decay within the photon bath of a stellar s-process scenario [6, 7, 8, 9, 10, 11]. Therefore, the electromagnetic coupling between the ground state and the low-lying isomeric state via low-lying intermediate states (IS) is of fundamental importance for the nucleosynthesis of ^{176}Lu and for tests of stellar models [6, 12, 13]. The possible coupling of these states is illustrated in Fig. 1. IS can be determined from the kinks in the yield curves observed in photoactivation experiments using bremsstrahlung photon beams (see, e.g., Ref. [14]). However, in such experiments the energy determination is limited to an accuracy of about 30 keV. On the other hand, in photon-scattering experiments the excitation energies of such IS can be measured with accuracies of better than 1 keV.

Photon-scattering experiments on ^{176}Lu were performed at the bremsstrahlung facility of the Stuttgart University [15]. Measurements using electron beams of 2.3 and 3.1 MeV delivered by the Dynamitron accelerator were carried out to achieve an optimum sensitivity, in particular in the low-energy range of astrophysical interest.

As a result of the present experiments a total of 29 transitions in ^{176}Lu have been found in the energy range from 1.3 MeV to 2.9 MeV and their transition strengths have been determined. For the lowest proposed IS at 838.6 keV an upper limit for the scattering-cross section integral of $I_s < 1.5$ eVb, corresponding to a minimum lifetime of $\tau \approx 1.5$ ps can be given. This limit is consistent with the result of a GRID measurement [9].

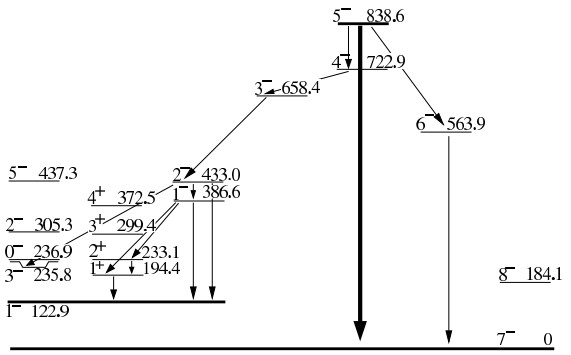

Fig. 1 *Level scheme showing a possible coupling between the ground state of ^{176}Lu and the isomer at 122.9 keV via the IS at 838.6 keV with a spin of 5^- and quantum number $K = 4^-$ (taken from Ref. [8]).*

[1] G.F. Grinyer, J.C. Waddington et al., Phys. Rev. C 67 (2003) 014302
[2] Y. Nir-El and G. Haquin, Phys. Rev. C 68 (2003) 067301
[3] M. S. Basunia, Nucl. Data Sheets 107 (2006) 791
[4] J. Audouze, W.A. Fowler and D. N. Schramm, Nature 238 (1972) 8
[5] M. Arnould, Astron. & Astrophys. 22 (1973) 311
[6] F. Käppeler, H. Beer and K. Wisshak, Rep. Prog. Phys. 52 (1989) 945
[7] N. Klay, F. Käppeler et al., Phys. Rev. C 44 (1991) 2801
[8] N. Klay, F. Käppeler et al., Phys. Rev. C 44 (1991) 2839
[9] C. Doll, H.G. Börner et al., Phys. Rev. C 59 (1999) 492
[10] K.T. Lesko, E.B. Norman et al., Phys. Rev. C 44 (1991) 2850
[11] J. Vanhorenbeeck, J.M. Lagrange et al., Phys. Rev. C 62 (2000) 015801
[12] F. Käppeler, Prog. Part. Nucl. Phys. 43 (1999) 419
[13] D. Belic, C. Arlandini et al., Phys. Rev. Lett. 83 (1999) 5242; Phys. Rev. C 65 (2002) 035801
[14] D. Belic, J. Besserer et al., Nucl. Instr. Meth. A 463 (2001) 26
[15] U. Kneissl, H.H. Pitz and A. Zilges, Prog. Part. Nucl. Phys. 37 (1996) 349

The Two-Step Gamma Cascade Method as a Tool for Studying Photon Strength Functions of Intermediate-Weight and Heavy Nuclei

F. Bečvář, J. Honzátko, M. Krtička, S. Pašić, **G. Rusev**, I. Tomandl

In press in Nucl. Instr. Meth. B

The method of two-step γ cascades (TSC) following the thermal-neutron capture is described. An example of two-step cascade data from measurements with ^{162}Dy target is given (cf. Fig. 1) together with interpretation of this data in terms of scissors-mode resonances built on excited levels in ^{163}Dy (cf. Fig. 2). With the aim of verifying the correctness of the method results of benchmark testing measurements with ^{56}Fe (cf. Fig. 3) are compared with the outcome of the GEANT3 simulations (cf. Fig. 4).

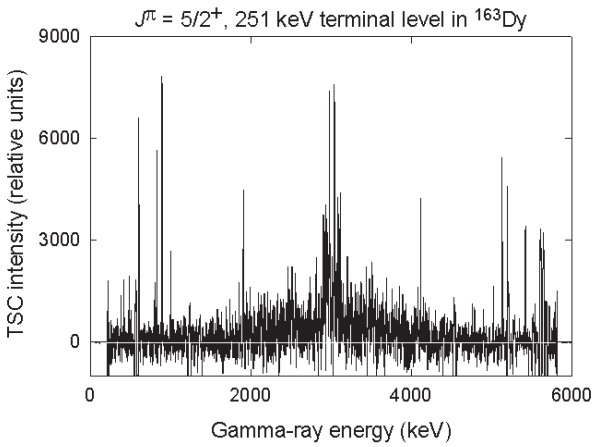

Fig. 1 *An example of a TSC spectrum measured in the thermal $^{162}Dy(n,\gamma)^{163}Dy$ reaction.*

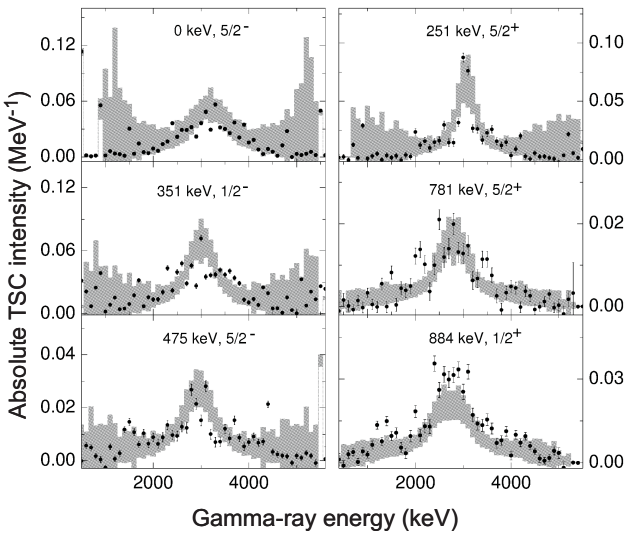

Fig. 2 *TSC spectra for 6 terminal levels in ^{163}Dy (data points) and their comparison with predictions of the statistical model (shaded areas). Energies and J^π values of the levels are indicated.*

The simulations clearly demonstrate that the TSC spectra represent clean data for studying decay properties of the levels in the quasi continuum with excitation energies $E_f + 1.5\text{MeV} < E_x < B_n - 1.5\text{MeV}$.

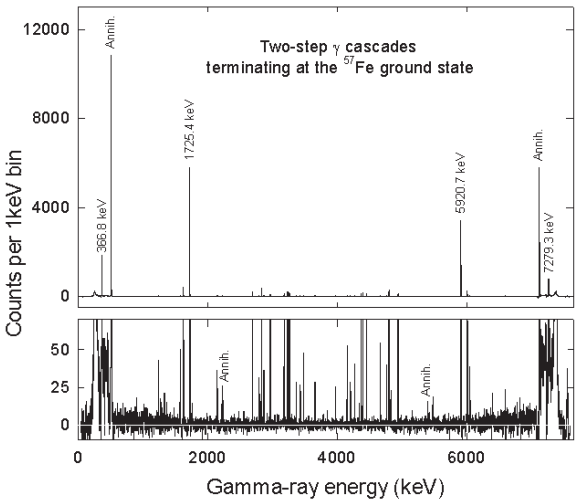

Fig. 3 *The spectrum of TSCs terminating at the ^{57}Fe ground state. Gamma-lines associated with positron annihilation are labeled, as well as lines belonging to the pair of the strong γ cascades. The inherent symmetry of the spectrum is apparent.*

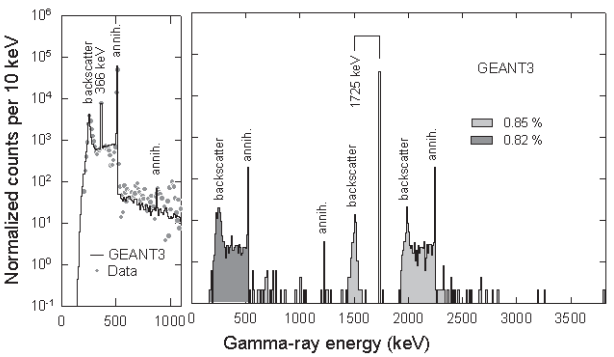

Fig. 4 *Left panel: a comparison between the data and the results of the simulation. In the simulation only two most prominent TSCs and the primary transition to the ^{57}Fe ground state were taken into account. Right panel: the results of simulations of the response of the detector system to the strongest TSC proceeding via the 1725.4 keV level; only the low-energy part of the spectrum is shown.*

Electromagnetic Excitations in Nuclei: from Photon Scattering to Photodisintegration

M. Erhard, C. Nair, R. Beyer, E. Grosse[1], A.R. Junghans, J. Klug, K. Kosev, N. Nankov, G. Rusev, K.D. Schilling, R. Schwengner, A. Wagner

Part of PhD thesis M. Erhard

Accepted by Proc. of Science (2007), PoS(NIC-IX)056

In explosive nucleosynthesis temperatures are high enough for photodisintegration reactions to occur, e.g. leading to the production of p-process nuclei. In order to understand the reaction rates of element production and element disruption we started an experimental program at the new bremsstrahlung facility of the superconducting electron accelerator ELBE of FZ Dresden-Rossendorf. The bremsstrahlung facility and the detector setup are designed such that the scattering of photons from nuclei and the photodisintegration of nuclei around the particle separation energies can be studied under optimized background conditions. In activation measurements with bremsstrahlung at end-point energy from 10.0 to 16.5 MeV (γ,p), (γ,n) and (γ,α) reactions of ^{92,100}Mo have been studied. Our activation yields can be described within a factor 2-3 or better with calculations using the cross sections from recent Hauser-Feshbach models.

[1] A.J. Koning, S. Hillaire et al., *Proc. Int. Conf. Nucl. Data for Science and Technology, ND2004*, Santa Fe, USA, 2004, AIP Conference proceedings 769 (2005) 177

[2] T. Rauscher and F.-K. Thielemann, At. Data and Nucl. Data Tables 88 (2004) 1

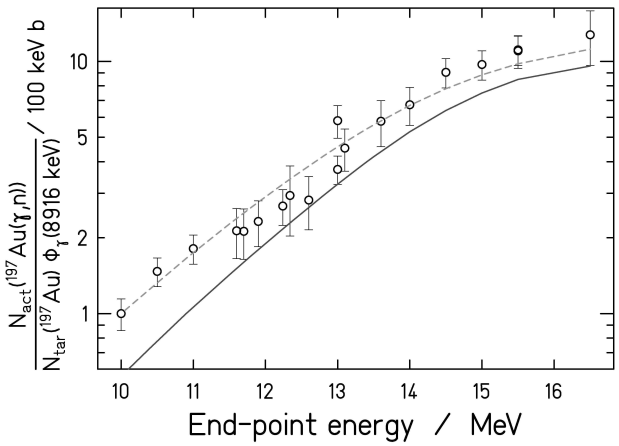

Fig. 1 *Preliminary activation yield of $^{197}Au(\gamma,n)$ measured at the target position. The experimental yield is normalized to the number of ^{197}Au atoms and to the absolute photon flux at the energy E_γ = 8916 keV. The data are compared to yield integrals computed with the cross sections from TALYS [1] and NON-SMOKER [2] using the absolute photon flux determined from known transitions in a sample containing ^{11}B.*

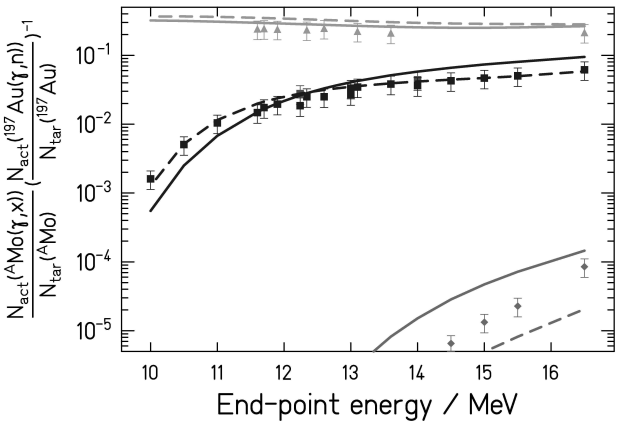

Fig. 2 *Measured activation yields at the photoactivation site for different Mo-Isotopes normalized to the activation yield from $^{197}Au(\gamma,n)$ irradiated simultaneously and to the number of the respective target atoms as a function of the bremsstrahlung end-point energy. The full symbols denote experimental yields from $^{100}Mo(\gamma,n)$ (triangles), $^{92}Mo(\gamma,p)$ + (γ,n) (squares), and $^{92}Mo(\gamma,\alpha)$ (diamond). The lines are calculated with photodisintegration cross sections from NON-SMOKER (full) and TALYS (dashed).*

[1] *also TU Dresden*

Photodisintegration Studies on p-Nuclei: The Case of Sm Isotopes

C. Nair, A.R. Junghans, M. Erhard, E. Grosse[1], K.D. Schilling, R. Schwengner, A. Wagner

Part of PhD thesis C. Nair

In explosive stellar environments like supernovae, the temperatures are high enough for the production of heavy neutron deficient nuclei, the so-called p-nuclei. These are thought to be produced in such scenarios either through chains of photodisintegration reactions like (γ,n), (γ,p) and (γ,α) on heavy seed nuclei or by a recently suggested mechanism interpreted as the νp process[1]. The precise knowledge of the cross sections of these reactions are of crucial importance for the prediction of the p-nuclei abundances in nucleosynthesis network calculations.

At the ELBE bremsstrahlung facility, photodisintegration studies on the astrophysically relevant p-nuclei ^{92}Mo and ^{144}Sm have been performed via the photoactivation technique. All the three types of photodisintegration reactions were observed for the two nuclei and in particular the (γ,α) reactions of the mentioned nuclei were studied for the first time. Bremsstrahlung endpoint energies chosen ranged from 10.0 to 16.5 MeV. Details and main results of the photoactivation studies on ^{92}Mo are comprised in [2].

Samples of fine Sm_2O_3 powder (mass $\approx$ 3 g, diameter 18 mm) were irradiated in the photoactivation site located behind the electron beam dump together with an Au sample. During the same experiment, another Au sample was irradiated at the target position in the bremsstrahlung cave together with a ^{11}B sample. By using the known ^{197}Au(γ,n) cross section and the known scattering cross section of transitions in ^{11}B we could estimate the photon flux in the electron beam dump. For more details of the experimental setup and method see, [2, 3].

The number of radioactive nuclei $N_{act}(E_0)$ produced in a photoactivation measurement is proportional to the integral of the absolute photon flux $\phi_\gamma(E,E_0)$ multiplied by the photodisintegration cross section $\sigma_{\gamma,x}(E)$ from the reaction threshold energy E_{thr} up to the bremsstrahlung spectrum end-point energy E_0:

$$N_{act}(E_0) = N_{tar} \cdot \int_{E_{thr}}^{E_0} \sigma_{\gamma,x}(E)\phi_\gamma(E,E_0)dE.$$

The symbol x stands for the emitted particle (i.e, n,p or α). N_{tar} is the number of target atoms in the sample. $N_{act}(E_0)$ can be experimentally determined with a low-level counting setup using the HPGe detector as

$$N_{act}(E_0) = N_\gamma(E_0,E_\gamma) \cdot \kappa_{corr}/(\epsilon(E_\gamma) \cdot p(E_\gamma)).$$

Here $N_\gamma(E_0,E_\gamma)$ denotes the full-energy peak counts of the observed transition corrected for dead-time and pile-up , $\epsilon(E_\gamma)$ and $p(E_\gamma)$ stand for the absolute full-energy peak efficiency of the detector and the emission probability of the photon for the energy E_γ, respectively. The factor κ_{corr} accounts for the decay losses during irradiation and measurement and this corrects the measured number of decays to the number of radioactive nuclei in the sample.

Measured reaction yields relative to the ^{197}Au reaction yield are as shown in fig. 1. The experimental data are compared with the yield integrals calculated with a simulated thick-target bremsstrahlung spectrum and photodisintegration cross sections predicted by Hauser-Feshbach models [4, 5]. The ^{144}Sm(γ,n) reaction cross section is dominant for energies above 10.5 MeV. Since ^{144}Sm(γ,p) has the reaction threshold at 6.3 MeV, it is necessary to do the experiment with endpoint energies between 6.3 MeV and 10.5 MeV in order to measure pure (γ,p) yields. Experiments in this regard are in progress.

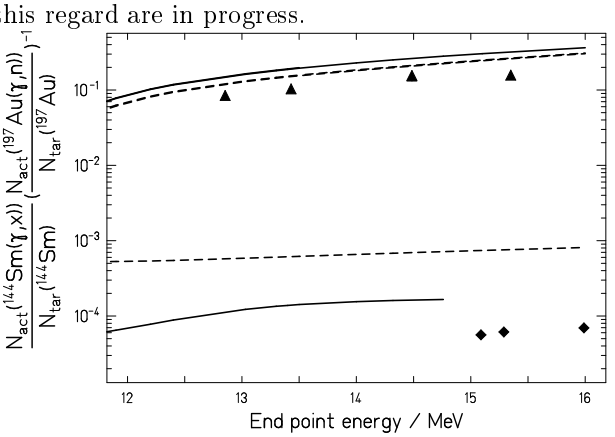

Fig. 1 *Experimental activation yields for photodisntegration reactions on ^{144}Sm isotopes normalized to the activation yield from ^{197}Au(γ,n) irradiated simultaneously. Symbols stand for ^{144}Sm(γ,n) (triangles) and ^{144}Sm(γ,α) (diamonds). The solid line shows calculations using cross sections from [4] and the dotted one stands for the predictions from [5]*

[1] C. Fröhlich et al., Phys. Rev. Lett. 96 (2006) 142502
[2] M. Erhard et al., PoS-(NIC-IX) 056 (2006)
[3] R. Schwengner et al., NIM A 555 (2005) 211
[4] T. Rauscher, F. -K. Thielemann, Atomic Data and Nuclear Data Tables 88 1(2004)
[5] A. J. Koning et al., AIP-(ND-2004) 769 (2005) 1154

[1] *also TU Dresden*

Commissioning of a Pneumatic Delivery System for Photoactivation Experiments at the Electron Accelerator ELBE

A. Wagner, J. Claussner[1], P. Crespo, M. Erhard, M. Fauth[2], E. Grosse[2], A. Hartmann, C. Nair, A.R. Junghans, K.D. Schilling, R. Schwengner, M. Sobiella, J. Steiner

The new facility for experiments on photodisintegration of nuclei using bremsstrahlung has been set into operation at the electron accelerator ELBE of the Forschungszentrum Dresden-Rossendorf [1]. In order to access short-lived nuclides with half-lives below 10 min, the irradiated samples are transported within about 5 s from the electron beam dump into a well-shielded low-level counting setup by means of a pneumatic delivery system. The whole system is hermetically closed in order to prevent leakage of activated air. The radioactive decay is measured by a coaxial high-purity Germanium (HPGe) detector with a relative efficiency of 90%. The data acquisition is based on an ORTEC[3] 919 multichannel analyzer system for long-term measurements of long-lived activities and a dedicated CAMAC-based list-mode data acquisition system for measurements with strongly varying count rates stemming from short-lived decays. The list-mode systems named CAP (CAMAC Acquisition by PCI) allows us to determine the precise dead time during data taking and the correction for signal pile-up in time slices down to 1 ms depending on the detector count rates. The list-mode system consists of NIM and CAMAC modular electronics which are read out by a LINUX-based personal computer. The data taking, analyzing, and visualizing software has been developed based on the Qt open source package[4].

As a first commissioning experiment we studied several (γ, n) reactions close to the neutron separation energies. Table 1 shows the parameters of the reactions leading to β-unstable nuclei. The photon emission following β-decay is used unambiguously to identify the amount of nuclei being activated. Several samples of Mo (≈0.8 g) and Sm_2O_3 (≈3 g) were irradiated for 15 min inside the electron beam dump and the decay was measured for 15 min after 13 s transport to the low-level counting setup. The fractional lifetime of the data taking system was always higher than 0.75.

From the energy dependent activation yields shown in Fig. 1 we conclude that the explicit identification of nuclei from photoactivation allows for a precise determination of activation yields of nuclei with short half lives.

The energy scale of the experimental data was adjusted by a factor of 0.96 to the value deduced from the measurement of the magnetic rigidity of the electron beam.

Reaction	S_n^{eff}	E_γ	$T_{\frac{1}{2}}$
$^{197}Au(\gamma,n)^{196}Au$	8.07 MeV	356 keV	6.2 d
$^{144}Sm(\gamma,n)^{143}Sm$	10.52 MeV	1057 keV	525 s
$^{144}Sm(\gamma,n)^{143m}Sm$	11.27 MeV	754 keV	66 s
$^{92}Mo(\gamma,n)^{91m}Mo$	13.33 MeV	653 keV	15 s

Table 1 *Reactions, effective neutron separation energies S_n^{eff}, photon energies E_γ, and decay half lives $T_{\frac{1}{2}}$ used in photoactivation experiments.*

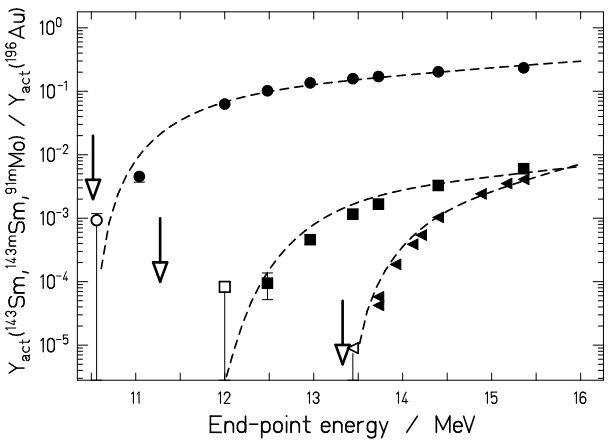

Fig. 1 *Photo-activation yields relative to the reaction $^{197}Au(\gamma,n)^{196}Au$ for $^{92}Mo(\gamma,n)^{91m}Mo$ (triangles), $^{144}Sm(\gamma,n)^{143}Sm$ (circles), and $^{144}Sm(\gamma,n)^{143m}Sm$ (squares). The effective neutron separation energies are marked by arrows. Open symbols denote the detection threshold for the lowest measured energies. Dashed lines show predictions from theoretical models [3].*

[1] K.D. Schilling et al., IKH Annual Report 2005, FZR-442 (2006) 42

[2] M. Fauth et al., this report, p. 52

[3] A. Koning et al., Proc. Int. Conf. Nuclear Data Science and Technology, ND2004, Santa Fe, NM, USA, AIP Conf. Proc. 769, 177 (2005)

[1] *Department of Research Technology, FZD*
[2] *also TU Dresden*
[3] *ORTEC Inc., Oak Ridge, TN 37830 U.S.A.*
[4] *Qt development framework, http://www.trolltech.com*

A CAMAC-Based Data Acquisition System for Photoactivation Experiments at the Electron Accelerator ELBE

M. Fauth[1], P. Crespo, M. Erhard, A.R. Junghans, C. Nair, K.D. Schilling, A. Wagner

A CAMAC-based data acquisition system named CAP (for CAMAC Acquisition through PCI) has been developed for photo-activation experiments at ELBE using high-purity germanium-detectors. The system enables to handle rapidly changing detector count rates from decaying radioactivities with strongly varying data-acquisition dead-times and detector pile-up by using list-mode data taking.

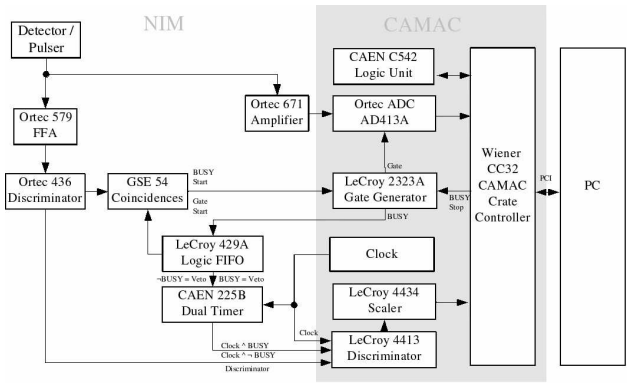

Fig. 1 *Electronics scheme of the CAP system.*

Fig. 1 shows the electronics chain implemented with CAP. The detector's preamplifier signal arrives at an ORTEC[2] 671 main amplifier and an ORTEC 479 fast filter amplifier.

The main amplifier provides a Gaussian-shaped signal for an ORTEC AD413 13-bit analog-to-digital converter read out by CAMAC through a WIENER[3] CAMAC to PCI computer interface. The fast filter amplifier produces a fast rise-time signal with 200 ns differentiation time which is fed into a discriminator. The discriminator signals are counted directly and gated by the data-acquisition dead-time logic using a fast LeCroy[4] 4434 scaler. The gated discriminator signal provides the ADC gate, as well. In parallel, a 1 MHz clock signal is processed in the same way which allows for a precise determination of the data taking time and an independent determination of the dead-time (and detector pile-up) correction. Fig. 2 shows the electronic timing diagram of the CAP system.

The software routines developed for CAP and the list-mode data-format are based on the routines developed for the data acquisition CAGE [1] (CAMAC Acquisition through GPIB and Ethernet). The system performance was analyzed using the decay of activated Sm_2O_3 samples where the various isotopes decay with significantly different half-lives. The plot in Fig. 3 shows three different decay curves for the full energy spectrum, the 103 keV transition from $^{154}Sm(\gamma,n)^{153}Sm(\beta^-)^{153}Eu$ with a half-live of 46.3 h, and the 1057 keV transition from $^{144}Sm(\gamma,n)^{143}Sm(\beta^+)^{143}Pm$ with a half-live of 8.83 min. We conclude that radioactivity from short-lived nuclei can be quantified even for strongly varying detector count rates.

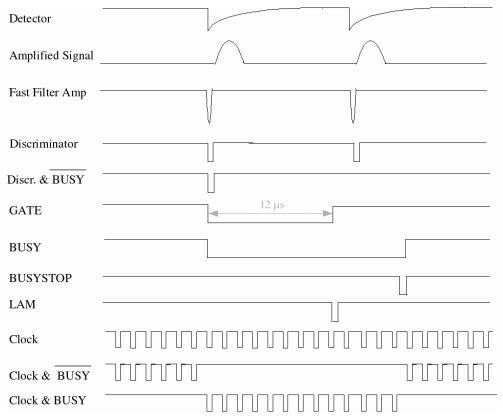

Fig. 2 *Electronic timing diagram of the CAP system.*

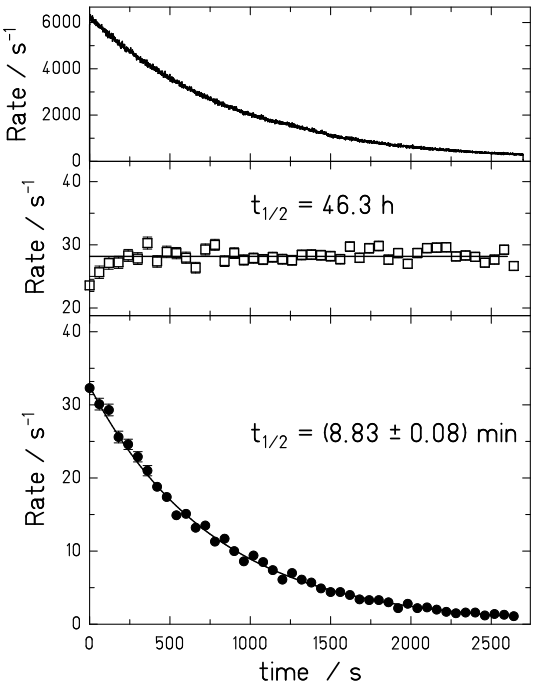

Fig. 3 *Data acquisition rate, rate of detected decays from* ^{153}Sm*, and rate of detected decays from* ^{143}Sm.

[1] http://www.fzd.de/FWK/MITARB/crespo/cage.html

[1] *also TU Dresden*
[2] *ORTEC Inc., Oak Ridge, TN 37830 U.S.A.*
[3] *WIENER, Plein & Baus GmbH, 51399 Burscheid, Germany*
[4] *LeCroy Corp., Chestnut Ridge, NY 10977 U.S.A.*

Improving the Timing Properties of the Photo-Fission Setup

K. Kosev, N. Nankov[1], M. Friedrich[2], **E. Grosse**[3], **A. Hartmann, K. Heidel, A.R. Junghans, K.D. Schilling, R. Schwengner, M. Sobiella, A. Wagner**

Part of PhD thesis K. Kosev

A double time-of-flight spectrometer is under construction which would eventually enable the detection of fission fragments produced by the high-intensity photon beam from bremsstrahlung at ELBE. In this spectrometer Micro-Channel Plate detectors play an important role. The quality of the timing information derived from them is crucial for the experiment.

In a standard setups, the electronic MCP signals are processed by capacitively coupled devices with low impedance (50 Ω) input. The low impedance input is necessary to preserve the signal shape using shielded 50 Ω coaxial cable transmission and hence the signal timing information. Since the MCP back and front signals in our setup are derived from thin rings with ill defined impedance, impedance matching problems arise, causing ringing and signal distortion. Although it is not impossible to build 50 Ω impedance signal collectors [1], an electronic matching is the easier and cheaper solution[2]. Consequently, a simple and fast capacitively coupled transimpedance amplifier has been developed (see Fig. 1).

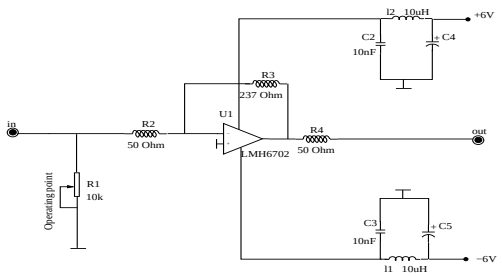

Fig. 1 *The circuit diagram.*

The amplifier is designed to be used with a high input and a low (50 Ω) output impedance without a coupling capacitor. The resistors R1 and R2 determine the operating point of the amplifier U1, the input impedance of the circuit and therefore the quality of the impedance matching. The amplifier U1 is an ultra-wideband monolithic OP-Amp (LMH6702, National Semiconductor) using inverting gain circuit. It has been optimised for exceptionally low harmonic distortion. The amplification formed by the input resistor R2 and the feedback resistor R3 does not exceed factor 4, yet improving the signal-to-noise ratio. R5 serves for impedance line matching. By mounting this circuit as close to the MCP detectors surface as possible, we succeed in preserving the signal rise time and improving the CFD sensitivity, because of the additional amplification.

Finally the setup is tested under beam conditions at the 5 MeV FZD TANDEM accelerator (see Fig. 2).

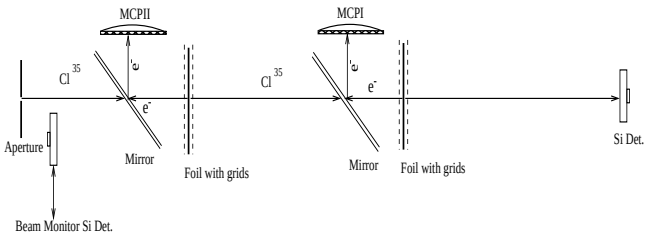

Fig. 2 *Experimental setup. The heavy ion beam enters the setup from the left. After interacting with the foils for secondary electron production, the accelerated electrons are deflected and detected by the MCPs.*

Our first test measurements with the transimpedance amplifiers show satisfactory results (see Fig. 3). It is also worth mentioning that the beam quality can also affect the observed timing resolutions [3].

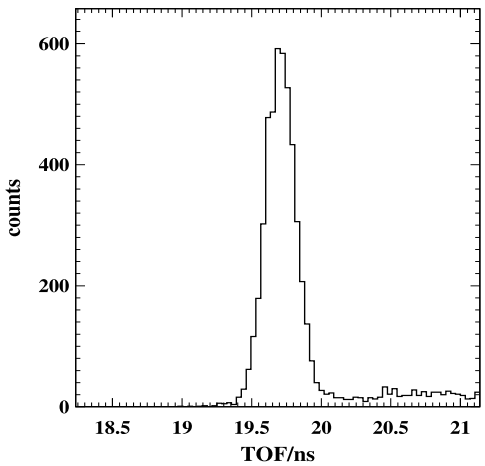

Fig. 3 *TOF spectrum between the two MCPs using transimpedance amplifiers for a ^{35}Cl beam of 40 MeV and foil-to-foil distance of 27 cm. The FWHM results in 240 ps. Assuming identical detectors, the apparent time resolution of one detector corresponds to 170 ps.*

[1] P. Wurz and L. Gubler, Rev. Sci. Instrum. 65 (1994) 871

[2] P. Schwartze et al., Rev. Sci. Instrum. 72 (2001) 3125

[3] K.Kosev et al., IKH Annual Report 2005, FZR-442 (2005) 12

[1] *INRNE, Sofia, Bulgaria*
[2] *Inst. of Ion Beam Physics and Materials Research, FZD*
[3] *also TU Dresden*

Low-Threshold Proton-Recoil Detectors for nELBE

R. Beyer, E. Grosse,[1] **K. Heidel, J. Hutsch, A.R. Junghans, J. Klug,** D. Légrády,[2] R. Nolte,[3] S. Röttger,[3] **M. Sobiella, A. Wagner**

Part of Diploma thesis R. Beyer

For experiments with neutrons at the new neutron time-of-flight source (nELBE) [1] at FZD, and at the existing bremsstrahlung facility [2] fast plastic-scintillation detectors with relatively high efficiency also for neutrons with kinetic energies below 100 keV have been developed [3].

The detectors are made from strips of EJ-200 and have a detection area of 1000 x 42 mm^2 and thicknesses of 11 or 22 mm. In order to determine the position of the detection reaction and to improve the signal to noise ratio, the scintillators are read out in coincidence by two Hamamatsu R2059-01 PMTs, one at each end. A dedicated VMEbus-based data acquisition (DAQ) setup was assembled. Two 32-channel QDCs (CAEN V792) integrate the analog signals of both PMTs to obtain the light output signal. One TDC (CAEN V1190A) is used to determine the timing information. The timing signals are delivered by CFDs (CFT5386), which are an inhouse development being optimized for the signals of the scintillator material used. The start for the time-of-flight (ToF) measurement is given by a reference signal (e.g. the timing signal of the ELBE accelerator). To obtain a low neutron detection threshold, the PMTs are operated at highest gain ($\sim 2{\cdot}10^7$) while the CFD threshold is set to about 50 mV, resulting in a trigger level just below the single-photo-electron peak (SEP) of the PMTs. By adjusting the trigger threshold relative to the SEP, one can set a quite stable and well reproduceable detection threshold [3].

From measurements with a collimated ^{90}Sr electron source one obtains a position resolution of about 5.3 cm (FWHM) and a time resolution of of about 670 ps (FWHM). For neutrons with a kinetic energy of 1 MeV and a flight path of 4 m this time resolution causes an energy resolution of less than $\Delta E/E = 0.5$ %. The efficiency of the detectors has been determined at Physikalisch-Technische Bundesanstalt (PTB), Braunschweig, with quasi-monoenergetic neutron fields from (p,n) reactions on ^{3}H or ^{7}Li [4]. The neutron yield is monitored by well-calibrated neutron counters [5]. In Fig. 1 the measured ToF spectra taken with one detector and a neutron energy of 73 keV are shown. In the upper panel the comparison of the time-of-flight spectra measured with and without a polyethylene shadow bar is shown. Both measurements have been normalised to the same neutron fluence. The width of the ToF peak is dominated by the energy loss of the proton beam inside the target which was simulated with the Monte-Carlo program TARGET [6]. The background subtracted spectrum is shown in the lower panel of Fig. 1 for comparison with the simulated spectrum. Even the background of scattered neutrons can be reproduced reasonably well. Six plastic scintillation detectors were calibrated at five different neutron energies E_n: 24, 73, 150, 560 and 1200 keV. The results of the efficiency determination are plotted in Fig. 2. The main result is, that for neutrons with a kinetic energy of only 24 keV, efficiencies of about ten percent were obtained for all detectors.

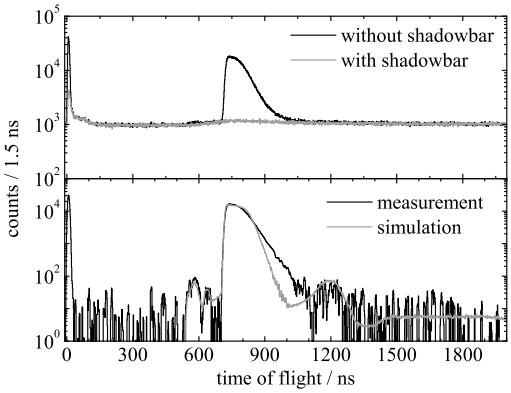

Fig. 1 *Measured ToF spectra for one detector at E_n = 73 keV (see text).*

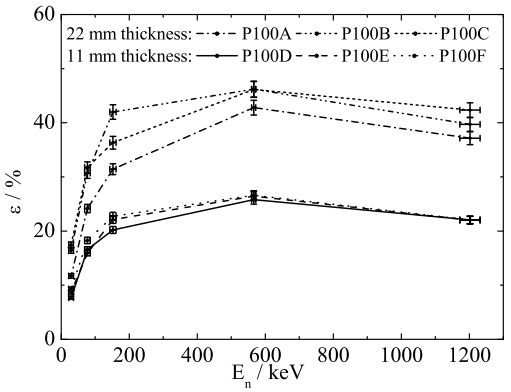

Fig. 2 *Measured intrinsic neutron-detection efficiency for 6 different detectors. The efficiency may vary due to different light collection efficiencies.*

[1] E. Altstadt, C. Beckert et al., Ann. Nucl. Ener. (2007) in press

[2] R. Schwengner, R. Beyer et al., Nucl. Instr. Meth. A 555 (2005) 211

[3] R. Beyer, E. Grosse et al., Nucl. Instr. Meth. A (2007) submitted

[4] H.J. Brede, M. Cosack et al., Nucl. Instr. Meth. 169 (1980) 349

[5] D. Schlegel, S. Guldbakke, PTB-6.41-02-03 (2002)

[6] D. Schlegel, PTB-6.42-05-2 (2005)

[1] *also TU Dresden* [2] *Inst. of Safety Research, FZD*
[3] *PTB Braunschweig*

A BaF_2 Detector Array for Neutron-Capture γ-Rays

J. Klug, E. Altstadt[1], C. Beckert[1], **R. Beyer,** H. Freiesleben[4], V. Galindo[1], M. Greschner[4], **E. Grosse**[also 4], **A.R. Junghans,** D. Légrády[1], B. Naumann[2], K. Noack[1], **G. Rusev, K.D. Schilling,** R. Schlenk[3], S. Schneider[3], K. Seidel[4], **A. Wagner,** F.-P. Weiss[1,also4]

Submitted to Nucl. Instr. Meth. A

The neutron time-of-flight system at ELBE will produce neutrons in the energy interval E_n = 50 keV−10 MeV, where there is a need for neutron cross section measurements for transmutation, fission and fusion reactor applications [1].

For measurements of neutron-capture γ-rays, a scintillation detector array covering up to 96 % of the total solid angle is being built from 42 BaF_2 crystals, each 19 cm long, having a hexagonal cross section with an inner diameter of 53 mm. Two adjacent inner rings of 12 crystals each are surrounded by an outer ring of 18 crystals. They are read out by fast, UV sensitive Hamamatsu R2059 photomultiplier tubes [2], able to measure both the slow and the fast component of the scintillation light, enabling pulse-shape discrimination to separate photon signals from intrinsic α-particle background. A fast digital data acquisition system based on the Acqiris DC282 digitiser [3] is under development.

The efficiency ε of the BaF_2 array due to (n,γ) reactions in a target of 1 cm^3 (7.87 g) of ^{56}Fe has been simulated. It depends on two mechanisms:

(1) The detailed behavior of the γ-cascades following neutron capture. A Monte Carlo code developed at FZD [4] was used to simulate cascades from capture of S-neutrons in ^{56}Fe by exciting levels with spin $\frac{1}{2}$ in ^{57}Fe. The excitation in ^{57}Fe was selected from the range $E_X = 7.6-15$ MeV, corresponding to capture of neutrons with energies $E_n = 0.0-7.4$ MeV. The γ-ray multiplicity and the individual γ-ray energies E_γ were determined in each cascade.

(2) The interactions in the crystals of the emitted γ-rays. Energy deposition tables for γ-ray transport in the array were created using MCNP5, where monoenergetic photons of energy E_{tab} were emitted isotropically from the ^{56}Fe target in steps of 0.5 MeV, up to $E_{tab} = 15$ MeV. The photons were traced through the setup, providing a step-by-step account of all interactions until final absorption or escape. This was done for 90000 γ-rays for each energy and resulted in a table containing the energy deposited in the 42 BaF_2 crystals in a (90000 × 42) array. The sum energy of all 42 entries for a γ-ray starting with energy E_γ may be anywhere between zero and E_γ, depending on how much energy was lost along the track (which may span over one or more crystals).

The calculation of ε proceeded by selecting a γ-ray with energy E_γ from a cascade and identifying the energy deposition table with E_{tab} closest to E_γ. One of the 90000 events was chosen by random, and the energy deposited in each of the 42 detectors was obtained by multiplying the entries with the scale factor E_γ/E_{tab}. This was done for all γ-rays in the cascade, giving the total energy. By repeating the process for all cascades, the instrumental multiplicity m, the energy distribution of the detected cascades, and ε were obtained. The calculation can be performed with several threshold requirements: a minimum energy E_{thr} deposited in each hit BaF_2 crystal, a minimum total energy E_{THR} in the array, and a minimum multiplicity m_{thr}. Thereby a comparison can be made with a real situation where, e. g., background reduction may call for coincident signals in at least two detectors.

Fig. 1 shows the response for neutrons in the range $E_n = 0.0 - 7.4$ MeV with (i) no condition, (ii) $E_{thr} \geq$ 300 keV combined with $E_{THR} \geq$ 7.6 MeV, and (iii) $E_{thr} \geq$ 300 keV plus $m_{thr} \geq 2$. In case (ii), only events above the neutron separation energy are studied, where the high threshold may allow also for $m = 1$ events. In (iii), coincident signals in at least two detectors are utilised instead of a high threshold on the total energy. The efficiencies are (i) $\varepsilon = 0.91$, (ii) $\varepsilon = 0.53$, and (iii) $\varepsilon = 0.67$.

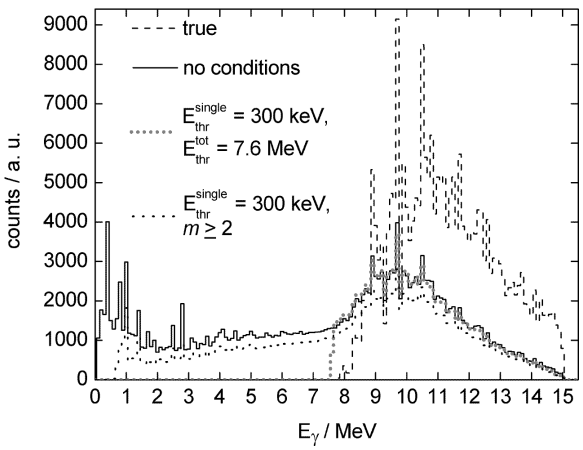

Fig. 1 *Total cascade energy (dashed line), and energy detected by the BaF_2 array under conditions indicated.*

[1] M. Herman (comp) INDC(NDS)-428 and INDC(NDS)-423, IAEA, Vienna, Austria (2001)

[2] http://www.hamamatsu.com

[3] http://www.acqiris.com

[4] G. Rusev, Ph.D. thesis, TU Dresden (2007)

[1] *Inst. for Safety Research, FZD*
[2] *Department for Techn. Infrastructure, FZD*
[3] *Department of Research Technology, FZD*
[4] *TU Dresden*

A Photo-Neutron Source for Time-of-Flight Measurements at the Radiation Source ELBE

J. Klug, E. Altstadt[1], C. Beckert[1], **R. Beyer,** H. Freiesleben[2], V. Galindo[1], M. Greschner[2], **E. Grosse** [also 2], **A. R. Junghans,** D. Légrády[1], B. Naumann[3], K. Noack[1], **G. Rusev, K.D. Schilling,** R. Schlenk[4], S. Schneider[4], K. Seidel[2], **A. Wagner,** F.-P. Weiss [1,also 2]

Submitted to Nucl. Instr. Meth. A

The radiation source ELBE at FZD uses the electron beam to produce various secondary beams. Electron beam intensities of up to $I_e = 1$ mA at energies up to $E_e = 10$ MeV can be delivered with a pulse width of 5 ps at FWHM.

With these parameters, the electron beam allows to generate sub-ns neutron pulses by stopping the electrons in a heavy (high atomic number) radiator and producing neutrons by bremsstrahlung photons through (γ,n) reactions. In order to enable measurements of energy-resolved neutron cross sections like (n,γ), (n,n$'\gamma$), (n,p), (n,α), and (n,f) at a time-of-flight arrangement with a short flight path of only a few meters, it is necessary to keep the volume of the radiator for neutron production as small as possible to avoid multiple scattering of the emerging neutrons, which would broaden the neutron pulses. It is the primary physics objective of this neutron source to measure neutron cross sections firstly for construction materials of fusion and fission reactors, for which it is important to select materials with low activation cross sections, and secondly for the handling of waste from such reactors, especially in order to find processes which transmute long-lived radioactive nuclides into short-lived and finally stable ones. Furthermore, experiments can be performed which address problems of nuclear astrophysics.

The power deposition of the electron beam in the small neutron radiator volume of 1 cm^3 reaches up to 25 kW. This is such a high power density that any solid high Z number material would melt. Therefore, the neutron radiator consists of liquid lead circulated by an electromagnetic pump. The heating power introduced by the electrons is removed through a heat exchanger in the liquid-lead circuit. Typical flow velocities of the lead are between 1 m/s and 5 m/s in the radiator section. From the thermal and mechanical point of view, molybdenum turned out to be the most suited target wall material in the region where the electrons impinge on the neutron radiator.

To reduce the radiation background at the measurement position, the neutrons are decoupled from the radiator at an angle of about 90° with respect to the impinging electrons. Particle transport calculations using the Monte Carlo codes MCNP and FLUKA predict a neutron source strength in the range of $7.9 \cdot 10^{12}$ n/s to $2.7 \cdot 10^{13}$ n/s for electron energies between $E_e = 20$ and 40 MeV. At the measuring place 3.9 m away from the radiator, a neutron flux of about $1.5 \cdot 10^7$ will be obtained. The short beam pulses allow for a neutron energy resolution better than 1 % for neutron energies between $E_n = 50$ keV and 5 MeV. The usable energies range up to about 10 MeV.

The complete setup has been installed in its final position in hall 123 of the ELBE building. The lead loop and the beamdump sit on a lifter that brings the device into position for the experiments, and that lowers it into a lead shield for radiation protection in the periods inbetween. The lifter was tested by raising and lowering it 40 times, giving deviations in vertical position of only 0.2-0.3 mm, and in horizontal position of 0.2 mm orthogonally to the electron beam and 0.7 mm in the direction of the electron beam.

Supplies of cooling water, argon, pressurized air and heating have been installed. The stainless-steel neutron beam collimator tube has been cast into the concrete wall between the halls 123 and 111c. Tungsten shutters to be used for sealing off the neutron beamline when using other experiment setups in hall 123 are under construction.

Several tests of filling and emptying the lead loop confirm the function of the valves, and a one-week uninterrupted run with heated lead demonstrates a stable mode of operation. An emergency shutdown was also successfully tested.

The hut containing the data-acquisition electronics is being installed on top of the experiment caves.

A comprehensive report on the technical aspects of the liquid-lead radiator is given in Ref.[1], while Ref. [2] accounts for simulations done to determine neutron beam characteristics and detector responses. The latter is also reported upon in another contribution to this annual report.

[1] A. Altstadt et al, A photo-neutron source for time-of-flight measurements at the radiation source ELBE, Ann. Nucl. Energy 34 (2007) 36

[2] J. Klug et al, Development of a neutron time-of-flight source at the ELBE accelerator, Nucl. Instr. Meth. A (to be submitted)

[1] *Inst. of Safety Research, FZD*
[2] *TU Dresden*
[3] *Department for Techn. Infrastructure, FZD*
[4] *Department of Research Technology, FZD*

Low-Energy Cross Section of the ^{7}Be(p,γ)^{8}B Solar Fusion Reaction from the Coulomb Dissociation of ^{8}B

F. Schümann, S. Typel, F. Hammache, K. Sümmerer, F. Uhlig, I. Böttcher, D. Cortina, A. Förster, M. Gai, H. Geissel, U. Greife, **E. Grosse**, N. Iwasa, P. Koczon, B. Kohlmeyer, R. Kulessa, H. Kumagai, N. Kurz, M. Menzel, T. Motobayashi, H. Oeschler, A. Ozawa, M. Ploskon, W. Prokopowicz, E. Schwab, P. Senger, F. Strieder, C. Sturm, S. Zhi-Yu, G. Surowka, **A. Wagner**, W. Walus

Published in Phys. Rev. C 73 (2006) 15806, 1-13

An exclusive measurement of the Coulomb breakup of ^{8}B into ^{7}Be + p at 254 A MeV was used to infer the low-energy ^{7}Be(p,γ)^{8}B cross section. The radioactive ^{8}B beam was produced by projectile fragmentation of 350 A MeV ^{12}C and separated with the FRagment Separator (FRS) at Gesellschaft für Schwerionenforschung in Darmstadt, Germany. The Coulomb-breakup products were momentum-analyzed in the KaoS magnetic spectrometer; particular emphasis was placed on the angular correlations of the breakup particles. These correlations demonstrate clearly that E1 multipolarity dominates within the angular cuts selected for the analysis. The deduced astrophysical S_{17} factors exhibit good agreement with the most recent direct ^{7}Be(p,γ)^{8}B measurements. By using the energy dependence of S_{17} according to the recently refined cluster model for ^{8}B of P. Descouvemont [1], we extract a zero-energy S factor of $S_{17}(0) = 20.6 \pm 0.8(\text{stat}) \pm 1.2(\text{syst})$ eV b. These errors do not include the uncertainty of the theoretical model to extrapolate to zero relative energy, estimated by Descouvemont to be about 5%.

[1] P. Descouvement, Phys. Rev. C 70 (2004) 065802

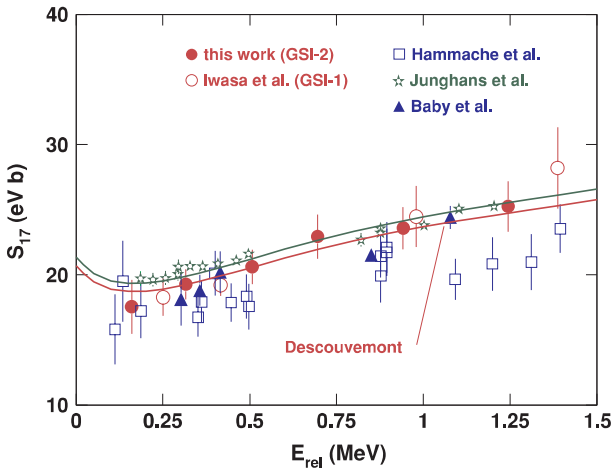

S_{17} from this work (filled circles) in comparison with direct measurements. The latter data were corrected for the contribution of the M1 resonance by the authors. The theoretical curves from [1] have been fitted to the most recent Seattle data (asterisks, upper curve) and the present data (lower curve).

Study of Radiative Proton Capture to the Ground State in ^{15}O

Gy. Gyürky[1], **M. Marta**, A. Formicola[2], **D. Bemmerer**, R. Bonetti[3], C. Broggini[4], F. Confortola[5], P. Corvisiero[5], H. Costantini[5], Z. Elekes[1], Zs. Fülöp[1], G. Gervino[6], A. Guglielmetti[3], C. Gustavino[2], G. Imbriani[7], M. Junker[2], A. Lemut[5], B. Limata[8], R. Menegazzo[4], P. Prati[5], V. Roca[8], C. Rolfs[10], C. Rossi Alvarez[4], E. Somorjai[1], O. Straniero[8], F. Strieder[10], F. Terrasi[9], H.P. Trautvetter[10]

Part of PhD thesis M. Marta

The previous LUNA studies of the ^{14}N(p,γ)^{15}O reaction have shown [1, 2, 3, 4] that the cross section at energies of astrophysical interest is a factor 2 lower with respect to the value adopted in the NACRE compilation, with significant astrophysical implications [5].
The main conclusion from the LUNA data has been confirmed by an independent study at higher energy [6]. However, a discrepancy amounting to 15 % of the total extrapolated S factor at energies corresponding to solar hydrogen burning remains between the R-matrix extrapolations of the different experiments [1, 6]. This discrepancy is due to the extrapolation of the capture to the ground state in ^{15}O, a transition that is strongly affected by interference effects between several resonances and the direct capture mechanism. Removing this discrepancy by precision cross section data would make it possible to study the solar center [7] by comparing the calculated flux of CNO neutrinos with the low energy neutrino data to be provided by the BOREXINO experiment at Gran Sasso.
A new experiment on ^{14}N(p,γ)^{15}O is currently underway, taking advantage of the uniquely low gamma-ray background for $E_\gamma \sim 7$ MeV [8] evident in the LUNA underground facility and of the segmentation of a Clover HPGe detector (see figure). The aim of this new study is to provide precision cross section data for the ground state capture at energies where the R-matrix fit can be effectively constrained.

[1] A. Formicola et al., Phys. Lett. B 591 (2004) 61
[2] G. Imbriani et al., Eur. Phys. J. A 25 (2005) 455
[3] A. Lemut et al., Phys. Lett. B 634 (2006) 483
[4] D. Bemmerer et al., Nucl. Phys. A 779 (2006) 297
[5] G. Imbriani et al., Astron. Astrophys. 420 (2004) 625
[6] R.C. Runkle et al., Phys. Rev. Lett. 94 (2005) 082503
[7] G. Fiorentini and B. Ricci, astro-ph/0310753 (2003)
[8] D. Bemmerer et al., Eur. Phys. J. A 24 (2005) 313
[9] Z. Elekes et al., Nucl. Inst. Meth. A 503 (2003) 580

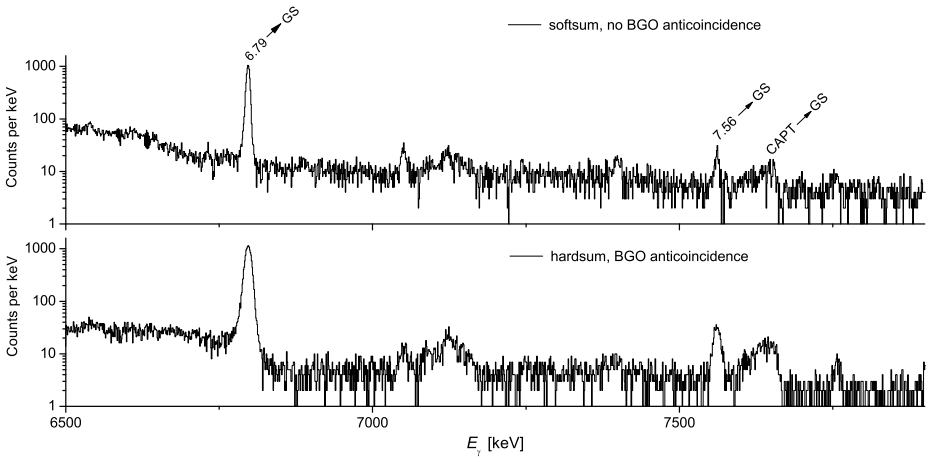

Gamma-ray spectra observed at LUNA with the ATOMKI Clover detector [9] above the $E = 259$ keV resonance. The software sum of the four segments (free running, softsum) is compared with the sum of the analog signals of the same segments (veto from the Clover BGO anticompton shield, hardsum).

[1] *Inst. of Nuclear Research (ATOMKI), Debrecen, Hungary*
[2] *INFN, Lab. Nazionali Gran Sasso (LNGS), Assergi (AQ), Italy*
[3] *Istituto di Fisica Generale Applicata, Univ. Milano, INFN Sezione Milano, Italy*
[4] *Istituto Nazionale di Fisica Nucleare (INFN), Sezione Padova, Italy*
[5] *Univ. Genova, INFN Sezione Genova, Italy*
[6] *Dipartimento di Fisica Sperimentale, Univ. Torino, and INFN Sezione di Torino, Italy*
[7] *Dipartimento di Scienze Fisiche, Univ. Napoli "Federico II", and INFN Sezione di Napoli, Italy*
[8] *Osservatorio Astronomico di Collurania, Teramo, and INFN Sezione Napoli, Italy*
[9] *Seconda Univ. di Napoli, Caserta, and INFN Sezione di Napoli, Italy*
[10] *Inst. für Experimentalphysik III, Ruhr-Univ. Bochum, Germany*

^{3}He(α,γ)^{7}Be cross section at low energies

Gy. Gyürky, F. Confortola, H. Costantini], A. Formicola, **D. Bemmerer**, R. Bonetti, C. Broggini, P. Corvisiero, Z. Elekes, Zs. Fülöp, G. Gervino, A. Guglielmetti, C. Gustavino, G. Imbriani, M. Junker, M. Laubenstein, A. Lemut, B. Limata, V. Lozza, **M. Marta**, R. Menegazzo, P. Prati, V. Roca, C. Rolfs, C. Rossi Alvarez, E. Somorjai, O. Straniero, F. Strieder, F. Terrasi, H.P. Trautvetter

Accepted in Phys. Rev. C (2007), nucl-ex/0702003

The flux of ^{7}Be and ^{8}B neutrinos from the Sun and the production of ^{7}Li via primordial nucleosynthesis depend on the rate of the ^{3}He(α,γ)^{7}Be reaction. In extension of a previous study [1] showing cross section data at 127 - 167 keV center of mass energy, the present work reports on a measurement of the ^{3}He(α,γ)^{7}Be cross section at 106 keV performed at Italy's Gran Sasso underground laboratory by the activation method. This energy is closer to the solar Gamow energy than ever reached before. The result is $\sigma = 0.567 \pm 0.029_{\rm stat} \pm 0.016_{\rm syst}$ nbarn. The data are compared with previous activation studies at high energy, and a recommended $S(0)$ value for all ^{3}He(α,γ)^{7}Be activation studies, including the present work, is given.

[1] D. Bemmerer *et al.*, Phys. Rev. Lett. 97 (2006) 122502

[2] J. Osborne *et al.*, Phys. Rev. Lett. 48 (1982) 1664 Nucl. Phys. A 419 (1984) 115

[3] R. Robertson *et al.*, Phys. Rev. C 27 (1983) 11

[4] B. N. Singh *et al.*, Phys. Rev. Lett. 93 (2004) 262503

[5] P. Parker and R. Kavanagh, Phys. Rev. 131 (1963) 2578

[6] K. Nagatani *et al.*, Nucl. Phys. A 128 (1969) 325

[7] H. Kräwinkel *et al.*, Z. Phys. A 304 (1982) 307

[8] T. Alexander *et al.*, Nucl. Phys. A 427 (1984) 526

[9] M. Hilgemeier *et al.*, Z. Phys. A 329 (1988) 243

[10] P. Descouvemont *et al.*, At. Data Nucl. Data Tables 88 (204) 203

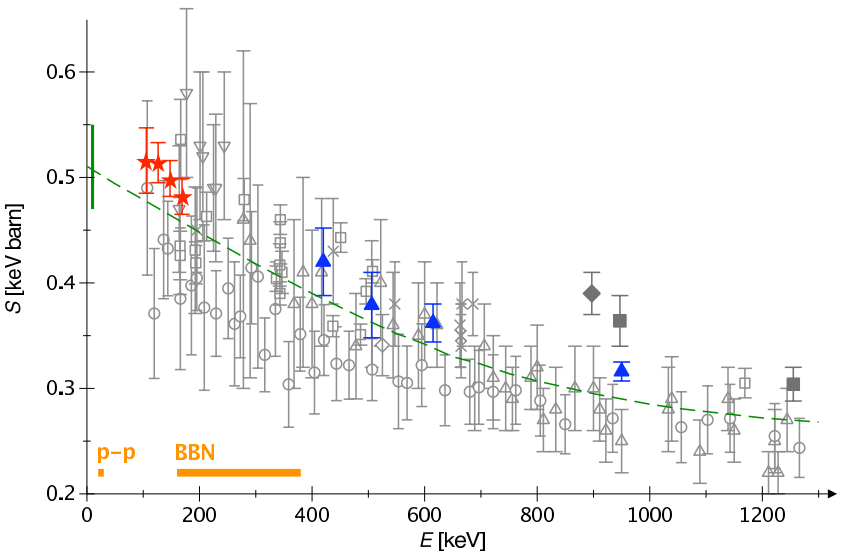

Astrophysical S factor for ^{3}He(α,γ)^{7}Be. Activation data: filled squares [2], filled diamonds [3], filled triangles [4], stars (present work and [1]). Prompt-γ data: triangles [5], inverted triangles [6], circles [7] (renormalized by a factor 1.4 [9]), squares [2], diamonds [8], crosses [9]. Dashed line: previously adopted R-matrix fit [10]. Horizontal bars: energies relevant for solar p–p hydrogen burning and for big bang nucleosynthesis.

Cooling Dynamics in Multi-Fragmentation Processes

T.X. Liu, W.G. Lynch, M.J. van Goethem, X.D. Liu, R. Shomin, W.P. Tan, M.B. Tsang, G. Verde, **A. Wagner**, H.F. Xi, H.S. Xu, W.A. Friedman, S.R. Souza, R. Donangelo, L. Beaulieu, B. Davin, Y. Larochelle, T. Lefort, R.T. de Souza, R. Yanez, V. Viola, R.J. Charity, L.G. Sobotka

Published in Europhys. Lett. 74 (2006) 806-812

Fragment energy spectra of neutron-deficient isotopes are significantly more energetic than those of neutron-rich isotopes of the same element. This trend is well beyond what can be expected for the bulk multi-fragmentation of an equilibrated system. It can be explained, however, if some of these fragments are emitted earlier through the surface of the system while it is expanding and cooling.

[1] W.A. Friedman, Phys. Rev. C, 42 (1990) 667
[2] W.P. Tan, et al., Phys. Rev. C, 68 (2003) 034609

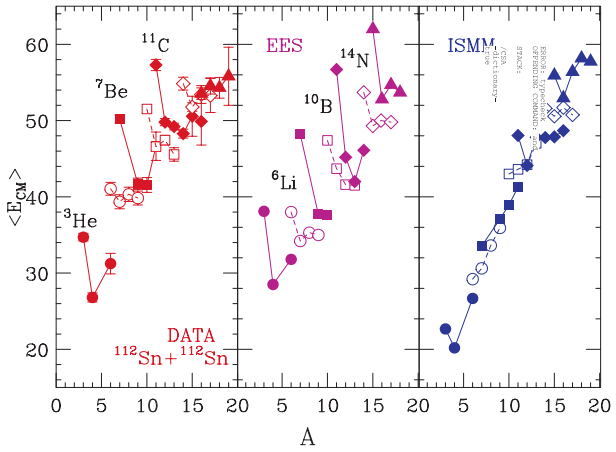

Left panel: experimental fragment mean kinetic energies. Middle panel: mean kinetic energies calculated with the EES[1] model. Right panel: mean kinetic energies calculated with the ISMM[2] model.